

QUANTIFYING PRECIPITATION CHANGES IN NORTHERN CYPRUS
UNDER THE INFLUENCE OF CLIMATE CHANGE

A THESIS SUBMITTED TO
THE BOARD OF GRADUATE PROGRAMS
OF
MIDDLE EAST TECHNICAL UNIVERSITY, NORTHERN CYPRUS CAMPUS

BY

AHMET SERHAT OKUR

IN PARTIAL FULFILLMENT OF THE REQUIREMENTS
FOR
THE DEGREE OF MASTER OF SCIENCE
IN SUSTAINABLE ENVIRONMENT AND ENERGY SYSTEMS PROGRAM

SEPTEMBER 2023

Approval of the Board of Graduate Programs

Prof. Dr. Cumali Sabah
Chairperson

I certify that this thesis satisfies all the requirements as a thesis for the degree of Master of Science

Asst. Prof. Dr. Canraş Batunlu
Program Coordinator

This is to certify that we have read this thesis and that in our opinion it is fully adequate, in scope and quality, as a thesis for the degree of Master of Science.

Asst. Prof. Dr. Hasan Zaifoğlu
Supervisor

Examining Committee Members

Asst. Prof. Dr. Hasan Zaifoğlu	Civil Engineering Prog. METU NCC	_____
Asst. Prof. Dr. Canraş Batunlu	Electrical and Electronics Engineering Prog. METU NCC	_____
Asst. Prof. Dr. İbrahim Bay	Civil Engineering Dept. EUL	_____

I hereby declare that all information in this document has been obtained and presented in accordance with academic rules and ethical conduct. I also declare that, as required by these rules and conduct, I have fully cited and referenced all material and results that are not original to this work.

Name, Last name : Ahmet Serhat, Okur

Signature :

ABSTRACT

QUANTIFYING PRECIPITATION CHANGES IN NORTHERN CYPRUS UNDER THE INFLUENCE OF CLIMATE CHANGE

Okur, Ahmet Serhat
Master of Science, Sustainable Environment and Energy Systems Program
Supervisor: Assist. Prof. Dr. Hasan Zaifoğlu

September 2023, 136 pages

There are some expected changes in the usual weather patterns of the Eastern Mediterranean due to the changing climate conditions of the region. In this study, the focus will be on the Northern Cyprus. The possible effects of climate change on precipitation trends which could be experienced in the future were examined. For that manner, the observational precipitation data and 14 climate models are adopted from EURO-CORDEX database for nine stations to create projections on future precipitation under two different climate scenarios (RCP4.5 and RCP8.5). First, a control period (1978-2005) was formed to check the accuracy of raw models compared to observational data. To correct the biases in the model data, two different bias correction methods of Empirical Quantile Mapping and Gamma Quantile Mapping were adopted. Afterwards, five best performing climate models were selected to create a multi-mean ensemble. Prior to analyze future simulations, observation data were analyzed to see if there was a trend in the precipitation between 1978-2015. Later, by using the multi-mean ensemble, simulations of near future (2024-2062) and far-future (2063-2100) are investigated to check changing trends of precipitation by applying Modified Mann-Kendall, Innovative Trend Analysis, and Sen's Slope Estimator methods. According to the results obtained with these analyzes, in general, all three trend tests in both climate scenarios predicted decreasing precipitation trends for the near future (2024-2062) on both annual and

seasonal basis. Trend tests for the far-future (2063-2100) detected an overall upward trend in the RCP4.5 scenario, both at annual and seasonal levels. However, all trend tests for the RCP8.5 scenario showed a downward trend in annual, winter, and spring season analysis. While a generally decreasing trend was detected in trend tests for the autumn season, a few number of stations with an ascending trend were also detected.

Keywords: Mediterranean, Northern Cyprus, Climate model, Bias Correction

ÖZ

KUZEY KIBRIS'TA İKLİM DEĞİŞİKLİĞİNİN ETKİSİ ALTINDA YAĞIŞ DEĞİŞİMLERİNİN ÖLÇÜLMESİ

Okur, Ahmet Serhat
Yüksek Lisans, Sürdürülebilir Çevre ve Enerji Sistemleri Programı
Tez Yöneticisi: Dr. Öğr. Üyesi Hasan Zaifoğlu

Eylül 2023, 136 sayfa

Değişen iklim koşulları nedeni ile Doğu Akdeniz'deki yağış düzenlerinde uzmanlar tarafından bazı değişiklikler öngörülmektedir. Bu çalışmanın odak noktası Kuzey Kıbrıs olarak belirlenmiştir. İklim değişikliğinin gelecekte yaşanabilecek yağış eğilimleri üzerindeki olası etkileri incelenmiştir. Bu amaçla dokuz farklı istasyon için yağış gözlem verileri ve 14 farklı iklim modelinin hem geçmiş hem de iki farklı iklim senaryosu (RCP4.5 ve RCP8.5) altındaki gelecekteki verileri EURO-CORDEX veri tabanından elde edilmiştir. Öncelikle, modellerin gözlemsel verilere kıyasla doğruluğunu kontrol etmek için bir kontrol dönemi (1978-2005) oluşturulmuştur. Model verilerindeki sapmaları düzeltmek için iki farklı sapma düzeltme yöntemi olan Empirical Quantile Mapping ve Gamma Quantile Mapping teknikleri benimsenmiştir. Bu düzeltme sürecinden sonra, multi-mean ensemble oluşturmak için en iyi performans gösteren beş iklim modeli seçildi. Gelecekteki simülasyonları analiz etmeden önce, 1978-2015 yılları arasında yağışta bir eğilim olup olmadığını görmek adına gözlem verileri analiz edildi. Daha sonra, multi-mean ensemble verileri kullanılarak, değişen yağış eğilimlerini kontrol etmek için yakın gelecek (2024-2062) ve uzak gelecek (2063-2100) simülasyonları Modified Mann-Kendall, Innovative Trend Analysis, ve Sen's Slope Estimator yöntemleri uygulanarak araştırıldı. Bu analizler ile elde edilen sonuçlara göre genel olarak her iki iklim senaryosunda da üç trend testi hem yıllık hem de mevsimsel bazda yakın gelecek

(2024-2062) için azalan yağış trendleri tahmin etmiştir. Uzak gelecek (2063-2100) için yapılan trend testleri, RCP4.5 senaryosunda hem yıllık hem de mevsimsel seviyelerde genel bir artış eğilimi tespit etti. Ancak RCP8.5 senaryosu için tüm trend testleri yıllık, kış sezonu ve ilkbahar sezonu analizlerinde düşüş eğilimi gösterdi. Sonbahar sezonu için trend testlerinde genel olarak azalan bir trend tespit edilmiş olsa da, yükselen trende sahip az sayıda istasyon da tespit edildi.

Anahtar Kelimeler: Akdeniz, Kuzey Kıbrıs, İklim modeli, Hata Düzeltme

To my family and friends

ACKNOWLEDGMENTS

The author wishes to express his deepest gratitude to his supervisor Assist. Prof. Dr. Hasan Zaifođlu for his guidance, advice, criticism, encouragements and insight throughout the research.

The author also wishes to express his gratitude to his friends and colleagues in the school and outside who made this experience unique and meaningful.

Last but not least, the author is highly grateful for all the support from his family members, especially his father Ahmet Okur, his mother Zeliha Okur, his older and younger brothers and his friend Hafsa Khalid. Without them, this whole journey would not have been possible.

TABLE OF CONTENTS

ÖZ	ix
ACKNOWLEDGMENTS	xii
TABLE OF CONTENTS	xiii
LIST OF TABLES	xvi
LIST OF FIGURES	xviii
LIST OF ABBREVIATIONS	xx
LIST OF SYMBOLS	xxii
CHAPTERS	
1. INTRODUCTION	1
1.1 Background of the Study	1
1.2 Statement of the Problem	3
1.3 Scope and Objective	8
1.4 Outline	9
2. LITERATURE REVIEW	11
2.1 Overview of Climate Models	11
2.1.1 Global Climate Models	11
2.1.2 Regional Climate Models	12
2.2 Downscaled Climate Datasets	15
2.3 Representative Concentration Pathway (RCP)	17
2.4 Bias Correction	18
2.5 Previous Studies About the Climate Models and Bias Correction	20
3. STUDY AREA AND DATASETS	25

3.1	Study Area and Rainfall In-situ Data	25
3.2	Simulation (Model) Data	27
4.	METHODOLOGY	29
4.1	Model Data Extraction.....	29
4.2	Bias Correction Application	31
4.2.1	Empirical Quantile Mapping (EQM)	32
4.2.2	Gamma Quantile Mapping (GQM).....	33
4.3	Trend Analysis.....	34
4.3.1	Modified Mann-Kendall Test (MMK).....	35
4.3.2	Sen’s Slope Estimator	38
4.3.3	Innovative Trend Analysis (ITA)	39
5.	RESULTS AND DISCUSSION.....	41
5.1	Evaluation of EURO-CORDEX Over Northern Cyprus.....	41
5.2	Implementation of Bias Correction Techniques	43
5.3	Trend Analysis of Observed Data	46
5.3.1	Observed Annual Trends	46
5.3.2	Observed Seasonal Trends.....	47
5.4	Trend Analysis of Future Simulations.....	50
5.4.1	Trend Analysis Results of RCP4.5 Scenario Simulation.....	51
5.4.2	Trend Analysis Results of RCP8.5 Scenario Simulation.....	56
6.	CONCLUSIONS AND RECOMMENDATIONS	63
6.1	Summary and Conclusions	63
6.2	Recommendations for Future Studies	65
	REFERENCES	67

APPENDICES

A. Bias Correction Tables81

B. Trend Analysis Tables97

LIST OF TABLES

TABLES

Table 3.1. Rainfall Station Details.....	27
Table 3.2. List of GCM-RCM Combinations.....	28
Table A.1. Results of Comparison Between Observation, Raw Model, and EQM Corrected Model for Mean Precipitation and SD.....	81
Table A.2. Results of Comparison Between Observation, Raw Model, and GQM Corrected Model for Mean Precipitation and SD.....	89
Table B.1. Observed MMK and SS Results for Annual Analysis.....	97
Table B.2. Observed ITA Results for Annual Analysis	98
Table B.3. Observed MMK and SS Results for Winter Season Analysis.....	99
Table B.4. Observed ITA Results for Winter Season Analysis.....	100
Table B.5. Observed MMK and SS Results for Spring Season Analysis	101
Table B.6. Observed ITA Results for Spring Season Analysis.....	102
Table B.7. Observed MMK and SS Results for Autumn Season Analysis.....	103
Table B.8. Observed ITA Results for Autumn Season Analysis.....	104
Table B.9. RCP4.5 Near-Future MMK and SS Results for Annual Analysis.....	105
Table B.10. RCP4.5 Near-Future ITA Results for Annual Analysis	106
Table B.11. RCP4.5 Near-Future MMK and SS Results for Winter Season Analysis	107
Table B.12. RCP4.5 Near-Future ITA Results for Winter Season Analysis.....	108
Table B.13. RCP4.5 Near-Future MMK and SS Results for Spring Season Analysis	109
Table B.14. RCP4.5 Near-Future ITA Results for Spring Season Analysis	110
Table B.15. RCP4.5 Near-Future MMK and SS Results for Autumn Season Analysis	111
Table B.16. RCP4.5 Near-Future ITA Results for Autumn Season Analysis.....	112
Table B.17. RCP4.5 Far-Future MMK and SS Results for Annual Analysis	113
Table B.18. RCP4.5 Far-Future ITA Results for Annual Analysis.....	114

Table B.19. RCP4.5 Far-Future MMK and SS Results for Winter Season Analysis	115
Table B.20. RCP4.5 Far-Future ITA Results for Winter Season Analysis.....	116
Table B.21. RCP4.5 Far-Future MMK and SS Results for Spring Season Analysis	117
Table B.22. RCP4.5 Far-Future ITA Results for Spring Season Analysis	118
Table B.23. RCP4.5 Far-Future MMK and SS Results for Autumn Season Analysis	119
Table B.24. RCP4.5 Far-Future ITA Results for Autumn Season Analysis.....	120
Table B.25. RCP8.5 Near-Future MMK and SS Results for Annual Analysis	121
Table B.26. RCP8.5 Near-Future ITA Results for Annual Analysis.....	122
Table B.27. RCP8.5 Near-Future MMK and SS Results for Winter Season Analysis	123
Table B.28. RCP8.5 Near-Future ITA Results for Winter Season Analysis	124
Table B.29. RCP8.5 Near-Future MMK and SS Results for Spring Season Analysis	125
Table B.30. RCP8.5 Near-future ITA results for spring season analysis	126
Table B.31. RCP8.5 Near-Future MMK and SS Results for Autumn Season Analysis	127
Table B.32. RCP8.5 Near-Future ITA Results for Autumn Season Analysis	128
Table B.33. RCP8.5 Far-Future MMK and SS Results for Annual Analysis.....	129
Table B.34. RCP8.5 Far-Future ITA Results for Annual Analysis	130
Table B.35. RCP8.5 Far-Future MMK and SS Results for Winter Season Analysis	131
Table B.36. RCP8.5 Far-Future ITA Results for Winter Season Analysis.....	132
Table B.37. RCP8.5 Far-Future MMK and SS Results for Spring Season Analysis	133
Table B.38. RCP8.5 Far-Future ITA Results for Spring Season Analysis	134
Table B.39. RCP8.5 Far-Future MMK and SS Results for Autumn Season Analysis	135
Table B.40. RCP8.5 Far-future ITA Results for Autumn Season Analysis.....	136

LIST OF FIGURES

FIGURES

Figure 1.1. Illustration of Greenhouse Effect	4
Figure 1.2. Average Temperature Variation from 1880 to 2022	4
Figure 1.3. Average Temperature Change for the Period 2081–2100 Compared to 1986–2005 Under Two Different Climate Scenarios	5
Figure 1.4. Change in Average Precipitation Simulations for 2081–2100 Compared to 1986–2005 Under Two Different Climate Scenarios	6
Figure 1.5. Deviation of Annual Mean Temperatures from The Reference Period of 1880–1899. The Mediterranean Basin Average is Represented by Blue Lines and The Earth’s Average is Represented by the Green Line	7
Figure 1.6. The Average Temperature Change Over Time, Related to the Period 1986-2005 from June to August for the Four Representative Concentration Pathway (RCP) Scenarios	8
Figure 2.1. Framework of a Global Climate Model (GCM)	12
Figure 2.2. Simulation Domain of EURO-CORDEX	17
Figure 3.1. Study Area and Stations	26
Figure 4.1. Methodology of the Study	29
Figure 4.2. Trend Analysis with ITA for Monotonic (a) and Nonmonotonic (b) Series	39
Figure 5.1. Comparison of Raw GCM-RCM Combinations Against Observed Data	41
Figure 5.2. Comparison of Raw, EQM, GQM, and Observed Data for 14 Combinations.....	45
Figure 5.3. ITA Results for Observation Data at Confidence Limits 90 (Left), 95 (Middle), and 99% (Right).	48
Figure 5.4. ITA Results for RCP4.5 Near-Future Annual Dataset at Confidence Limits 90 (Left), 95 (Middle), and 99% (Right).....	52
Figure 5.5. ITA Results for RCP4.5 Far-Future Annual Dataset at Confidence Limits 90 (left), 95 (Middle), and 99% (Right).	55

Figure 5.6. ITA Results for RCP8.5 Near-Future Annual Dataset at Confidence Limits 90 (Left), 95 (Middle), and 99% (Right).....	58
Figure 5.7. ITA Results for RCP8.5 Far-Future Annual Dataset at Confidence Limits 90 (Left), 95 (Middle), and 99% (Right)	60

LIST OF ABBREVIATIONS

ABBREVIATIONS

AMMA	African Monsoon Multidisciplinary Analyses
AR5	The IPCC's fifth Assessment Report
BC	Bias Correction
CA	Central America
CDO	Climate Data Operators
CLARIS	Climate Change Assessment And Impact Studies
CORDEX	Coordinated Regional Downscaling Experiment
CRCM	Canadian Regional Climate Model
DJF	December-January-February
DT	Delta Change
ECHAM	European Centre-Hamburg
ENSEMBLES	Ensembles-Based Predictions of Climate Changes and Their Impacts
EQM	Empirical Quantile Mapping
ESGF	Earth System Grid Federation
EURO-CORDEX	European Coordinated Regional Climate Downscaling Experiment
EUR11	Domain with a resolution of 0.11°
EUR44	Domain with a resolution of 0.44°
GCM	Global Climate Model
GHG	Greenhouse Gasses
GPCC	Global Precipitation Climatology Centre
GQM	Gamma Quantile Mapping
GRIB	GRIdded Binary
HadGEM	Hadley Centre Global Environment Model version
HadRM	Hadley Centre Regional Environment Model version
HDF	Hierarchical Data Format
HIRLAM	High-Resolution Limited Area Model
IMN	Instituto Meteorológico of Costa Rica
IPCC	Intergovernmental Panel on Climate Change
ITA	Innovative Trend Analysis
LOCI	Local Intensity Scaling

LS	Linear Scaling
JJA	June-July-August
MAM	March-April-May
MANC	Meteorological Authority of Northern Cyprus
MMK	Modified Mann-Kendall Trend Test
NARCCAP	North American Regional Climate Change Assessment Program
NetCDF	Network Common Data Form
PRUDENCE	Prediction Of Regional Scenarios And Uncertainties
RACMO	Dutch Regional Atmospheric Climate Model
PB	Percent Bias
PT	Power Transformation
QM	Quantile Mapping
RCM	Regional Climate Model
RCP	Representative Concentration Pathway
RegCM3	U.S. Regional Climate Model Version 3
REMO	German Regional Climate Model
SD	Standard Deviation
STARDEX	Statistical And Regional Dynamical Downscaling of Extremes
SON	September-October-November
WRF	Weather Research Forecasting

LIST OF SYMBOLS

SYMBOLS

a	Time series (Mann-Kendall)
b	Time series (Mann-Kendall)
B	Bias-correcting factor
Corr	Correlation confidence limits (ITA)
c_j	Individual data points within the time series (Mann-Kendall)
c_i	Individual data points within the time series (Mann-Kendall)
$ Cn(H) $	Determinant of the correlation matrix
$[Cn(H)]^{-1}$	Inverse matrix
DF	Empirical cumulative distribution function,
DF^{-1}	Inverse of DF for observation
DF_m	DF for model data
$E(S)$	Mean variance
H	Hurst coefficient
n	Total number of observations
n^*	Length of the time series
P_{mod}	Model value of precipitation
P_{obs}	Observed value of precipitation
Q	Slope (Sen's slope)
R_i	Ranking of the de-trended series x_{li}
S	Test statistic (Mann-Kendall)
S^*	Trend slope (ITA)
SSD	Slope standard deviation (ITA)
TI	Trend indicator (ITA)
$V(S)^H$	Unbiased estimate
$V(S)^{HF}$	Estimate with bias.
$Y_{cr,d}$	Value of corrected rainfall data for the model on d th day
$Y_{m,d}$	Value of uncorrected rainfall data for the model on d th day
Z	Standardized (Mann Kendall)
Zc	Transposed vector of the corresponding normal variates Z ,
$[\Gamma(\alpha)]$	Gamma function

α	Shape parameter
β	Scale parameter
Φ^{-1}	Reverse standard normal distribution function with a mean of 0 and a standard deviation of 1.
ρ_l	Autocorrelation function at lag l for a specific H value
γ_0	Variance of z_i .
μ_H	Mean
σ_H	Standard deviation

CHAPTER 1

INTRODUCTION

1.1 Background of the Study

It is a well-known fact that since the beginning of the geological time the Earth's climate has never been constant, and it has been fluctuating. However, it has been observed that frequency of these fluctuations is increasing with every year. Majority of the scientists believe that the amount of greenhouse gases (GHG) released by the human activities have crucial impact on the latest changes in the climate. Such activities have drastically risen in 18th century with the Industrial Revolution resulting in increasing the atmospheric concentrations of some of the GHGs, such as carbon dioxide by 50% and methane by 150% [1]. This is the highest level reached by these gases in the last 3 million years [2]. Because of the careless use of fossil fuels like coal, oil, and natural gas, the concentration of greenhouse gases has increased, causing major global climate change. In particular, it is important to comprehend how the Earth's climate changes and influences hydrologic variables, such as precipitation, in order to assess how future water resource availability will be affected by the climate change.

The Mediterranean region has been the focus of research thus far on the worldwide impacts of climate change. According to the literature [3], there is an increase in mean temperature and a decrease in precipitation rates in the Mediterranean Region. Additionally, there is a noticeable rise in the intensity and number of occurrences of extreme weather events, including floods and droughts. Consequently, it is of utmost importance to conduct localized assessments of precipitation characteristics for each country situated within this region.

The island of Cyprus, situated in the eastern Mediterranean basin, struggles with water shortage under the influence of the Mediterranean climate. In the past few years, there has been a noticeable decline in precipitation in this particular region [4]. However, whether at the national or local level, there is a lack of comprehensive literature covering climate change estimates, especially for Northern Cyprus. Additionally, the limited studies available either analyzed earlier editions of global climate change scenarios [5] or concentrated on variables other than precipitation [6]. Hence, this research focuses on Northern Cyprus, a region that has already witnessed shifts in precipitation patterns. The main purpose of this research is to examine the changing trends of precipitation indicators in the northern part of the island. The analysis integrates observational data from weather stations spanning the years from 1978 to 2015, alongside regional climate model simulations including historical periods (1978-2005), near-future (2024-2062) and far-future (2063-2100). Additionally, a validation step is carried out in which the station observations are compared with the model's historical data.

The major goal of this research is to address a knowledge gap in Northern Cyprus by examining changes in precipitation totals on an annual, seasonal, and monthly scale. The examination of the trends across various time periods will yield valuable insights into historical and anticipated climate studies within the basin. These findings can subsequently guide the development of targeted adaptation and mitigation strategies developed specifically for the basin's requirements.

The analysis of trends in precipitation holds a significant role within the context of sustainability, as it offers crucial insights into the intricate dynamics of evolving weather patterns and their potential ramifications on diverse ecosystems, societies, and economies. Through the examination of prolonged precipitation patterns, researchers have the ability to discern shifts in rain distribution, encompassing alterations in precipitation levels, seasonal fluctuations, and modifications in extreme climatic incidents. These discoveries furnish indispensable knowledge for comprehending the regional consequences of climate shifts, involving potential transformations in water availability, agricultural outputs, management of water

resources, and the overall equilibrium of the environment. The establishment of sustainable developmental strategies greatly hinges on precise climate projections, and the analyses of precipitation trends provide valuable data capable of influencing decisions concerning water resource management, agricultural practices, the advancement of infrastructure, readiness for disasters, and a multitude of other considerations. In its essence, the insights yielded by examinations of precipitation trends empower decision-makers, scientists, and stakeholders alike, guiding them to make well-informed choices that bolster the enduring sustainability of our planet and its intricately interconnected systems.

1.2 Statement of the Problem

A greenhouse gas is a kind of gas that absorbs and releases radiant radiation to trap heat in the Earth's atmosphere [7]. The main GHGs in the atmosphere are ozone (O₃), methane (CH₄), water vapor (H₂O), nitrous oxide (N₂O), and carbon dioxide. These gases enable Earth to become warmer by trapping the heat inside the atmosphere [8]. When the solar energy is absorbed at Earth's surface, it radiates back to the atmosphere as heat to make its way back to the space. However, as seen in Figure 1.1, the most of this heat cannot make its way out of the atmosphere to space since it is captured by the greenhouse gases in the atmosphere. This mechanism is called greenhouse effect. As a result, more the GHG levels in the atmosphere, more the heat will be trapped. When the level of GHG levels reaches an excessive amount and starts to trap more heat than it should be, the average temperature of Earth increases in an uncontrolled and dangerous way. This increase in the Earth's temperature is referred as Global Warming [9]. In a more scientific way, Global Warming can be described as the extended rise in Earth's average temperature caused by human caused acts, mainly fossil fuel usage, by increasing the GHG levels in the atmosphere [10]. As it is illustrated in Figure 1.2, the average temperature of the Earth has increased approximately 1°C since the late 19th century.

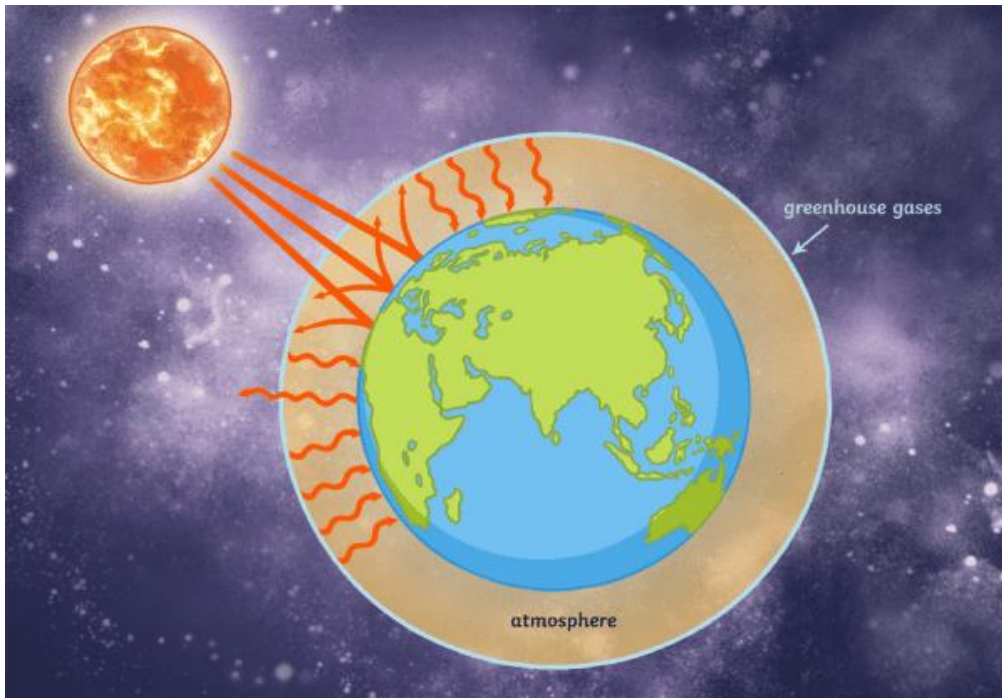


Figure 1.1. Illustration of Greenhouse Effect [11]

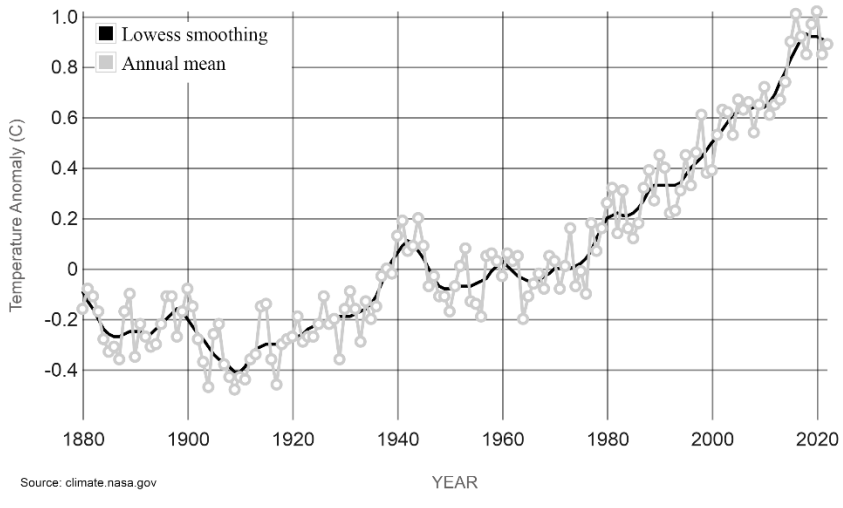


Figure 1.2. Average Temperature Variation from 1880 to 2022 [12]

According to the Intergovernmental Panel on Climate Change (IPCC) fifth assessment report [13], different parts of the planet will experience different fluctuations in temperature. The temperature increase will be stronger in certain places than others. For instance, as seen in Figure 1.3, the lands and high latitudes are predicted to see the most dramatic warming, particularly in the Northern Hemisphere. The biggest contributor to the rising temperature in polar locations is ice melt. In certain areas, the previously highly reflective ice surface is being replaced by a darker soil cover that has a greater capacity to absorb sunlight. as it disappears, boosting warming and future melting in a positive feedback cycle.

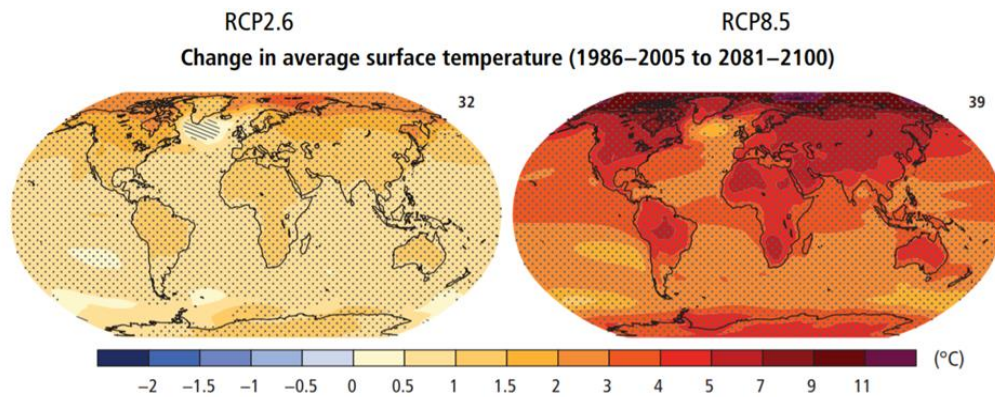


Figure 1.3. Average Temperature Change for the Period 2081–2100 Compared to 1986–2005 Under Two Different Climate Scenarios [13].

Model-based predictions of future changes in precipitation for two different emission pathways RCP2.6 and RCP8.5 are shown on maps in Figure 1.4. According to this, the high latitude regions and the part of the Pacific Ocean near equator are predicted to undergo a rise in yearly average rainfall by the year 2100 when heavy emission scenario is taken into account. However, many wet areas in mid-latitudes are projected to see a rise in average rainfall, whereas several dry regions in mid-latitudes and regions with semi-tropical climates may see a reduction. On the other

hand, the expected fluctuations in rainfall under the RCP2.6 scenario are often small, corresponding to a difference of less than 10%.

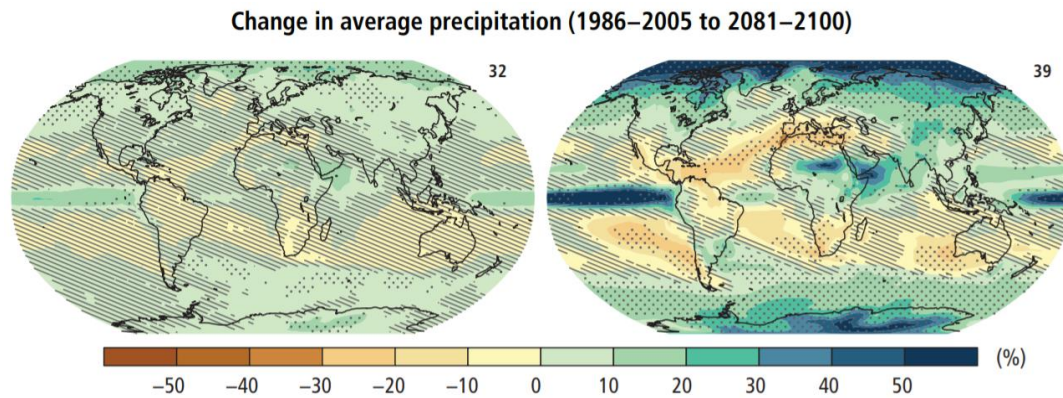


Figure 1.4. Change in Average Precipitation Simulations for 2081–2100 Compared to 1986–2005 Under Two Different Climate Scenarios [14].

The Mediterranean climate, which has hot, dry summers and wet winters, is what gives Mediterranean region their distinctive characteristics [15]. This geographical area includes sections of Europe, Africa, and Asia. According to scientific assessments of global climate scenarios, the Mediterranean region is known as one of the hotspot locations in Earth in terms of having a potential to experience effects of climate change [16]. Average annual temperature in this region is currently 1.4°C higher than they were between 1880 and 1899, exceeding current trends in global warming, which are most noticeable during the summer (Figure 1.5). Moreover, by 2100, the Mediterranean is expected to undergo a temperature increase ranging from 2°C to 6°C based on which RCP scenario is being targeted. Temperatures for summer season are shown in Figure 1.6. In the future years, both frequency and severity of the heat waves and extreme temperature events are expected to rise [17]. Moreover, the long-term assessments conducted in the Mediterranean region indicate a tendency towards warmer and drier annual mean conditions. Since 1950, there has been a notable rise in both the occurrence and severity of dry spells experienced in

the Mediterranean [18]. Forecasts predict an extension in the duration of dry spells in terms of days [19] along with a decrease in precipitation, particularly during the summer months and with significant regional variations.

In the light of all this, this study's findings will be valuable for further research on the effects of climate change because they provide information that decision-makers can utilize to make sustainable decisions about how to manage water supplies in the Northern Cyprus, which is also located in the Mediterranean region. Additionally, it aims to include comprehensive statistically supported findings on the anticipated changes in precipitation totals to understand the consequences locally.

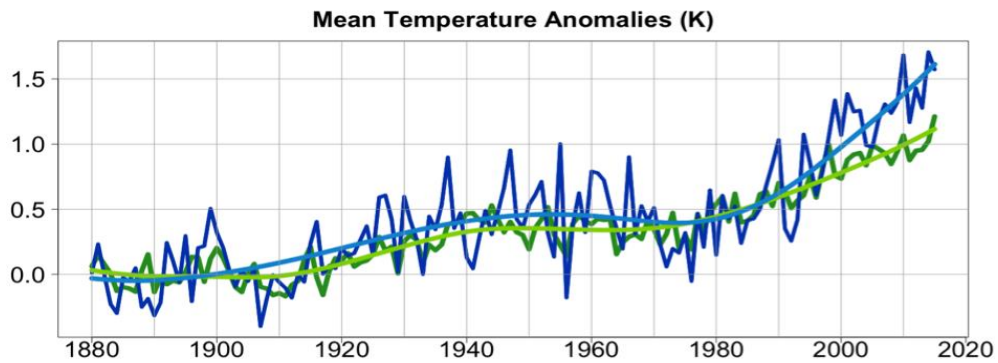


Figure 1.5. Deviation of Annual Mean Temperatures from The Reference Period of 1880–1899. The Mediterranean Basin Average is Represented by Blue Lines and The Earth's Average is Represented by the Green Line [20]

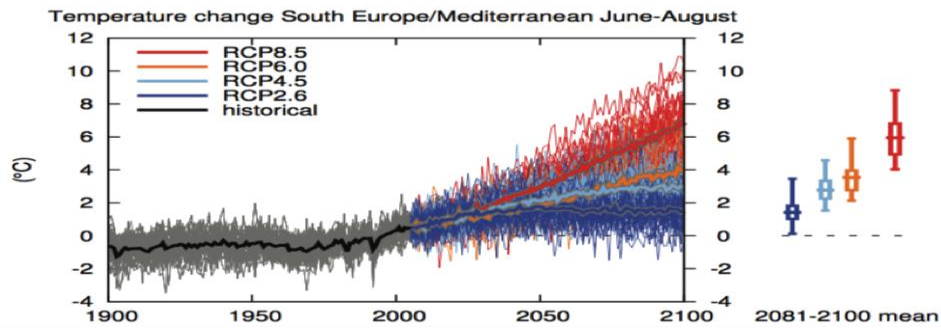


Figure 1.6. The Average Temperature Change Over Time, Related to the Period 1986-2005 from June to August for the Four Representative Concentration Pathway (RCP) Scenarios [21]

1.3 Scope and Objective

The main aim of this study is to understand the potential impacts of climate change on precipitation amounts for the future in the Northern Cyprus region.

The following are the precise objectives of this study within the scope:

- To evaluate the accuracy of various EURO-CORDEX climate models over Northern Cyprus in predicting historical precipitation records.
- To assess the effectiveness of two commonly employed bias correction techniques in enhancing the quality of projected data series for all selected stations, using observed data as a basis.
- To explore the local changes in precipitation for observed data across annual, seasonal, and monthly timeframes.
- To analyze alterations in precipitation patterns under two distinct emission pathways for future projections.

1.4 Outline

This thesis is divided into six chapters, each with its own distinct content, which is briefly summarized below:

Chapter 1: The background of the study, the statement of the problem, and the scope and objectives are summarized.

Chapter 2: The general overview of climate models, bias correction approaches, representative concentration pathways, and previous studies in literature are reviewed.

Chapter 3: The description of study area, the observed precipitation series, and climate model datasets are outlined.

Chapter 4: The methodology of the study including model data extraction, bias correction methods, and trend tests are given in detail.

Chapter 5: The findings from the examination of raw climate model data, the application of bias correction methods, and trend analysis are presented, together with a discussion of the significance of these results for the study area.

Chapter 6: Summary and conclusion of the study are presented.

CHAPTER 2

LITERATURE REVIEW

2.1 Overview of Climate Models

2.1.1 Global Climate Models

General or global circulation models (GCMs) employ mathematical formulas to replicate the Earth's climate. These models simulate various processes, interactions, and feedbacks involving the atmosphere, oceans, and ecosystems. These models serve as crucial tools for providing reasonably accurate climate information at global, hemispheric, and continental scales. They assist in comprehending present climate conditions as well as potential future climate scenarios in the presence of increased greenhouse gas levels [22].

As illustrated in Figure 2.1, in GCMs framework vertical and horizontal grid cells exist to correspond specific regions on the surface of Earth. In every individual grid cell, GCMs analyze a range of elements, which involve the relationships among water vapor and clouds in the atmosphere, the influence of aerosols on radiation and precipitation (both direct and indirect consequences), variations in snow coverage and sea ice, the accumulation of heat in soils and oceans, the flow of heat and moisture across surfaces, and the extensive movement of heat and water by the atmosphere and oceans [23].

GCMs commonly employ a horizontal resolution ranging from 100 to 300 km. Nevertheless, the outputs of GCMs still exhibit limitations in terms of their geographical and time-dependent resolutions [24]. These constraints emerge from a variety of factors, such as imperfect conceptualization, the application of spatial averaging, and the omission of localized characteristics. Consequently, directly

utilizing GCM outputs for local scaled studies can lead to unreliable results [25]. Moreover, GCMs are unable to provide sufficient geographical specifics in various areas characterized by tight continental enlargements, high mountains, and sharp inclines, as the elevation-dependent nature of rainfall is inadequately displayed [26]. Furthermore, GCMs do not offer dependable data for most hydrologically pertinent factors, such as rainfall and temperature, at scale finer than 200 km on a monthly or daily basis. This level of resolution is notably coarse when compared to the finer-scale nature of hydrologic processes [27].

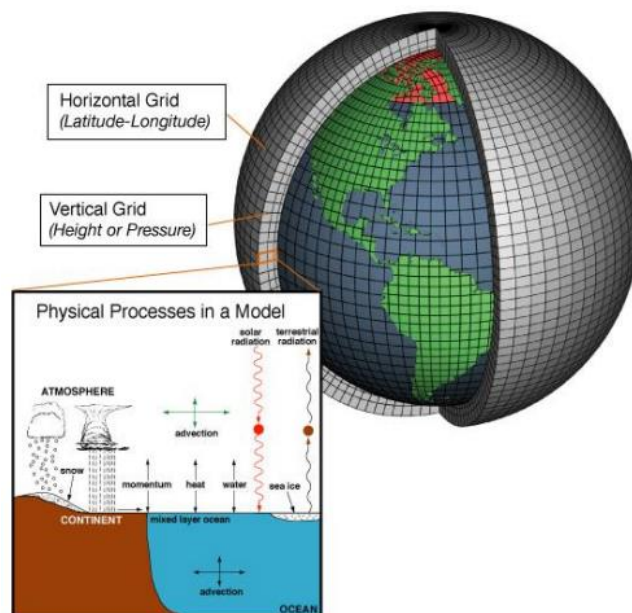


Figure 2.1. Framework of a Global Climate Model (GCM) [28]

2.1.2 Regional Climate Models

At both the national and local levels, there is a rising demand from decision-makers for climate information. This need results from the requirement to handle the risks related to anticipated climate changes and their possible effects. While it is easy to find projections of general climate change towards the latter part of twenty-first

century from sources like the Intergovernmental Panel on Climate Change [29], these predictions do not fully meet the requirements of risk management at a local scale, highlighting the need for regional or local forecasts for the next 5-10 years. To meet the increasing demand, a wide range of assessments focusing on impacts and vulnerabilities have been conducted at different scales, encompassing global, regional, and local levels. These assessments aim to findings that are at a finer level of resolutions than original projections. To obtain such outcomes, it is common practice to utilize blend of approaches and metrics, each carrying its distinct presumptions, advantages, and constraints. However, these crucial factors are often inadequately conveyed in reports, which can leave readers unable to comprehend potential inconsistencies among different studies. Often, information at the global or continental level is directly applied to create impact maps at the local level, disregarding the fact that this broader-scale information does not adequately capture variations specific to the regional level. [30].

A method known as downscaling has been implemented into global scale studies to fulfill the need for regional scaled studies. Downscaling enables the derivation of climate projections at the specific scales desired by decision makers, allowing for more tailored and localized assessments [31]. The term ‘downscaling’ refers to the application of dynamical or statistical methods to obtain information about the climate at a higher resolution level than the GCM data [32]. The downscaling methods that are often employed are statistical and dynamical downscaling.

Statistical downscaling operates by establishing statistical correlations between regional scale data obtained from observations and global scale data extracted from GCMs. By assuming the constancy of these relationships over time, GCM output can be downscaled to individual stations. Statistical downscaling offers advantages such as computational efficiency and user-friendliness [33]. Nevertheless, it is limited in its ability to capture relationships that do not exist in historical data and may not be suitable for regions where a substantial connection between global scale information and regional observations is lacking [34].

On the other hand, dynamical downscaling techniques encompass the utilization of Regional Climate Models (RCMs) with enhanced resolution to drive input from GCMs to regional scales. These RCMs are employed within a restricted geographic region, employing primary constraints derived from a driving GCM [35]. The enhanced benefit of RCMs comes from their capacity to capture the signals of changing climate that might not be detected in the GCMs lower resolutions [36]. RCMs demonstrate greater reliability in reproducing local precipitation patterns as they explicitly consider mesoscale atmospheric processes than GCMs. Consequently, they provide improved representation of the effects of topography on regional-scale precipitation [37].

RCMs exhibit improved performance compared to GCMs primarily due to their higher spatial resolutions (ranging from 12.5 to 50 km), which allows for improved depiction of geographical characteristics such as landforms. Furthermore, RCMs utilize parameterization techniques for sub-grid scales and comprehensive land surface schemes to improve the representation of physical processes. This leads to outputs that are spatially and physically coherent, making them appropriate for various climate-related applications. [38]. The preference towards RCMs arises from their capability to offer more accurate outcomes when investigating the effects of climate change at smaller scales, as opposed to GCMs. [39].

To obtain a more accurate estimate of how the climate in the future will be and its associated uncertainties, ensemble downscaling simulations have been conducted using various combinations of RCMs and GCMs. However, it is important to note that RCMs may still exhibit systematic biases, and therefore, direct utilization of their outputs is not recommended as it may lead to misleading information [40]. Thus, the bias between model and observation data should be carefully considered when interpreting the results [41].

RCMs are created by organizations equipped with the essential computational capacities and technical proficiencies. Different RCMs exhibit variations in terms of their operating way. Some of the widely utilized models in studies that are used for downscaling climate change include U.S. Regional Climate Model Version 3

(RegCM3), Canadian Regional Climate Model (CRCM), UK Met Office Hadley Centre's Regional Climate Model Version 3 (HadRM3), German Regional Climate Model (REMO), Dutch Regional Atmospheric Climate Model (RACMO), and the German HIRHAM, which combines the dynamics of the High-Resolution Limited Area Model (HIRLAM) and the European Centre-Hamburg (ECHAM) models [30].

Even though the previously mentioned models were initially designed for North America and Europe, by adjusting them these models could be used to simulate data belongs to the other regions. This means that multiple RCMs can be applied to a specific area. However, it should be noted that downscaled outcomes may vary depending on the choice of RCM(s) employed. It is crucial to acknowledge that a single RCM is unlikely to yield completely reliable results. Thus, researchers should exercise caution when interpreting the findings, considering the assumptions and limitations of dynamical downscaling. In numerous comprehensive downscaling investigations and initiatives, a range of RCMs are employed to form a multi-model ensemble, enabling validation against observational data.

2.2 Downscaled Climate Datasets

Several international projects have been initiated to facilitate dynamical downscaling intercomparisons, including, “Ensembles-Based Predictions of Climate Changes and Their Impacts (ENSEMBLES), North American Regional Climate Change Assessment Program (NARCCAP), and Coordinated Regional Downscaling Experiment (CORDEX), Prediction Of Regional Scenarios And Uncertainties For Defining European Climate Change Risks And Effects (PRUDENCE), A Europe-South America Network For Climate Change Assessment And Impact Studies (CLARIS), African Monsoon Multidisciplinary Analyses (AMMA), Statistical And Regional Dynamical Downscaling Of Extremes For European Regions (STARDEX)” [42]. These initiatives aim to enhance our understanding of regional climate variations by evaluating the outputs of different downscaling models in a coordinated manner.

Since it was specifically employed in this study, CORDEX has received the most attention of all of them. The aim of CORDEX is to enhance and synchronize scientific endeavors and utilization of downscaling in local scale via an international collaboration [43]. The primary objectives of CORDEX involve enhancing the comprehension of global and regional atmospheric occurrences related to weather and climate, including their variations and alterations, via the use of process of downscaling, to assess and enhance models and techniques for downscaling regional climate, to generate globally coordinated collections of regional downscaled projections, and to facilitate interaction and sharing of knowledge with stakeholders utilizing regional climate data.

The EURO-CORDEX community has emerged as a prominent participant within CORDEX, involving over 30 modeling groups to simulate the European climate under various scenarios. The projection domain is shown in Figure 2.2. They have made RCM simulations openly available to public, notably through the Earth System Grid Federation (ESGF). Additionally, numerous groups within the EURO-CORDEX community have provided diverse RCM data in various CORDEX regions. Additionally, historical and climate change projections are conducted in accordance with the approved CORDEX protocol [44]. The simulations encompass the resulting timeframes: For the evaluation process (ERA-Interim) from 1989 to 2008; for the control process from 1951 to 2005; and for the future projections from 2006 to 2100. The projections are conducted within a single domain with two resolutions: the EUR44 domain with a resolution of 0.44° and the EUR11 domain with a resolution of 0.11° .

There are two ways of downscaling GCMs coarse data into finer RCM data. In the first one, EUR11 data is obtained by downscaling directly from GCMs through RCMs. In the second way, there is a need for intermediate step. First GCM data is needs to be downscaled to EUR44, and then it can be downscaled to EUR11. For both 0.11° (which separates the CORDEX framework from the others) and 0.44° resolutions data sets are available through ESGF data sharing platform.

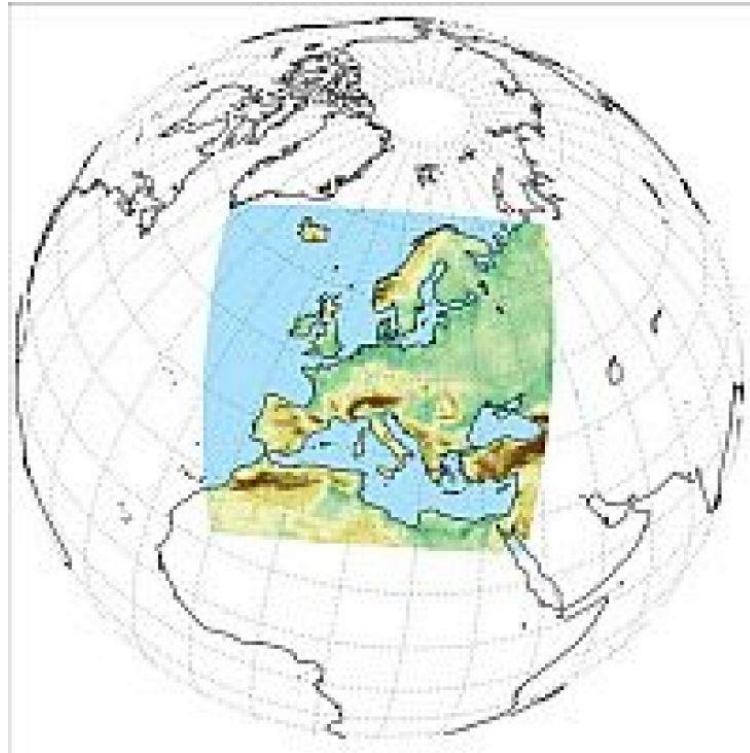


Figure 2.2. Simulation Domain of EURO-CORDEX [45]

2.3 Representative Concentration Pathway (RCP)

A Representative Concentration Pathway (RCP) stands as a designated trajectory for greenhouse gas concentrations embraced by the IPCC. The IPCC's fifth Assessment Report (AR5) in 2014 employed a set of four distinct pathways, purposefully utilized for climate modeling and research endeavors. The described pathways encompass diverse potential climate scenarios, each contingent upon the quantity of greenhouse gases (GHG) released into the atmosphere in the forthcoming years. The designated RCPs, initially referred to as RCP2.6, RCP4.5, RCP6.0, and RCP8.5, derive their names from the potential range of radiative forcing values projected for the year 2100 (2.6, 4.5, 6.0, and 8.5 W/m², correspondingly) [46].

RCP 2.6 represents a pathway characterized as "very stringent" [47]. As per the IPCC's guidelines, RCP 2.6 mandates a notable reduction in carbon dioxide (CO₂)

emissions, commencing by 2020 and reaching complete cessation by the end of 21st century. The IPCC classifies RCP4.5 as a mid-level scenario [48]. Emissions in this pathway reach their peak approximately by 2040 and subsequently begin to decrease [49]. RCP4.5 is regarded as the most plausible baseline scenario in consideration of the finite nature of non-renewable energy resources [50]. Emissions in RCP6.0 reach their highest point around the year 2080 before gradually decreasing [46]. The RCP6.0 scenario involves a substantial rate of greenhouse gas emissions and represents a stabilization pathway where the total radiative forcing is maintained at a stable level till the end of the century. After 2100, through the implementation of various technologies and strategies aimed at reducing greenhouse gas emissions. In RCP8.5, emissions exhibit a continuous upward trend throughout the 21st century. Despite being considered very improbable since AR5, the possibility of such a scenario still exists due to limited comprehension of feedback mechanisms [51]. RCP8.5 is commonly regarded as the foundational premise for worst-case climate change scenarios.

2.4 Bias Correction

As mentioned earlier, RCMs are extremely useful for downscaling coarser GCM data into local scale, nevertheless, the RCM data might still exhibit biases as highlighted in previous studies [52]. Consequently, utilizing RCM outputs directly as input for hydrological models poses a significant challenge. Because the biases observed in RCMs can be attributed to multiple factors, such as errors in boundary conditions inherited from GCMs, inadequately determined surface characteristics due to limited spatial resolution, inaccuracies stemming from numerical resolutions, and integrated model parameterizations [53]. This dependence on model resolution becomes crucial [54]. The reliability of RCMs varies depending on the season and region, with lower accuracy in simulating summer precipitation compared to other seasons, such as autumn and winter. This is primarily due to challenges in modeling heat driven rainfall [55].

Moreover, RCMs exhibit enhanced performance in areas characterized by moderate climate conditions compared to tropical regions. This is due to the fact that rainfall in tropical regions is mainly driven by thermal circulation and occurs on a sub-daily temporal scale [56]. Conversely, the local feedbacks and forcings within RCMs can result in diverse climate change responses across distinct regions worldwide [57]. For example, to address the lack of certainty linked to simulations, it is recommended to employ multiple combinations of GCM-RCMs alongside various emission scenarios [58]. Despite the substantial enhancement provided by RCMs in terms of temporal and spatial resolutions compared to GCMs simulations, there remains a disparity in scale among the simulated values of rainfall at the grid cell level and the data obtained at the point scale [59]. Consequently, it holds great importance to appropriately adjust the variables simulated by RCMs prior to their utilization in driving a hydrological model, particularly in dry regions where the hydrology is highly responsive to fluctuations in the climate [60].

The process of bias correction involves modifying simulated data that contain biases to align them with observations [61]. The purpose of bias correction methods is to enhance the quality of RCM outputs by eliminating methodical biases in the generated data, thereby enabling their utilization in studies [62]. However, it should be emphasized that majority of the bias correction techniques under the assumption of the relation between historical observations and historical model driven data will stay same in the future as well. Thus, the aim of these techniques is not to alter original signals of changing climate but to establish a statistical relationship between historical data from models and observations, with the intention of utilizing this relationship to rectify future simulations as well [63]. Numerous techniques have been developed to modify the meteorological parameters derived RCMs, encompassing techniques that span from straightforward scaling methods to intricate distribution mapping approaches. The most commonly used methods to correct biases are Linear Scaling (LS), Local Intensity Scaling (LOCI), Delta Change (DT), Power Transformation (PT), Quantile Mapping (QM), Empirical Quantile Mapping (EQM) and Gamma Quantile Mapping (GQM) [64].

2.5 Previous Studies About the Climate Models and Bias Correction

Since several climate models and bias correction methods have been employed in climate change research, it is crucial to review the prior studies covering the Mediterranean region, which includes the island of Cyprus, to understand the superior model data sets and bias correction approaches. A brief review of the literature was conducted for this purpose, and the highlights are provided in the following paragraphs.

Menendez et al. (2010) [65] evaluated the performance of six different bias correction techniques to fix the biases in RCMs. In this study, an observational dataset covering monthly precipitation climatology on a 1x1 km grid, derived from historical rain-gauge observations was carefully chosen originated from the Instituto Meteorológico of Costa Rica (IMN) [66] and spanned the period from 1951 to 1995. To assess general consistency of the IMN climatology simulation on a regional scale, conducted a comparative analysis using the dataset from the well-established Global Precipitation Climatology Centre (GPCC) [67]. In this study, data pertaining to cumulative monthly rainfall data from five GCMs were employed. These models were downscaled by dynamical techniques adopting their data from the RCA4 driving RCM [68], and they were accessible through CORDEX initiative, specifically for the Central America (CA) region. Information extracted from CORDEX-CA models spans from the year 1950 to 2100 and exhibits a spatial resolution of $0.44^\circ \times 0.44^\circ$ (approximately 50km). The purpose of this domain is to accurately simulate significant large-scale circulation patterns that significantly influence the regional climate within Central America. Furthermore, to process the monthly rainfall data from the HadGEM2-ES GCM, the researchers utilized the Met Office Hadley Centre HadRM3P as their driving RCM. These simulations were carried out at a spatial resolution of about $0.22^\circ \times 0.22^\circ$ (approximately 25 km) over the CA region, encompassing the period from 1950 to 2100. In this investigation, the emission scenarios known as RCP were incorporated. Given the considerable divergence in emissions trends, encompassing both steady development and fast industrialized growth, this study took into account RCPs 2.6, 4.5, and 8.5. The

purpose was to offer a more comprehensive outlook on potential impacts of the climate change in the future.

Mehran et al. (2014) [69] was examined different BC methods employing a two-sample cross-validation technique. This approach entailed partitioning of the rainfall data from both observations and GCM-RCM couplings into a 30-year calibration interval (1951–1980) and a 15-year validation interval (1981–1995). The decision to divide the data in this manner was mainly driven by the temporal extension and data quality of the observational database to maintain consistency. During the implementation of the diverse BC techniques, customized R functions were employed. The primary objective was to rectify the biases present in the validation period (1981–1995) time series data. As a result of this process, it was founded that EQM and DT were the two most effective methods in terms of fixing biases between observed data and model simulations. Consequently, these two methods were meticulously employed to rectify the precipitation projection biases arising from each GCM-RCM combination for three distinct 30-year future periods: “the near future (2011–2040), mid-future (2041–2070), and far-future (2071–2100).” In general, the findings from the future ensemble-mean, which have undergone bias correction, suggest a decline in rainfall from the near to far-future periods, specifically during the dry season (DJF and MAM), for a significant portion of the country under both RCP4.5 and 8.5 scenarios. These results indicate notably drier conditions in the climatic regions that drain toward the Pacific Ocean. On the contrary, predominantly the projections indicate increased rainfall levels during the arid season under RCP2.6.

Todaro et al. (2022) studied [70] the historical and projected regional climate conditions at five designated locations in Mediterranean Region. These locations were distributed across Portugal, Spain, Tunisia, Greece, and Turkey. For each designated location, initially the precipitation and temperature records are examined to identify any regional patterns in the observed time series. Subsequently, the output obtained from the observation data were utilized to perform statistical downscaling and bias correction on a set of 17 GCM-RCM combinations with a resolution of

0.11°-0.11° (nearly 12.5km) obtained from the EURO-CORDEX initiative [71]. The observed data for the period 1976-2005 was compared to the simulation data obtained from the GCM-RCM coupling for the same period to detect the biases and fix them. Once the bias correction process was completed, the future analysis was conducted using two distinct RCPs [72]: namely, RCP4.5 and RCP8.5. The data that underwent bias correction were employed to assess the future alterations in local precipitation for short-term (2021–2040), medium-term (2041–2060), and long-term (2076–2095) periods compared to the reference period (1986-2005).

Precipitation projections carry a higher degree of uncertainty, with variations concerning the reference period often lacking robustness. The variations among different models are substantial, amplifying over time, and frequently surpasses the projected changes in future. Nevertheless, methodical shifts changes are anticipated in specific seasons. Greece, for instance, is expected to experience robust decreases in winter precipitation for nearly all future periods and both scenarios (ranging from -7% to -31%), alongside a substantial increase in autumn precipitation during the short-term for RCP4.5 (+10%) and RCP8.5 (+5%). Portugal, on the other hand, is projected to encounter robust precipitation decreases during summer (ranging from -16% to -61%) and autumn (ranging from -17% to -35%) for all periods and scenarios. Spain is also estimated to have robust reductions in spring (-2% to -24%) and autumn precipitation (-3% to -10%) for nearly all periods and scenarios, alongside a strong rise in summer rainfall during the short-term under RCP4.5 (+7.5%). In Tunisia, substantial and strong declines are anticipated in spring (ranging from -12% to -29%) and winter precipitation (ranging from -0.3% to -11%). Finally, Turkey is projected to experience robust decreases in summer precipitation (ranging from -13% to -29%) and robust increases in autumn precipitation (ranging from +3% to +10%).

Zittis et al. (2020) investigated the extreme precipitation indicator for Cyprus in 21st century [73]. In this study, an independent regional climate simulation focused on the eastern Mediterranean region, spanning from 1981 to 2100. To accomplish this, the Weather Research and Forecasting (WRF) model [74] was employed as a

dynamic downscaling tool [75], which was later compared to 26 GCM-RCM couplings from EURO-CORDEX datasets. To assess the model output, a daily 1×1 km gridded dataset for precipitation was used with high resolution, encompasses the period from 1980 to 2010. Moreover, to explore the future climate, two distinct 30-year periods under RCP8.5 climate scenario were chosen: one representing the middle of the 21st century (MID, from 2031 to 2060) and the other signifying the anticipated climate conditions by the end of 21st century (END, from 2071 to 2100). Based on the results of the new simulation (WRF), it appears that shift to a more arid and hotter climate are expected to persist throughout the 21st century. The anticipated alterations in various aspects of precipitation also indicate a shift towards more challenging climatic conditions. Interestingly, contrary to global trends observed in previous studies, the absolute 30-year daily rainfall extremes are anticipated to decline in most of the Cyprus grid cells by mid-century (around four-fifths) and by the end of the 21st century (about three-quarters). the projected decrease in precipitation may hold noteworthy consequences for forthcoming flood incidents, highlighting the necessity for a thorough examination of shifts in extreme rainfall occurrences.

Impacts of changing climate on the precipitation patterns over the island of Cyprus were examined in Giannakopoulos et al. (2010) [76]. While the observational data for the time period 1977-1990 was obtained from meteorological stations on the island, the daily model rainfall data was attained from the RACMO2 RCM with its grid spacing of 25km x 25km [77], and extracted from simulations conducted within the ENSEMBLES project were utilized for this study. Regarding the estimated precipitation, the model displayed satisfactory performance, although it tended to slightly minimize high precipitation levels when measured against the observed data. Thus, in general, outcomes of the evaluation process provide positive indications for utilizing this RCM data to simulate possible impacts of change in the climate over Cyprus. According to the predictions for future precipitation alterations, this study demonstrated Cyprus's susceptibility to change in climate in both future periods. The simulated future scenarios point towards a decline in rainfall levels. The most

significant decrease was observed seasonally during the 2071–2100 period, with a reduction in winter rainfall and a decrease in autumn. On the other hand, during the period of 2021–2050 precipitation exhibited a decline in winter but during autumn, an increase was observed.

CHAPTER 3

STUDY AREA AND DATASETS

3.1 Study Area and Rainfall In-situ Data

Cyprus's climate is typical of the eastern Mediterranean, with moderate winters and hot and dry summers. It has summers with a section of its region classified as hot and arid according to the Köppen-Geiger system [78]. During the winter period, the climate exhibits a mild and temperate nature, with occasional rainfall. Conversely, in the summer months, the influence of the summer Asian Thermal Low can be distinctly observed [79]. This particular weather pattern results in high temperatures and abundant sunshine during summer. During the winter season, the typical daytime temperature falls within the range of 12°C to 15°C. Conversely, in the coastal regions during summer, the average maximum temperature rises to 32°C. Deeper inland areas experience even higher temperatures, with the maximum temperature frequently reaching 40°C [76].

On average, Cyprus receives approximately 470 mm of annual precipitation [80]. The Troodos Mountains, covering nearly 30% of the land area, serve as the primary water source for the island [81]. Nonetheless, the period of rainfall persists from November until March, with the primary portion of precipitation (approximately 60%) concentrated between December and February. The occurrence of rainfall is typically linked to the movement of moisture-laden maritime air currents toward the North, particularly over high-altitude terrains (Kostopoulou & Jones, 2007b). The winter precipitation closely correlates with the development of cyclonic weather patterns in the area. Despite this, the occurrence of isolated thunderstorms during summer is not uncommon. However, they contribute to only 5% of the total yearly

rainfall [83]. The region's distinct dryness throughout the summer months holds noteworthy ramifications for diverse socio-economic domains.

The temporal and spatial variability of the rainfall totals during the observation period of 1976-2015 and projection period of 2025-2100 is investigated throughout the northern part of Cyprus. In this context, this study involves nine strategically selected rainfall stations, namely Girne, Lefkoşa, Magusa, Karpaz, Boğaz, İskele, Güzelyurt, Kantara, and Lefke. The designated study area and the specific rainfall stations can be visualized in Figure 3.1, and the details regarding the characteristics of the stations, including their geographic coordinates, altitudes and observation periods, are presented in Table 3.1.

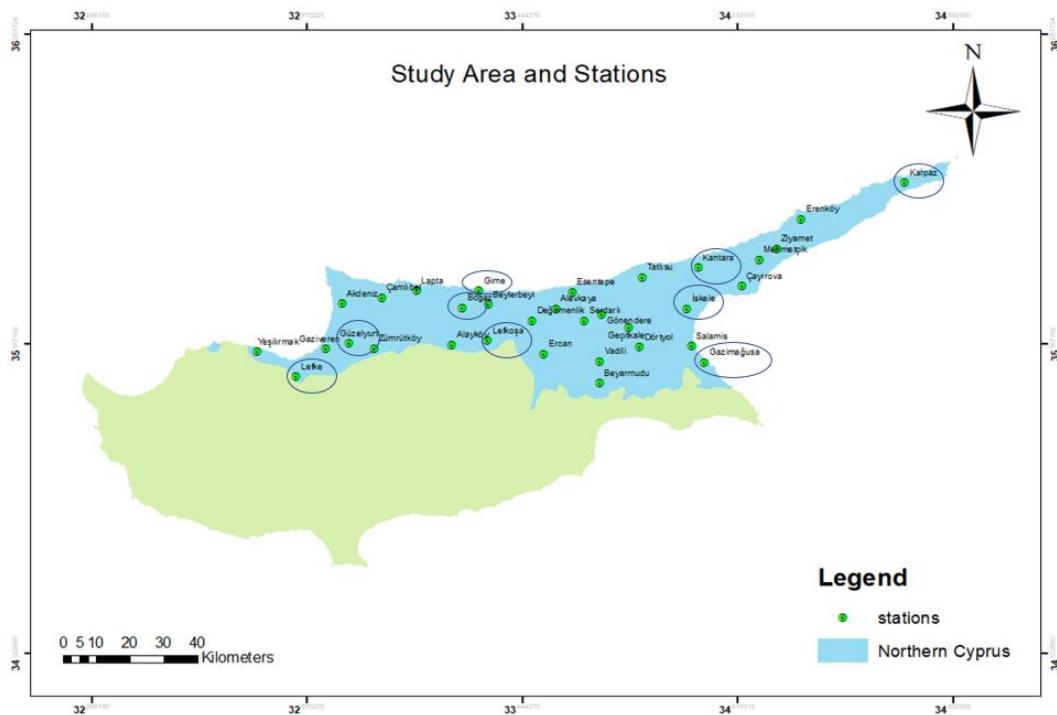


Figure 3.1. Study Area and Stations

Table 3.1. Rainfall Station Details

Station	Latitude (°N)	Longitude (°E)	Altitude (m)	Data Length
Boğaz	33.28484	35.28825	300	1976-2015
Lefkoşa	33.35194	35.19639	134	1976-2015
Girne	33.33139	35.34194	10	1978-2015
Magusa	33.93556	35.13639	10	1978-2015
Karpaz	34.37917	35.59889	136	1978-2015
Güzelyurt	32.98194	35.18889	52	1978-2015
Lefke	32.84091	35.09664	129	1978-2015
İskele	33.88444	35.28611	39	1978-2015
Kantara	33.91361	35.40056	480	1978-2015

The in-situ rainfall datasets are obtained from the Meteorological Authority of Northern Cyprus (MANC) providing essential information derived from direct measurements and monitoring stations strategically situated across the region. To guarantee the credibility and uniformity of the data, [84] a thorough examination is performed, encompassing the assessment of data series to identify any instances of missing values, estimating them as needed, and detecting any improbable or exceptional values. The careful and thorough method employed in this study aims to remove any biases or artificial influences from the collected time series data, ensuring its integrity and trustworthiness. Our rigorous data collection and quality control processes guarantee the reliability and precision of this vital information, forming a strong basis for subsequent analyses and interpretations.

3.2 Simulation (Model) Data

The datasets are crucial in unraveling the intricacies of regional climate dynamics. To achieve a comprehensive investigation, we rely on the esteemed CORDEX simulations. These datasets provide a vast and high-resolution compilation of climate model outputs, tailored to precisely capture regional complexities. The utilization of

CORDEX datasets ensures a robust foundation for data-driven analysis and empowers us to derive meaningful understanding of how climate change affects the environment and societies within the region.

The daily historical model data obtained from the EURO-CORDEX project database (<http://www.euro-cordex.net/>) is at the highest available spatial resolution of 0.11° (~12.5 km) for the time period between 1949 and 2005. The incorporation of this high-resolution CORDEX dataset significantly enhances the precision of representations for both regions of low and high precipitation, such as Cyprus. For the purposes of this investigation, a total of 14 distinct GCM-RCM combinations were carefully selected. Table 3.2. provides a listing of the specific GCM-RCM combinations chosen for this research.

Moreover, the best five performing GCM-RCM couplings from the initial 14 combinations were utilized to create a multi-mean ensemble for the future projection data extraction. The future projections were segmented into two distinct periods: near (2024-2062) and far future (2063-2100), with consideration for two representative concentration pathways of RCP 4.5 and RCP 8.5.

Table 3.2. List of GCM-RCM Combinations

Combination no	Driving Global Model (GCM)	Regional Climate Model (RCM)
1	CNRM-CERFACS-CNRM-CM5 (r1i1p1)	DMI-HIRHAM5_v2
2	CNRM-CERFACS-CNRM-CM5 (r1i1p1)	KNMI-RACMO22E_v2
3	CNRM-CERFACS-CNRM-CM5 (r1i1p1)	RMIB-UGent-ALARO-0_v1
4	CNRM-CERFACS-CNRM-CM5 (r1i1p1)	SMHI-RCA4_v1
5	ICHEC-EC-EARTH (r3i1p1)	KNMI-RACMO22E_v1
6	IPSL-IPSL-CM5A-MR (r1i1p1)	SMHI-RCA4_v1
7	MOHC-HadGEM2-ES (r1i1p1)	CLMcom-CCLM4-8-17_v1
8	MOHC-HadGEM2-ES (r1i1p1)	MOHC_HadREM_v1
9	MOHC-HadGEM2-ES (r1i1p1)	DMI-HIRHAM5_v1
10	MOHC-HadGEM2-ES (r1i1p1)	KNMI-RACMO22E_v2
11	MPI-M-MPI-ESM-LR (r1i1p1)	CLMcom-CCLM4-8-17_v1
12	MPI-M-MPI-ESM-LR (r1i1p1)	MPI-CSC-REMO2009_v1
13	NCC-NorESM1-M (r1i1p1)	DMI-HIRHAM5_v2
14	NCC-NorESM1-M (r1i1p1)	GERICS-REMO2015_v1

CHAPTER 4

METHODOLOGY

Within the methodology section, a comprehensive account of the framework and techniques utilized to collect, analyze, and interpret the data, ensuring the utmost integrity and validity of our findings is presented. The flow chart of this study is given in Figure 4.1.

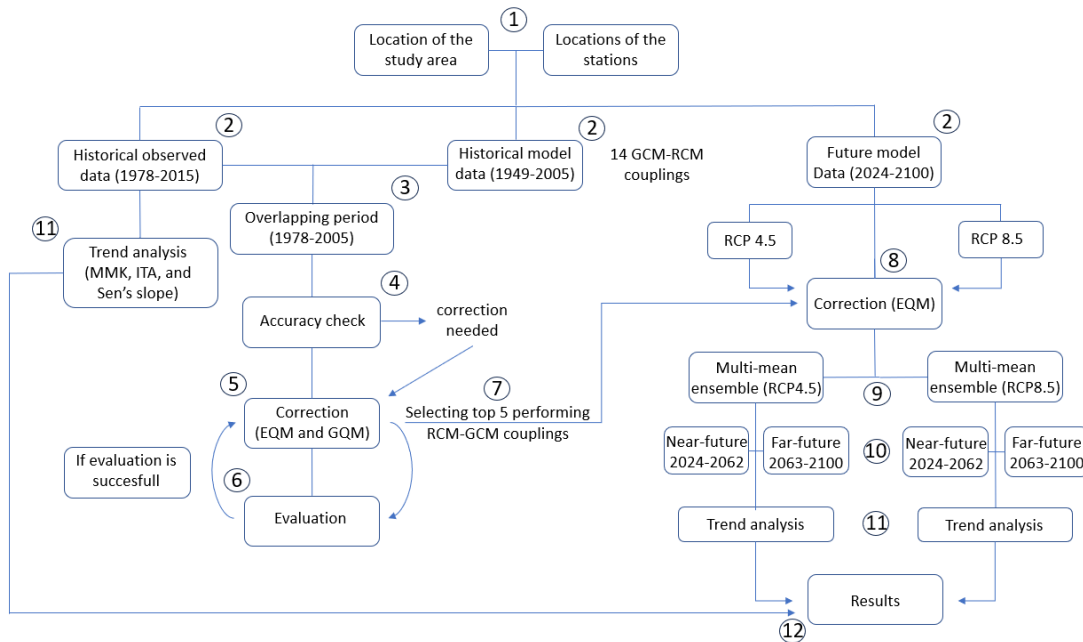


Figure 4.1. Methodology of the Study

4.1 Model Data Extraction

The precipitation data from the EURO-CORDEX project is extracted using the Climate Data Operators (CDO) software. The CDO is an open-source software widely employed in climate science and meteorology to efficiently manipulate and

analyze climate data [85]. Offering a suite of command-line tools, CDO enables researchers and scientists to perform diverse operations on climate data, such as extraction, aggregation, interpolation, masking, and mathematical calculations. Supporting various file formats commonly used in climate modeling, CDO also facilitates data re-gridding, time averaging, and sub-setting, making it a valuable resource for processing, and preparing large-scale climate datasets for further analysis and research. Due to its versatility and effectiveness, CDO finds widespread use in climate studies, helping experts handle the complexities of climate data and derive meaningful insights from extensive and diverse datasets. CDO demonstrates its versatility with multiple data formats, including: NetCDF (Network Common Data Form), GRIB (GRIdded Binary), HDF (Hierarchical Data Format), and GRIB 2.

The EURO-CORDEX datasets come in the NetCDF format (.nc), making them readily accessible for extraction using CDO. The EURO-CORDEX dataset serves as a valuable resource for understanding regional climate dynamics, while the CDO software offers powerful tools for efficiently handling and analyzing large-scale climate data. Through the implementation of CDO, a series of data processing tasks, including spatial and temporal aggregation, interpolation, and masking, enabling the extraction of relevant precipitation information tailored to our research objectives are performed.

Following CDO commands were implemented in given order to extract daily precipitation data from EURO-CORDEX datasets: Initially, the datasets sourced from EURO-CORDEX were seamlessly merged in chronological order, a necessary step due to their segmented nature spanning 3 to 5 years each. To ensure consistency, all data corresponding to February 29 were excluded from the unified dataset, given its quadrennial occurrence. Subsequently, a localized dataset specific to the island of Cyprus was curated, pinpointing the region through its coordinates. This deliberate isolation of Cyprus-centric data streamlined the analytical process significantly. Later, data corresponding to individual rainfall stations were meticulously processed

point by point. Lastly, the transformation of these data from NetCDF format to Excel format marked the concluding phase of this intricate procedure.

4.2 Bias Correction Application

Implementing bias correction techniques, a critical process aimed at enhancing the accuracy and reliability of climate model outputs. In this section, the selected bias correction methodologies are presented, outlining the algorithms and techniques utilized for aligning the model outputs with historical observations. Two bias correction techniques were utilized in this study: EQM and GQM, since the ability of these two techniques to fix biases in the precipitation simulations was suggested to be superior to the other methods as it is mentioned in literature review. Later, the accuracy of datasets that are fixed by these two methods were compared to each other to decide which method is better to fix data for our study area and stations.

In order to facilitate the implementation and evaluate the effectiveness of the two bias correction methods, it is essential to establish a synchronized time interval between historical observations and model data. This synchronization ensures a direct comparison of historical values on identical dates both before and after bias correction, allowing for the examination of differences between the datasets. The primary goal is to determine whether the bias correction techniques successfully minimize disparities between historical model and observation data, and to quantitatively measure the extent of this reduction. By aligning the time intervals, researchers can accurately assess the reliability and impact of bias correction techniques, gaining valuable insights into their ability to harmonize climate model outputs with observed data.

The observational data covered the period from 1978 to 2015, while the historical model data extended from 1949 to 2005. To synchronize these datasets, the calibration period between 1978 and 2005 was chosen. Within this calibration period, the percent bias (PB) of climatological mean and standard deviation of precipitation series were calculated to evaluate the differences between the in-situ

observed and historical model data before bias correction. The PB can be calculated as follows:

$$PB = \frac{\sum_i^n P_{obs} - P_{mod}}{\sum_i^n P_{obs}} \times 100 \quad (1)$$

where P_{obs} and P_{mod} stand for observed and model value of precipitation, respectively and n represents the total number of observations.

Afterward, each bias correction technique is individually implemented on the precipitation data during the calibration period, resulting in the creation of bias-corrected historical model data. The corrected data are subsequently compared to the historical observed data, and PB values are calculated for the climatological means and standard deviations of series.

As with historical model data, biases are also present in future model data. Consequently, these biases necessitate correction, similar to the approach taken for historical data models. To achieve the correction in projection precipitation series, a procedure similar to the one applied to historical model data is essential. In this regard, a correction relationship must be established between the model's historical data and the observed historical data. This is accomplished through a calibration period, considering the disparities between the data during this timeframe. For this study, the calibration period of 1978-2005 is employed. The correction relationship derived from this calibration period is eventually employed to rectify future projections. The same correction relationship obtained from the calibration period is applied to each of the future projections analyzed across two distinct time intervals: near future (2024-2062) and far future (2063-2100).

4.2.1 Empirical Quantile Mapping (EQM)

Empirical Quantile Mapping (EQM) is a widely used technique to correct biases in climate science and hydrology. This method aims to rectify systematic biases in climate model outputs by aligning them with observed data. The process involves matching the cumulative distribution function (CDF) of the model-simulated values

to that of the observed data, using quantiles. By empirically estimating the quantile mapping function, the model outputs are adjusted to account for any discrepancies between the modeled and observed distributions. EQM offers a non-parametric approach, making it versatile and applicable across different variables and regions. Its effectiveness lies in its ability to maintain the statistical characteristics of the observed data while enhancing the reliability of climate projections, thus providing more accurate and informative results for evaluating the consequences of climate changes and formulating strategies for adaptation.

The equation can be represented as follows [65]:

$$Y_{cr,d} = DF_o^{-1}[DF_m(Y_{m,d})] \quad (2)$$

where DF represents the empirical cumulative distribution function, DF_o^{-1} represents the inverse of DF for observation, DF_m represents DF for model data, $Y_{cr,d}$ represents the value of corrected rainfall data for the model on d th day, and $Y_{m,d}$ represents the value of uncorrected rainfall data for the model on d th day.

4.2.2 Gamma Quantile Mapping (GQM)

Gamma Quantile Mapping is another widely employed bias correction technique for precipitation data in climate science studies. Acknowledging the non-Gaussian characteristics often exhibited by precipitation, this technique applies a gamma distribution transformation to both observed and model-simulated data. By estimating the parameters of the gamma distribution for both datasets, quantiles are computed, enabling the establishment of a mapping function. This function aligns the model-simulated precipitation values with the corresponding observed quantiles, effectively correcting potential biases. The gamma quantile mapping approach ensures a more accurate representation of precipitation patterns, enhancing the reliability of climate projections and facilitating informed decision-making in the face of changing precipitation regimes. As a robust and utilized bias correction

method, GQM holds significant promise in advancing climate impact assessments and adaptation strategies.

The equations for gamma quantile mapping are as follows [86]:

$$f_{\gamma}(x | \alpha, \beta) = x^{\alpha-1} * \frac{1}{\beta^{\alpha} * \Gamma(\alpha)} * e^{-\frac{x}{\beta}}; x \geq 0; \alpha, \beta > 0 \quad (3)$$

Where α is the the shape parameter, β is the scale parameter, and $\Gamma(\alpha)$ is the gamma function. The gamma distribution is characterized by two key parameters: the shape parameter α and the scale parameter β . The shape parameter α defines the distribution's shape characteristics, while the scale parameter β governs the spread or dispersion of the Gamma distribution.

4.3 Trend Analysis

Examining trends in precipitation has become a crucial aspect of climate and environmental studies. Researchers analyze historical precipitation data over extended periods to identify potential patterns and fluctuations in precipitation series. Understanding these trends holds immense importance for various reasons, including assessing the impact of climate change, pinpointing regions susceptible to droughts or floods due to heavy rainfall, and evaluating the efficacy of water resource management strategies. Advanced statistical techniques and computational models are harnessed to derive valuable insights from the data, helping scientists determine whether there are significant increases, decreases, or no apparent trends in precipitation over time. Such knowledge empowers decision-makers, enabling them to make well-informed choices concerning infrastructure, agriculture, disaster readiness, and conservation efforts. Ultimately, this investigation of precipitation trend analysis plays a pivotal role in advancing our understanding of the intricate interactions within climate systems, leading to the formulation of sustainable and adaptable approaches to address the challenges arising from a dynamic climate.

In this study, a Modified Mann-Kendall (MMK) test and an innovative trend analysis (ITA) are used for trend detection in annual and seasonal precipitation series. Also,

these two different trend tests are applied to both observational and future projections to check the direction (i.e. negative or positive) and the significance of the trends (i.e. very weak, weak, strong, very strong). In addition, the Sen's slope estimator is employed to evaluate the magnitude of the existing trends.

4.3.1 Modified Mann-Kendall Test (MMK)

The Mann-Kendall method [87] is a commonly used statistical tool employed to identify trends in time-series data, without the need for strict assumptions about data distribution. This non-parametric approach focuses on detecting monotonic trends, characterized by consistent directional changes over time [88]. To achieve this, the method assigns ranks to data points based on their values and computes Kendall's Tau, which quantifies the correlation between data pairs in the original and comparison sequences. The resulting test statistic (S) is then standardized (Z) to facilitate hypothesis testing, where positive or negative Z values indicate increasing or decreasing trends, respectively, with the magnitude of Z denoting trend strength [89]. Embracing diverse applications, the Mann-Kendall method proves especially valuable in fields like climate studies, environmental monitoring, hydrology, and ecological research. It provides valuable insights into long-term trends in time-dependent data, particularly when conventional parametric techniques may not be suitable. The equations for Mann-Kendall test are as follows:

To initiate the Mann-Kendall test for two time series, $a = a_1, a_2, \dots, a_k$ and $b = b_1, b_2, \dots, b_k$, of length k , the first step involves computing the indicator function $\text{sgn}(c_j - c_i)$, where c_i and c_j are individual data points within the time series.

$$\text{sgn}(c_j - c_i) = \begin{cases} 1 & c_i < c_j \\ 0 & c_i = c_j \\ -1 & c_i > c_j \end{cases} \quad (4)$$

The indicator function reveals whether the difference between measurements at time i and j is positive, negative, or zero. Subsequently, the mean and variance of this quantity are calculated, denoted as $E(S)$.

$$E(S) = 0 \quad (5)$$

$$\text{var}(S) = \frac{k(k-1)(2k+5)}{18} \quad (6)$$

$$S = \sum_{i < j} \text{sgn}(c_j - c_i) \quad (7)$$

The statistic S is proven to exhibit asymptotic normality by Kendall (1975) [90] with its mean and variance being equivalent to those in Eqs. (6) and (7). To assess the significance of trends, the standardized test statistic Z , calculated as:

$$Z = \left(\frac{S}{\sqrt{\text{var}(S)}} \right) \quad (8)$$

S value is used to decide the direction of the trend: $S < 0$ indicates a negative trend, $S > 0$ indicates a positive trend. The p -values corresponding to Z values can be used to decide how strong the trend is. For instance, $p > 0.1$ means very weak trend, $0.05 < p < 0.1$ means weak trend, $0.01 < p < 0.05$ means strong trend, and $p < 0.01$ means very strong trend.

In the MMK examinations, the corresponding normalized versions of the rank for the series devoid of trends are derived using the subsequent formula:

$$Z_i = \Phi^{-1}\left(\frac{R_i}{n+1}\right) \text{ for } i=1:n \quad (9)$$

In this context, R_i represents the ranking of the de-trended series x_i^1 , n stands for the length of the time series, and Φ^{-1} symbolizes the reverse standard normal distribution function with a mean of 0 and a standard deviation of 1. The scaling coefficient, also known as the Hurst coefficient denoted as H , is calculated through the process of maximizing the log likelihood function as proposed in the research by McLeod and Hipel in 1978 [90]. This estimation of H demonstrates an approximate normal distribution, particularly in situations where the true H value is 0.5, indicating no correlation. The correlation matrix linked to a specific Hurst coefficient, H , is determined using the subsequent equation:

$$C_n(H) = [\rho_{|j-i|}], \text{ for } i = 1:n, j = 1:n, \quad (10)$$

$$\rho_l = \frac{1}{2}(|l + 1|^{2H} - 2|l|^{2H} + |l - 1|^{2H}), \quad (11)$$

In this equation, ρ_l represents the autocorrelation function at lag l for a specific H value, and it remains unaffected by the time scale of data aggregation within the time series (Koutsoyiannis 2003) [91]. The H value is determined by maximizing the log likelihood function of H , as illustrated in the equation below:

$$\log L(H) = -\frac{1}{2} \log |C_n(H)| - \frac{Z^T [C_n(H)]^{-1} Z}{2\gamma_o}, \quad (12)$$

In this context, where $|C_n(H)|$ signifies the determinant of the correlation matrix $[C_n(H)]$, Z^T represents the transposed vector of the corresponding normal variates Z , $[C_n(H)]^{-1}$ stands for the inverse matrix, and γ_o signifies the variance of z_i . The Eq. (7) can be numerically solved for various H values, and the particular value for which $\log L(H)$ attains its maximum value is considered as the definitive H value for the given series of observations, x_i . In this investigation, the H value is computed within the range of 0.50 and 0.98, utilizing an incremental step of 0.01. The significance level of H is established by employing the mean (μ_H) and standard deviation (σ_H) when H equals 0.5 (assuming a normal distribution). This determination is carried out through the utilization of the following equations [92]:

$$\mu_H = 0.5 - 2.87n^{-0.9067} \quad (13)$$

$$\sigma_n = 0.7765n^{-0.5} - 0.0062 \quad (14)$$

The importance of H is established through the application of μ_H and σ_n in Eq. (8). Within this investigation, significance levels of 5% and 10% were employed to ascertain the importance of H in relation to rainfall. The Hurst coefficient serves as a metric for assessing the long-term memory or persistence within the series. This study followed the approach outlined by Hamed (2008) [92] to determine the significance of the H value. If the significance of H is confirmed, the variance of S is computed using the subsequent equation for the provided H :

$$V(S)^{H'} = \sum_{i < j} \cdot \sum_{k < l} \cdot \frac{2}{\pi} \sin^{-1} \left(\frac{\rho|j-i| - \rho|i-l| - \rho|j-k| + \rho|i-k|}{\sqrt{(2-2\rho|i-j|)(2-2\rho|k-l|)}} \right) \quad (15)$$

The computation of ρ_1 is accomplished through the utilization of Eq. (11) with the designated H value, while $V(S)^{H'}$ signifies the estimate with bias. The determination of the unbiased estimate, $V(S)^H$, involves the multiplication by a bias-correcting factor B , as shown below:

$$V(S)^H = V(S)^{H'} \times B \quad (16)$$

where B is a function of H as below

$$B = a_0 + a_1H + a_2H^2 + a_3H^3 + a_4H^4 \quad (17)$$

The parameters $a_0, a_1, a_2, a_3,$ and a_4 in Eq. (17) depend on the data's sample size, n . The specific values of these coefficients are provided by Hamed (2008). The determination of the significance of the Mann-Kendall test involves substituting $V(S)^H$ for $V(S)$ in Eq. (4).

4.3.2 Sen's Slope Estimator

The Sen's slope estimator, introduced by Sen [93], has found extensive application in hydro-meteorological time series analysis to estimate the slope or the rate of change [94]. To obtain an estimation of the slope denoted as Q , calculations of the slopes for all pairs of data points are conducted.

$$Q_i = \frac{x_j - x_k}{j - k}, i = 1, 2, \dots, N, j > k \quad (18)$$

In the case where the time series comprises n values, a total of $N = n(n - 1)/2$ slope estimates, denoted as Q_i , can be obtained. The Sen's slope estimator is determined as the median among these N Q_i values. These slopes, calculated from the N values, are arranged in ascending order, and the Sen's estimator corresponds to the median of this collection of slopes

$$Q_{\text{med}} = \begin{cases} Q_{|(N+1)/2|} & \text{if } N \text{ is odd} \\ \frac{Q_{|N/2|} + Q_{|(N+2)/2|}}{2} & \text{if } N \text{ is even} \end{cases} \quad (19)$$

4.3.3 Innovative Trend Analysis (ITA)

While there exist widely adopted methods for identifying trends, their reliability is subject to restrictive assumptions. These assumptions include the independence of the time series structure, normal distribution of data, and sufficient data length. Moreover, calculating the trend magnitude (slope) typically necessitates using regression approaches, which introduce new assertions, impacting the theoretical validation in real-world scenarios. Successful water resources management necessitates not only recognizing trends but also distinguishing between sudden and gradual changes. Conversely, a different approach, Innovative Trend Analysis (ITA) overcomes such problems. ITA method enables studies to avoid such these assumptions and allows for visual examination to determine the presence of trends [95]. Various researchers have applied this method in trend identification studies involving diverse datasets, such as precipitation, streamflow, temperature data [96].

Before implementing the ITA method, it is essential to examine it thoroughly. The ITA approach views a time series as two half subseries extracted from the original parent time series. Both halves are sorted in ascending order and subsequently plotted against each other to visualize the scatter diagram. In the same graph, a straight line with a 45-degree angle (1:1) is drawn as a reference for a no-trend situation. If the points lie above (or below) the line, it indicates an increasing (or decreasing) trend, as illustrated in Figure 4.2.

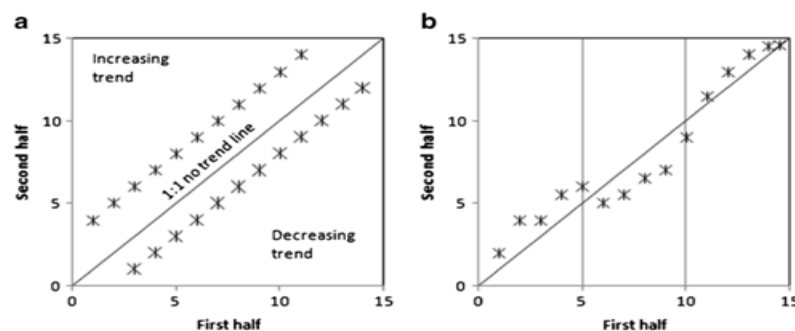


Figure 4.2. Trend Analysis with ITA for Monotonic (a) and Nonmonotonic (b) Series [97]

To apply ITA technique an RStudio package ‘innovtrend’ is implemented. By the implementation of this package, trend slope (S), trend indicator (TI), slope standard deviation (SSD), correlation confidence (Corr) limits at 90, 95, and 99% are calculated. Herein, trend slope is used to decide the direction of the trend. Positive trend slope value indicates a positive trend while negative slope indicates a negative trend. The trend indicator and correlation confidence limits are however used to decide the significance of the trend. Where, $|TI| > |Corr_{99}|$ indicates a very strong trend, $|TI| > |Corr_{95}|$ indicates a strong trend, $|TI| > |Corr_{90}|$ indicates a weak trend, and $|TI| < |Corr_{90}|$ indicates a very weak trend.

CHAPTER 5

RESULTS AND DISCUSSION

5.1 Evaluation of EURO-CORDEX Over Northern Cyprus

In this section, firstly, the performance of selected GCM-RCM couplings was analyzed to test their performance without a bias correction. For this manner, the climatological precipitation mean of historical observed data for nine different rainfall stations were plotted against 14 different historical model data. Results are given in Figure 5.1.

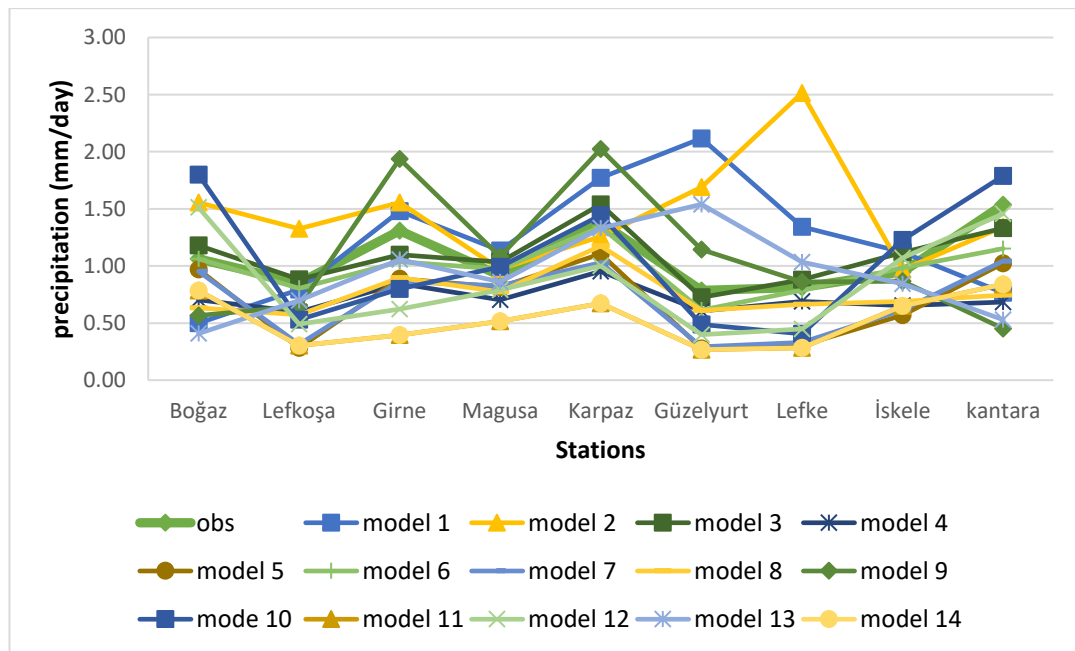


Figure 5.1. Comparison of Raw GCM-RCM Combinations Against Observed Data

The examination of the spatially mean precipitation cycle in Cyprus reveals significant disparities between uncorrected GCM-RCM outputs and actual observations. As a result, it is not advisable to directly employ GCM-RCM precipitation projections in local climate change investigations pertaining to the Cyprus region. In general terms, regardless of the GCM-RCM combination, there are differences between the observation and model values. Each of the models encounters challenges when attempting to replicate the observed higher levels of precipitation seen in the climatic regions along this particular section of the Mediterranean. Additionally, the intricate climate processes at play within these areas, as well as the intricate land and coastal formations between the northeastern and southwestern portions of the country, contribute to a performance that heavily relies on the specific location being considered.

As it was expected, the average %bias varies for each GCM-RCM combination. The average %bias for each combination ranges between 10% to 53%. The detailed results are given in Table A.1. The overall results suggest that the Combinations 1, 2, and 3, tend to overestimate the precipitation (+0.16, +0.40, +0.02 mm/day, respectively) while Combinations 4, 5, 6, 7, 8, 9, 10, 11, 12, 13, and 14 tend to underestimate (-0.35, -0.37, -0.09, -0.37, -0.32, -0.003, -0.01, -0.54, -0.20, -0.14, -0.54 mm/day, respectively).

When the average %bias values are investigated, except the combinations of 3 and 6, all models have a relatively high biases: 48%, 53%, 11%, 31%, 38%, 10%, 37%, 28%, 35%, 33%, 51%, 32%, 34%, 51% for the combinations 1-14 respectively. Given that even the most optimal combinations exhibit an average bias of no less than 10%, the implementation of bias correction becomes exceedingly essential for the study area.

Moreover, the comparisons of climatological standard deviations were performed for each station, considering both historical observed and historical model values. This analysis revealed notable disparities between the observations and model simulations, similar to the findings in the precipitation means. In further elaboration, the standard deviation values were computed for nine stations separately and then

they are averaged using the measurements from each GCM-RCM combination. The same process was carried out for the values derived from the historical observed dataset. Subsequently, standard deviation values obtained from GCM-RCM combinations were compared to the ones obtained from observation values. The detailed outcomes of this comparison are presented in Tables A.1 and A.2.

Consequently, the standard deviation discrepancies between observed and model data were calculated for each station. Moreover, to perform a comprehensive analysis, the average standard deviation differences across all stations were computed for each GCM-RCM combination. After examining these findings, noticeable distinctions were evident between the standard deviations of GCM-RCM combinations and those of the observed data. These disparities ranged from 25% to 53%. The results for each combination are 35%, 33%, 30%, 25%, 42%, 30%, 39%, 27%, 40%, 30%, 52%, 32%, 26%, 53% for the combinations 1-14 respectively.

5.2 Implementation of Bias Correction Techniques

The results of bias correction techniques are presented in Figure 5.2 and the detailed results are given in Table A.1, Table A.2. Based on the overall results, it can be concluded that both bias correction techniques demonstrated efficacy in rectifying the simulations. Except for the Boğaz station in Comb6, the EQM method successfully reduced biases across all stations for all models. Additionally, the average bias values decreased from the initial range of 10%-53% to a much lower range of 0.6%-1.1%. The detailed results are in the order of 0.7%, 1.0%, 0.9%, 1.1%, 0.7%, 0.6%, 0.8%, 1.1%, 0.6%, 0.6%, 0.8%, 1.1%, 0.6%, and 0.8% for the GCM-RCM combinations 1-14.

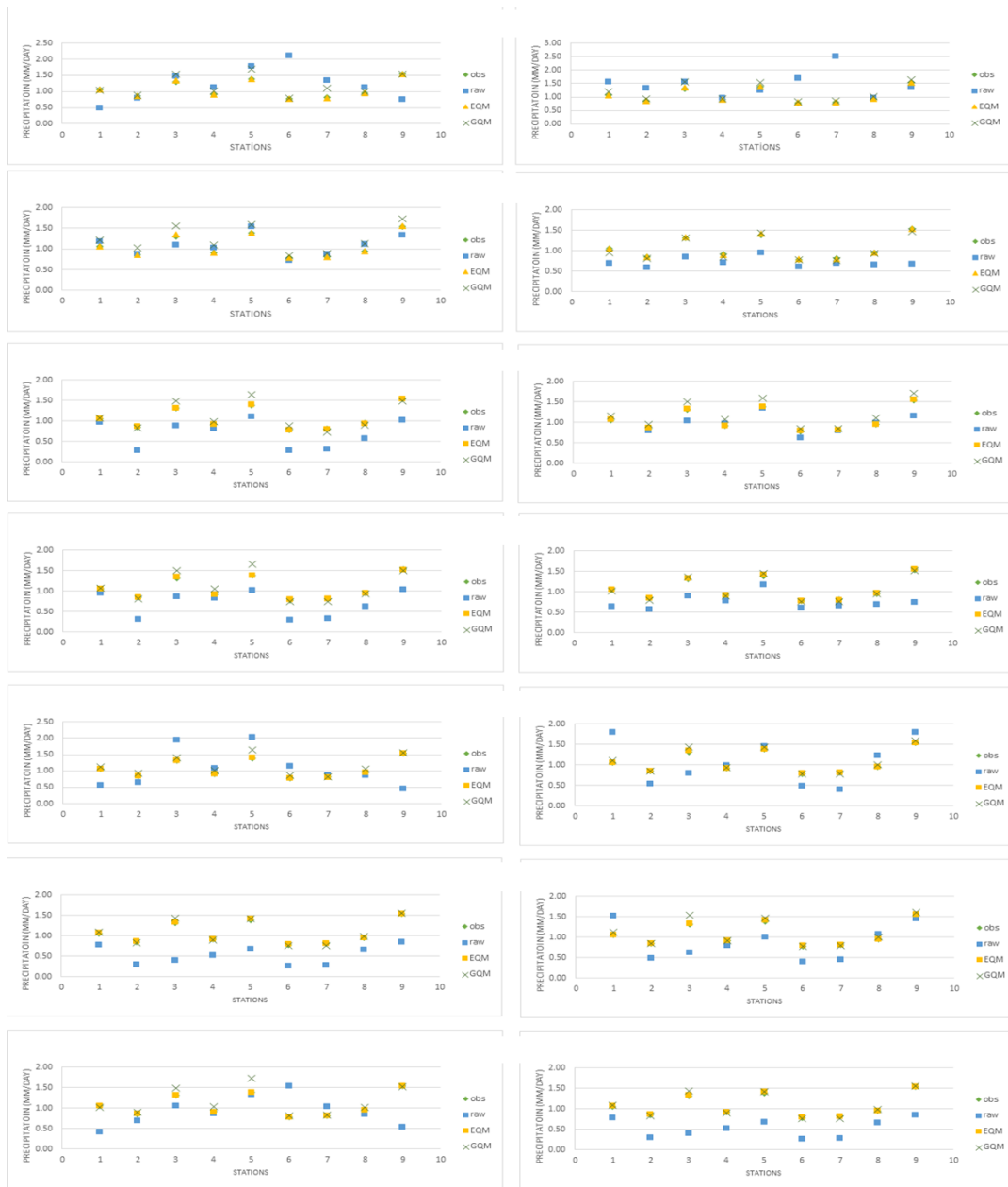
Though not as significant as the changes observed in precipitation means, the standard deviation values also demonstrated noteworthy improvement following the bias correction phase (Table A.1). Improvements were apparent in all stations across all other combinations except Magusa and Karpaz stations for the comb1, Boğaz station for comb2, Lefkoşa station for comb8 and comb13. Furthermore, the average

%bias of the SD for each combination was calculated. The average %bias decreased from the initial range of 25%-53% to a much narrower range of 2%-4%. The detailed results for each RCM-GCM combination are 2%, 3%, 3%, 4%, 2%, 2%, 2%, 4%, 2%, 2%, 3%, 4%, 2%, 3% for the combinations 1-14 respectively.

On the contrary, while the GQM method generally contributed to reducing biases, it did not exhibit the same level of effectiveness as the EQM method. A thorough analysis of the data presented in Table A.2 indicates that the average bias values varied between 4% and 15% following the application of the GQM method. The results for the combinations 1-14 are 11%, 9%, 15%, 4%, 9%, 12%, 8%, 4%, 8%, 4%, 4%, 5%, 8%, 4% respectively. Moreover, GQM method was unable to correct biases in a total of 20 stations across five different GCM-RCM combinations (three stations from Comb2, seven stations from Comb3, six stations from Comb6, one station from Comb7, one station from Comb8, and two stations from Comb13).

Similar to the EQM results, the standard deviation values in this context also exhibited a lesser degree of improvement compared to the precipitation means after undergoing the bias correction process (Table A.2). Upon examining a total of 126 data series for all nine stations across 14 GCM-RCM combinations, 106 series indicated improvement, while 20 series showed a decline. Additionally, %bias of average SD values were calculated for each combination. It is observed that the %bias of the average SD values across 14 combinations decreased from initial range of 25%-53% to the range of 6%-19%.

Based on the results across 14 distinct GCM-RCM combinations against observations, the selection process identified Comb5, Comb6, Comb9, Comb10, and Comb13 as the optimal five combinations that exhibited the closest representation of precipitation data for the Northern Cyprus region. Therefore, these five combinations were used to analyze future projections of this region.



Note: Stations 1-9 are respectively: Boğaz, Lekosa, Girne, Magusa, Karpaz, Güzelyurt, Lefke, İskele, Kantara

Figure 5.2. Comparison of Raw, EQM, GQM, and Observed Data for 14 Combinations

5.3 Trend Analysis of Observed Data

Prior to delving into the analysis of future simulations, the historical observed data was examined using MMK and ITA techniques to explore existing precipitation trends for the years 1978-2015. While examining the MMK approach, the parameters, such as test statistics, p -values and Sen's slope were investigated at 10%, 5%, and, 1% significance level. In the case of the ITA method, the values of trend slope, trend indicator, and the confidence limits (90%, 95%, 99%) were investigated.

5.3.1 Observed Annual Trends

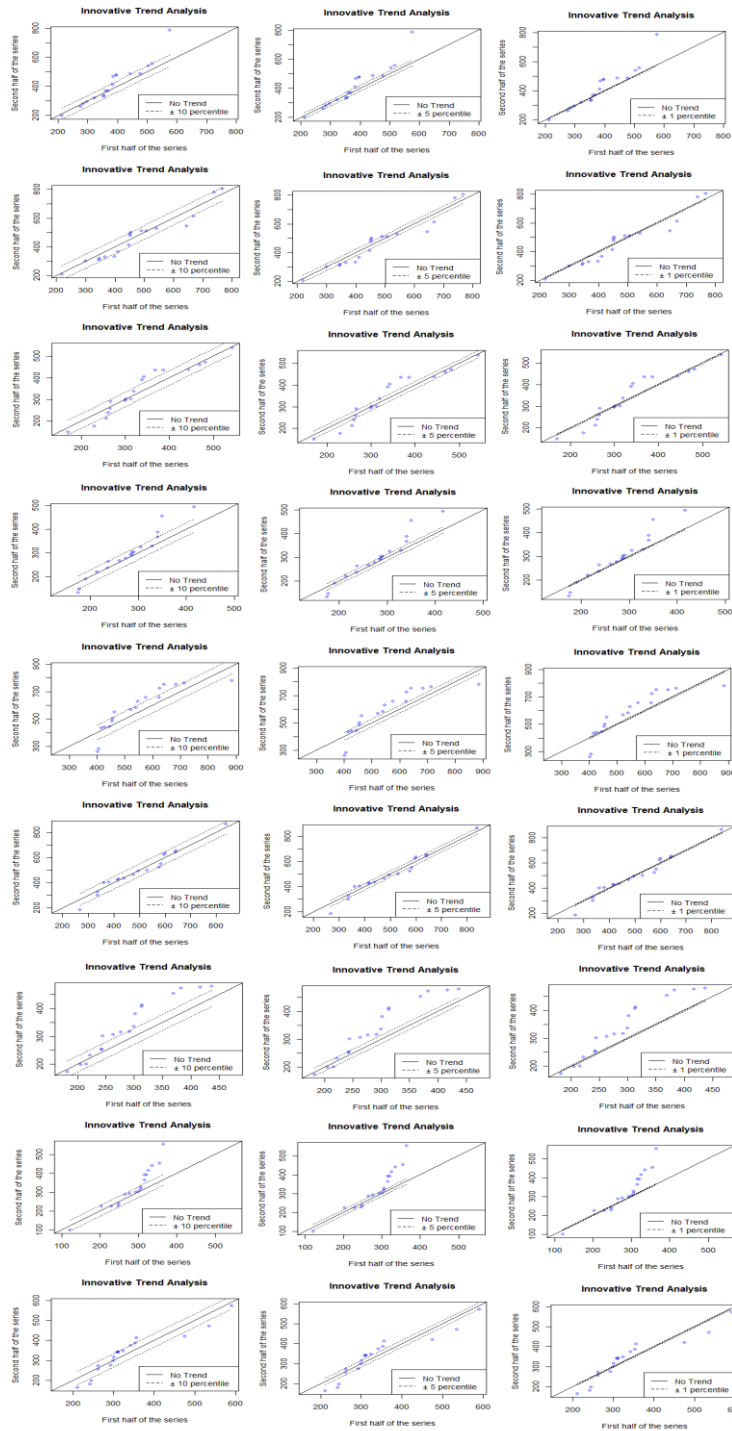
The findings of annual trends are presented in Tables B.1, and B.2 and Figure 5.3. These results revealed that there were divergent variations across various stations when examining annual trends. These disparities were evident not only in the trajectory of the trend but also in its strength. Furthermore, there were discrepancies between the findings of ITA and MMK at certain stations. In accordance with MMK data, upward trends were identified at Boğaz, Güzelyurt, Kantara, Lefke, Lefkoşa, and Magusa stations, whereas a declining trend was evident at Girne, İskele, and Karpaz stations. Conversely, the stations exhibiting an increase according to ITA were Boğaz, İskele, Güzelyurt, Kantara, Lefke, and Lefkoşa, while a descent was noted at Girne, Karpaz, and Magusa stations. MMK identified a very weak trend for Girne, İskele, Karpaz, and Lefkoşa stations, a strong trend for Boğaz station, and a very strong trend for Güzelyurt, Kantara, Lefke, and Magusa stations. On the other hand, ITA discerned a very weak trend for İskele, Karpaz, and Magusa stations, a weak trend for Girne station, a strong trend for Boğaz and Karpaz stations, and a very strong trend for Güzelyurt, Lefke, and Lefkoşa stations. Sen's slope values indicated an increase of 2.2, 1.1, 1.8, 2.4, 1.0, and 1.6 mm/year at Boğaz, Güzelyurt, Kantara, Lefke, Lefkoşa, and Magusa stations, respectively, and a decrease of 0.2, 0.1, and 0.1 mm/year at Girne, İskele, and Karpaz stations, respectively. The outcomes with very weak trend strengths corresponds with the findings of Seyhun and Akıntuğ (2013) [90] and Alpert et al. (2002) [98], who identified statistically

insignificant trends using the Mann-Kendall test for the yearly precipitation data recorded in Cyprus.

It is worth to highlight that the findings from this study in terms of significance and trend directions diverged from those found in the research. As indicated by Onyutha (2016) [99], uncertainties within datasets and statistical methodologies can impact trend analyses in hydrometeorology, leading to varying results. The presence of ties and prolonged patterns within data might challenge the foundational assumptions of nonparametric trend tests, as used in this study, which require time-acquired data to be independent and identically distributed. To mitigate uncertainties associated with data in trend analyses, an extension of the data record length can be employed. Additionally, the choice of trend tests can significantly contribute to uncertainty due to the existence of persistent fluctuations in the series [99]. Consequently, the adoption of multiple trend tests to evaluate the variability in hydrologic variables was considered essential for ensuring heightened reliability within the study.

5.3.2 Observed Seasonal Trends

The outcomes pertaining to the winter season have been presented in Tables B.3 and B.4. From these findings, it becomes apparent that MMK identified a decreasing trend solely in Kantara and Lefkoşa stations, while it recognized an ascending trend in the rest of the stations. Conversely, ITA identified an upward trend across all stations. ITA categorized the trend strength as very weak for Kantara station which is parallel to results obtained by Seyhun and Akıntuğ [90], strong for Girne and Magusa stations, and very strong for Boğaz, İskele, Güzelyurt, Karpaz, Lefke, and Lefkoşa stations. Conversely, MMK ascribed the trend strength as very weak for Girne, İskele, Kantara, Karpaz, and Lefkoşa stations, weak for Güzelyurt and Magusa stations, strong for Lefke station, and very strong for Boğaz station.



Note: Results are given in the order of Boğaz, Girne, İskele, Güzelyurt, Kantara, Karpaz, Lefke, Lefkoşa, and Magusa station.

Figure 5.3. ITA Results for Observation Data at Confidence Limits 90 (Left), 95 (Middle), and 99% (Right).

The results of MMK for the stations Girne, İskele, Kantara, Karpaz and Lefkoşa are in line with Seyhun and Akıntuğ [90] since they also found insignificant trends for the same stations for the winter period. Sen's slope analysis revealed an increase of 2.0, 0.3, 0.2, 0.6, 0.4, 0.9, and 1.0 mm/season for Boğaz, Girne, İskele, Güzelyurt, Karpaz, Lefke, and Magusa stations. It identified a reduction of 0.6 and 0.2 mm/season for Kantara and Lefkoşa stations.

The outcomes pertaining to the spring season have been presented in Tables B.5 and B.6. From these findings, it becomes apparent that MMK identified a decreasing trend solely in Boğaz, Girne Karpaz, and Magusa stations, while it recognized an ascending trend in İskele, Güzelyurt, Kantara, Lefke, and Lefkoşa stations. On the other hand, ITA identified an upward trend in Güzelyurt, Kantara, Karpaz, Lefke, and Lefkoşa stations while it detected a decreasing trend in Boğaz, Girne, İskele, and Magusa stations. Decreasing trends for the stations Girne and İskele and Increasing trends for the station Lefkoşa were also detected by Seyhun and Akıntuğ [90].

The ITA categorized the trend strength as very weak for Güzelyurt station, strong for Karpaz and Magusa stations, and very strong for Boğaz, Girne, İskele, Kantara, Lefke, and Lefkoşa stations. Conversely, MMK ascribed the trend strength as very weak for Girne, İskele, Kantara, Karpaz, and Lefkoşa stations, weak for Boğaz, İskele, Güzelyurt, Karpaz, Lefkoşa, and Magusa stations, very strong for Girne, Kantara, and Lefke stations. Sen's slope analysis revealed an increase of 0.1, 0.3, 0.8, 0.6, and 0.4 mm/season for İskele, Güzelyurt, and Kantara stations. It identified a reduction of 0.2, 0.8, 0.2, and 0.1 mm/season for Boğaz, Girne, Karpaz, and Magusa stations. Results of MMK for the stations Girne, İskele, Kantara, Karpaz, and Lefkoşa and Results of ITA for the stations Güzelyurt are in line with Hilal et al. [100]in terms of strength of the trend.

The results corresponding to the Autumn season have been given within Tables B.7 and B.8. From these findings, it emerges that MMK detected a declining trend in İskele, Güzelyurt, and Karpaz stations, while it acknowledged an ascending trend in Boğaz, Girne, Kantara, Lefke, Lefkoşa, and Magusa stations. Conversely, ITA

identified an upward trend in Boğaz, Lefke, Lefkoşa, and Magusa stations, but it detected a decrease in Girne, İskele, Güzelyurt, Kantara, and Karpaz stations. Results of MMK for the stations Boğaz, Girne, Kantara, Lefke, Lefkoşa, and Magusa and results of ITA for the stations Boğaz, Lefke, Lefkoşa, and Magusa are showing similarities with the findings of Seyhun and Akıntuğ [90].

ITA classified the trend strength as very weak for İskele, Kantara, and Lefkoşa stations, weak for Boğaz and Magusa stations, strong for Girne and Güzelyurt stations, and very strong for Karpaz and Lefke stations. On the contrary, MMK attributed the trend strength as very weak for Boğaz, Girne, İskele, Güzelyurt, and Kantara stations, weak for Lefkoşa station, strong for Karpaz and Magusa stations, and very strong for Girne station. Sen's slope analysis unveiled an increase of 0.3, 0.3, 0.1, 0.8, 0.3, and 0.4 mm/season for Boğaz, Girne, Kantara, Lefke, Lefkoşa, and Magusa stations, respectively. It identified a reduction of 0.1, 0.1, and 1.0 mm/season respectively for İskele, Güzelyurt, and Karpaz stations. The results of MMK for the stations Boğaz, Girne, İskele, Güzelyurti, Kantara, and Lefkoşa and Results of ITA for the stations İskele, Kantara, Lefkoşa, Boğaz, and Magusa are in line with Hilal et al. [100] in terms of strength of the trend since they detected no trend in these stations.

5.4 Trend Analysis of Future Simulations

As detailed in Section 5.1, the first step in assessing future simulations was to subject the top-performing five GCM-RCM combinations to EQM-based bias correction. Following that, the bias corrected datasets were combined into a uniform multi-mean ensemble dataset by averaging. Subsequently, this dataset was partitioned into two distinct time frames: the near future (2024-2062) and the far-future (2063-2100). Employing the ITA and MMK methodologies, each timeframe was analyzed for nine different stations within the context of two distinct climate scenarios of RCP4.5 and RCP8.5, with the objective of assessing the prevailing trends in precipitation. Each era was examined using the ITA and MMK techniques, which included the study of two unique climatic scenarios to examine the prevalent precipitation patterns.

Throughout this assessment, annual and seasonal analyses, except summer season, were conducted.

5.4.1 Trend Analysis Results of RCP4.5 Scenario Simulation

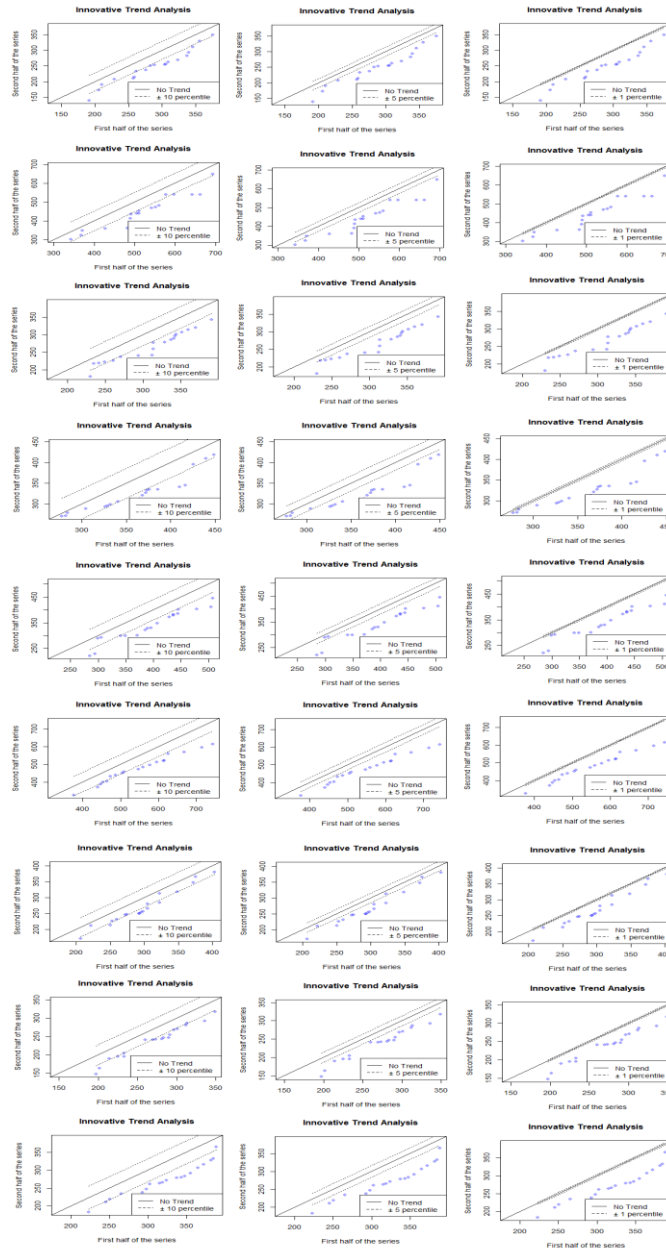
5.4.1.1 Investigation of trends for near future

The results of the annual trends for the near future are given in Tables B.9 and B.10 and Figure 5.4. The findings suggested that the MMK has observed a very strong declining trend consistently present at all stations. When considering the values of Sen's slope, the recorded precipitation levels for Boğaz, Girne, İskele, Güzelyurt, Kantara, Karpaz, Lefke, Lefkoşa, and Magusa stations were found to be 2.1, 3.1, 2.3, 1.4, 3.2, 4.2, 1.6, 1.6, and 2.5 mm/year in a decreasing manner, correspondingly. Furthermore, upon close examination of the outcomes derived through ITA, it was evident that they aligned with the MMK findings, revealing a very strong decreasing trend across all stations. These findings are in agreement with the results of Philandras et al. [101], which detected decrease in long term precipitation trends up to 30% for several countries located in eastern Mediterranean region.

When examining the seasonal variations for the near future, similar to the annual results, both MMK and ITA techniques identified declining trends in precipitation across all stations. However, in contrast to the yearly evaluations, during the spring season, ITA identified a trend that was noticeably weak at the Boğaz station, but MMK reported trends of variable intensities across several stations for both the spring and autumn seasons.

Both MMK and ITA has underscored a very strong decreasing trend across all stations in winter season, as given in Tables B.11 and B.12. Upon analyzing simulations encompassing the winter period using the MMK approach, the recorded decreases were 1.0, 2.1, 1.2, 0.7, 1.3, 2.6, 0.6, 0.6, and 1.4 mm/season at Boğaz,

Girne, İskele, Güzelyurt, Kantara, Karpaz, Lefke, Lefkoşa, and Magusa stations, respectively.



Note: Results are given in the order of Boğaz, Girne, İskele, Güzelyurt, Kantara, Karpaz, Lefke, Lefkoşa, and Magusa station.

Figure 5.4. ITA Results for RCP4.5 Near-Future Annual Dataset at Confidence Limits 90 (Left), 95 (Middle), and 99% (Right).

During the spring season, as given in Tables B.13 and B.14, both techniques has indicated downward trends, however, variations emerged in the significance of these trends. While ITA identified very strong trends across all stations, except Boğaz station, MMK identified trends of varying strengths. It detected very weak trends for Boğaz, Girne, Lefke, and Lefkoşa stations, weak trend for Güzelyurt station, strong trend for İskele station, and very strong trends for Kantara, Karpaz, and Magusa stations. When analyzing the magnitudes of trends in precipitation totals through Sen's slope, the findings unveiled reductions of 0.1, 0.3, 0.5, 0.2, 0.6, 0.9, 0.2, 0.2, and 0.4 mm/season Boğaz, Girne, İskele, Güzelyurt, Kantara, Karpaz, Lefke, Lefkoşa, and Magusa stations, respectively.

The trend results for the autumn season are given in Tables B.15 and B.16. According to these, ITA has identified a very strong downward trend for all stations, while MMK depicted weak trends for Girne and İskele stations, strong trends for Boğaz and Güzelyurt stations, and very strong decreasing trends for Kantara, Karpaz, Lefke, Lefkoşa, and Magusa stations. Furthermore, as indicated by the outcomes derived from Sen's slope estimator, reductions ranging from 0.2 to 0.7 mm/season were observed. The results of the seasonal analysis are in line with the findings of Gainnakopoulos et al. (2010) since they also detected 6-18% of decrease in precipitation for the near future period in Cyprus [76].

5.4.1.2 Investigation of trends for far future

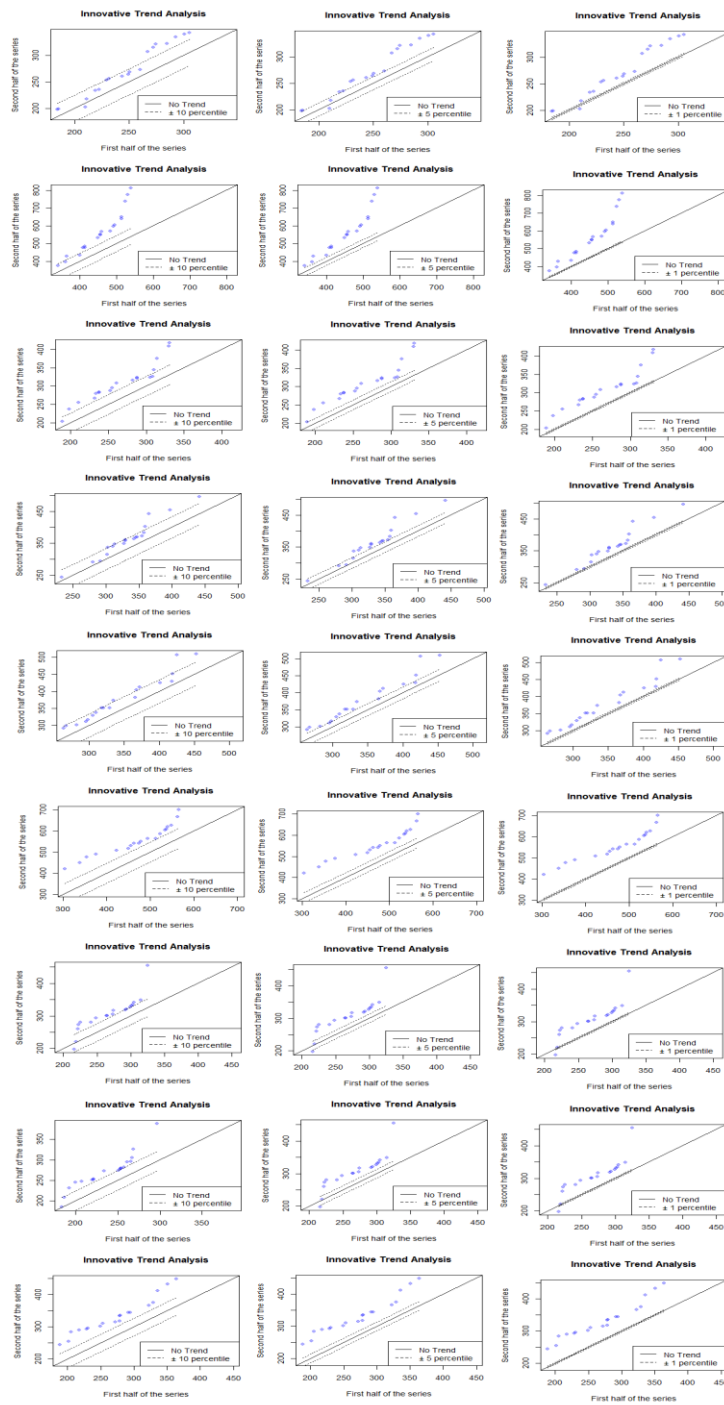
Examining the annual trend results given in Tables B.17, B.18 and Figure 5.5, it becomes evident that an upward trend was observed through both trend tests. Nonetheless, the variations detected in the significance of the existing trends. ITA identified very strong upward trends across all stations, whereas MMK pointed to a weak trend for Kantara, strong trend for Boğaz, and very strong increase sing trends for Girne, İskele, Güzelyurt, Karpaz, Lefke, Lefkoşa, and Magusa stations. When examining Sen's slope values, the increase in precipitation levels at Boğaz, Girne,

İskele, Güzelyurt, Kantara, Karpaz, Lefke, Lefkoşa, and Magusa stations were calculated as 0.9, 5.7, 1.3, 1.4, 0.7, 3.9, 1.7, 1.4, and 2.7 mm/year, respectively.

Upon reviewing the outcomes of the winter season analysis stated in Tables B.19 and B.20, it is apparent that both MMK and ITA have identified a very strong increasing trend across all stations. Additionally, delving into Sen's slope values, it becomes evident that an increase in precipitation levels was observed with increments of 1.5, 5.3, 1.3, 1.2, 1.5, 2.8, 1.0, 1.3, and 1.9 mm/season recorded at Boğaz, Girne, İskele, Güzelyurt, Kantara, Karpaz, Lefke, Lefkoşa, and Magusa stations, respectively. The results of annual and winter precipitation are in a good agreement with the findings of Lelieveld et al. [102].

For the spring season, while both MMK and ITA methods exhibited conformity in terms of identifying the same directional results (increase or decrease) at the corresponding stations, discrepancies raised regarding the significance of these trends (Tables B.21 and B.22). Through the application of both MMK and ITA analyses, decreasing trends were identified at Boğaz, İskele, Kantara, and Magusa stations, whereas ascending trends were discerned for Girne, Güzelyurt, Karpaz, Lefke, and Lefkoşa stations. The MMK classified the strength of trends as very weak for Boğaz, Girne, İskele, and Magusa stations; weak for Kantara and Lefkoşa stations; strong for Güzelyurt and Karpaz stations; and very strong for Lefke station. In response, ITA evaluated the trend strengths as very weak for Girne, İskele, Güzelyurt, Karpaz, and Magusa stations, weak for Lefkoşa station, and very strong for Boğaz, Kantara, and Lefke stations. When assessing the acquired Sen's slope measurements, a reduction in precipitation levels of 0.1, 0.1, 0.4, and 0.1 mm/season was detected at the Boğaz, İskele, Kantara, and Magusa stations, correspondingly. Conversely, a rise of 0.2, 0.3, 0.4, 0.5, and 0.3 mm/season was observed in Girne, Güzelyurt, Karpaz, Lefke, and Lefkoşa stations, respectively.

Examining the outcomes for the autumn season shown in Table B.23 and B.24, similar directional trends were identified for the same stations in both methodologies, resembling the spring season.



Note: Results are given in the order of Boğaz, Girne, İskele, Güzelyurt, Kantara, Karpaz, Lefke, Lefkoşa, and Magusa station.

Figure 5.5. ITA Results for RCP4.5 Far-Future Annual Dataset at Confidence Limits 90 (left), 95 (Middle), and 99% (Right).

However, the disparities emerged in terms of trend significance. Following analyses conducted through MMK and ITA, downward trends were discerned at Boğaz, Kantara, and Lefkoşa stations, whereas upward trends were observed at Girne, İskele, Güzelyurt, Karpaz, Lefke, and Magusa stations. The MMK classified the trend significance as very weak for Girne, İskele, Güzelyurt, Karpaz, Lefke, Lefkoşa, and Magusa stations, very strong for Boğaz and Kantara stations. Conversely, ITA assessed trend strengths as very weak for Lefkoşa station, very strong for Boğaz, Girne, İskele, Güzelyurt, Kantara, Karpaz, and Magusa stations. In terms of the extracted Sen's slope measurements, the reductions of 0.6, 0.9, and 0.2 mm/season were identified at Boğaz, Kantara, and Lefkoşa stations, respectively. On the other hand, increments of 0.5, 0.2, 0.1, 0.6, and 0.2 mm/season were noted at Girne, İskele, Güzelyurt, Karpaz, Lefke, and Magusa stations, respectively. The results of spring season for the stations Boğaz, İskele, Kantara, and Magusa and the results of autumn season for the stations Boğaz, Kantara, and Lefkoşa are parallel to the outcomes of Hadjinicolaou et al. [103] since they also projected a slight decrease in precipitation for the second half of the century. In addition, the results of the remaining stations align with the findings of Todaro et al. [70], which stated that slight increase in precipitation is expected for some of the countries located in eastern parts of the Mediterranean region.

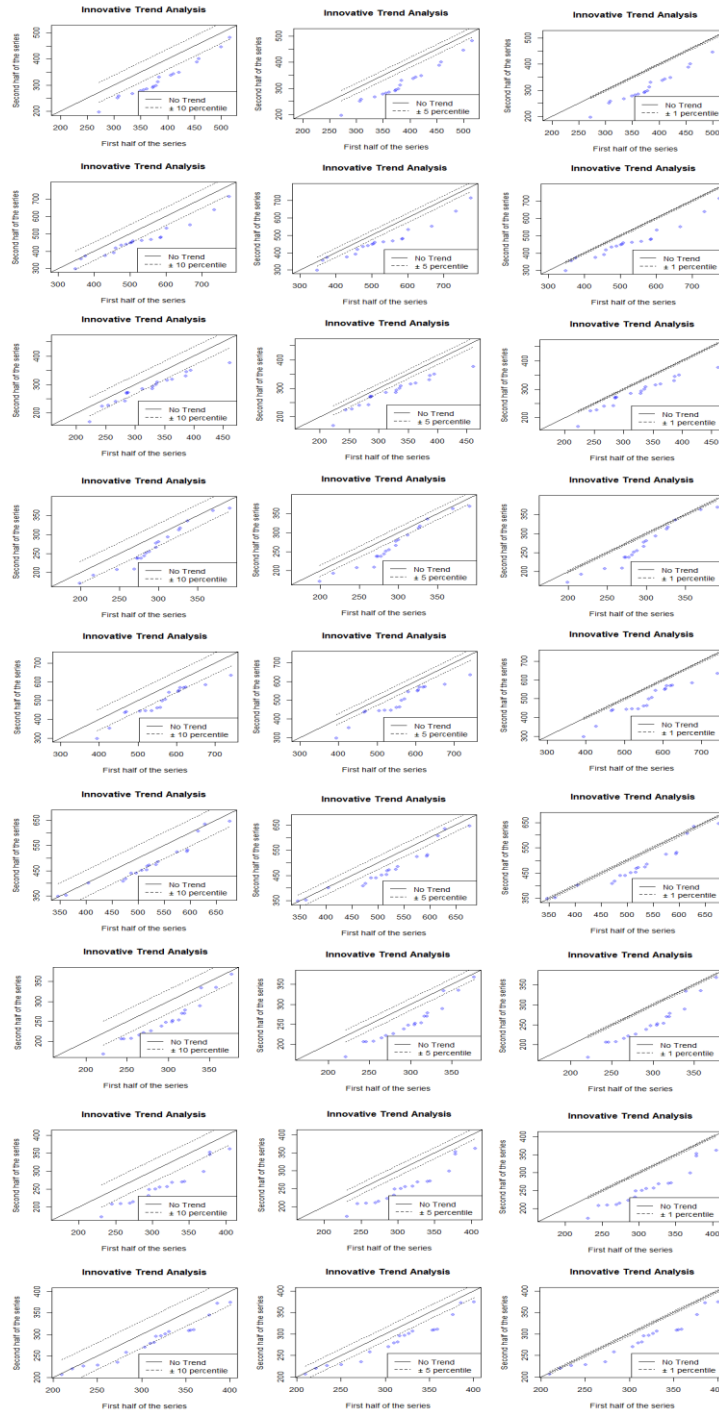
5.4.2 Trend Analysis Results of RCP8.5 Scenario Simulation

5.4.2.1 Investigation of trends for near future

Upon reviewing the findings related to annual trends shown in Tables B.25, B.26, and Figure 5.6, it becomes evident that MMK and ITA outcomes exhibited alignment both in terms of the directional trend and its significance. According to results yielded by both trend tests, very strong decreasing trends were observed across all stations. The Sen's slope analysis resulted as reductions of 2.3, 3.1, 1.4, 1.3, 2.2, 1.9, 2.1, 2.3, and 1.1 mm/year at Boğaz, Girne, İskele, Güzelyurt, Kantara, Karpaz, Lefke, Nicosia, and Magusa stations, respectively.

During the winter season, although both methodologies displayed consistency in identifying the same directional trends for the stations, the discrepancies emerged regarding the significance of these trends (Tables B.27 and B.28). Following assessments undertaken using both MMK and ITA, a declining trend was established for each station. In this context, the MMK categorized trends as very weak for Boğaz, Girne, and Karpaz stations, weak for Güzelyurt station, strong for Kantara station, and very strong for İskele, Lefke, Lefkoşa, and Magusa stations. Conversely, ITA categorized trend strengths as very weak for Girne station, strong for Güzelyurt station, and very strong for Boğaz, İskele, Kantara, Karpaz, Lefke, Lefkoşa, and Magusa stations. Upon close examination of the computed Sen's slope values, it is observable that the quantities of precipitation showcase a decline of 0.2, 0.4, 0.5, 0.6, 0.6, 0.1, 0.4, 0.5, and 0.6 mm/season at Boğaz, Girne, İskele, Güzelyurt, Kantara, Karpaz, Lefke, Nicosia, and Magusa stations, correspondingly.

For the spring season, similar to the winter season, MMK and ITA found the same results for the same stations in terms of the direction of the trend, once again the results they found in terms of the strength of these trends differed (Tables B.29 and B.30). As a result of the analyzes made with MMK and ITA, decreasing trends were determined for Boğaz, Girne, İskele, Güzelyurt, Kantara, Lefke and Lefkoşa stations. On the other hand, increasing trends were detected for Karpaz and Magusa stations. MMK determined the trend significance as very weak for İskele, Karpaz and Magusa stations, weak for Girne station, strong for Kantara station, and very strong for Boğaz, Güzelyurt, Lefke, and Lefkoşa stations. On the other hand, according to the ITA method, a very weak trend was detected in Girne station, while very strong trends were detected in all the remaining stations. Considering the obtained Sen's slope values, a decrease was detected in the amount of precipitation as 0.7, 0.3, 0.2, 0.3, 0.6, 0.7, and 0.8 mm/season, respectively, at Boğaz, Girne, İskele, Güzelyurt, Kantara, Lefke, and Lefkoşa stations. However, an increase of 0.1 and 0.1 mm/season was detected at Karpaz and Magusa stations.



Note: Results are given in the order of Boğaz, Girne, İskele, Güzelyurt, Kantara, Karpaz, Lefke, Lefkoşa, and Magusa station.

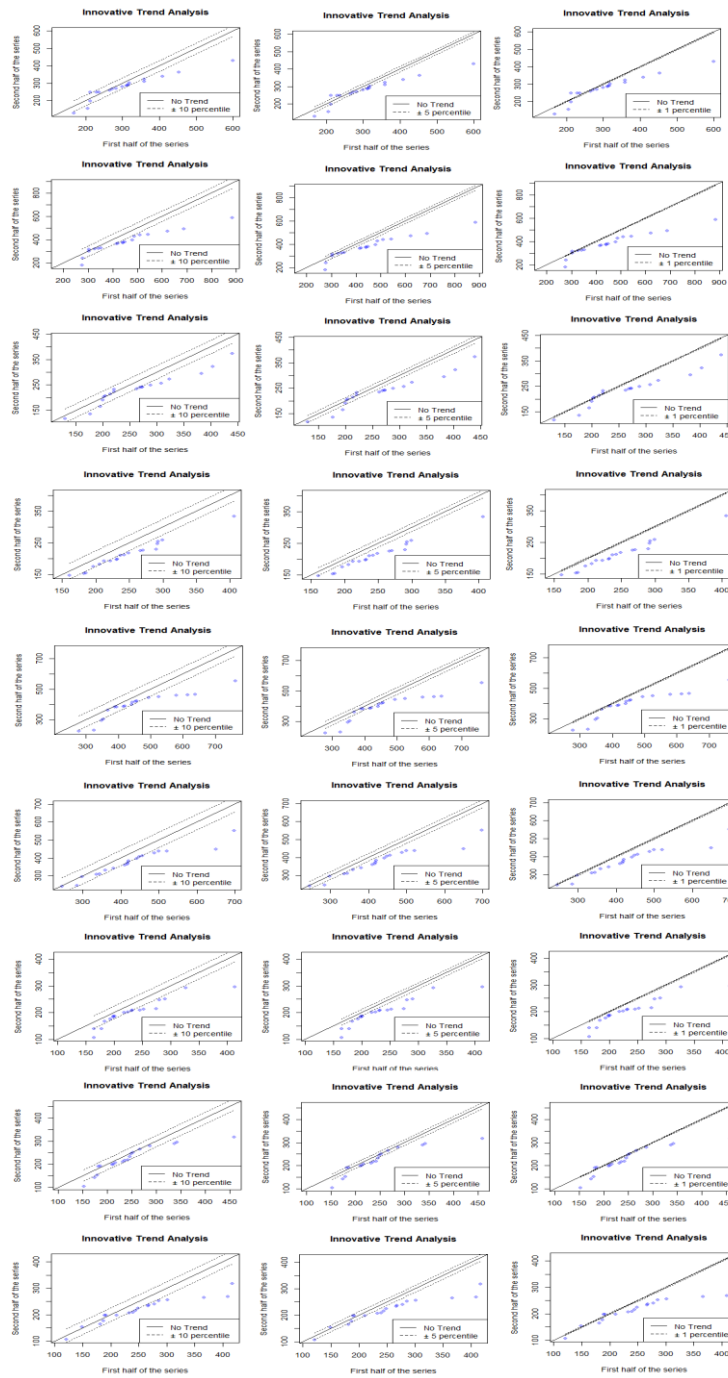
Figure 5.6. ITA Results for RCP8.5 Near-Future Annual Dataset at Confidence Limits 90 (Left), 95 (Middle), and 99% (Right).

Upon reviewing the outcomes of the autumn season given in Tables B.31 and B.32, an apparent congruence was observed in the findings of both methodologies. The analyses conducted using both MMK and ITA techniques consistently identified very strong decreasing trends across all stations. The Sen's slope values correspondingly align with this trend, marking a decline in precipitation amounts of ranging from 0.6 to 1.8 mm/season. The results obtained for the annual and seasonal precipitation totals are in a good alignment with the findings of Giannakopoulos et al. [76], and Babaousmail et al. [104] since a decreasing trend detected in almost all the stations and the strength of the trends are generally strong with a few exceptions.

5.4.2.2 Investigation of trends for far future

Examining the results pertaining to annual trends stated in Tables B.33 and B.34, and Figure 5.7, it is evident that the MMK and ITA results showed consistency in both the direction and significance of the trend. The findings from both tests demonstrated very strong decreasing trends across all stations. The Sen's slope analysis indicated a reduction of 1.6, 3.2, 1.4, 2.0, 2.3, 2.9, 1.5, 1.1, and 1.4 mm/year at the stations of Boğaz, Girne, İskele, Güzelyurt, Kantara, Karpaz, Lefke, Lefkoşa, and Magusa, respectively.

In relation to the analysis of the winter season given in Tables B.35 and B.36, both ITA and MMK indicated declining patterns across all stations. The MMK displayed strong trends for Boğaz, Girne, and Magusa stations, while it identified very strong trends for İskele, Güzelyurt, Kantara, Karpaz, Lefke, and Magusa stations. On the other hand, ITA determined very strong downward trends for all stations. In addition, based on the outcomes from the Sen's slope analysis, a reduction in precipitation was identified with rates of 1.1, 1.9, 0.9, 0.9, 1.8, 2.4, 0.9, 1.0, and 1.2 mm/season for Boğaz, Girne, İskele, Güzelyurt, Kantara, Karpaz, Lefke, Lefkoşa, and Magusa stations, respectively.



Note: Results are given in the order of Boğaz, Girne, İskele, Güzelyurt, Kantara, Karpaz, Lefke, Lefkoşa, and Magusa station.

Figure 5.7. ITA Results for RCP8.5 Far-Future Annual Dataset at Confidence Limits 90 (Left), 95 (Middle), and 99% (Right)

During the spring season, both analysis techniques exhibited a downward trend for each station (Tables B.37 and B.38). Parallel to the winter season findings, ITA identified very strong trends across all stations, while MMK indicated very weak trends for İskele, Lefke, and Lefkoşa stations, a weak trend for Boğaz station, a strong trend for Karpaz station, and very strong trends for Girne, Güzelyurt, Kantara, and Magusa stations. This was concluded based on the Sen's slope values, which also confirmed a decline in precipitation levels with rates ranging from 0.1 to 0.6 mm/season. Annual and seasonal findings for winter and spring seasons are parallel to the studies of Giannakopoulos et al. [76] and Philandras et al. [101] in terms of the direction of the trend and its Sen's slope analysis.

During the autumn season given in Tables B.39 and B.40, in contrast to the preceding two seasons, a distinctive pattern emerged where both decreasing and increasing trends were identified across certain stations. The MMK test showed upward trends for İskele, Lefkoşa, and Magusa stations, while indicating declining trends for Boğaz, Girne, Güzelyurt, Kantara, Karpaz, and Lefke stations. Meanwhile, ITA method largely agreed with MMK regarding the trend direction for these same stations, but it detected a rising trend at Kantara station, diverging from MMK. According to the MMK approach, it indicated very weak trends for Girne, İskele, Kantara, Lefkoşa, and Magusa stations, and very strong trends at Boğaz, Güzelyurt, Karpaz, and Lefke stations. Conversely, ITA revealed very weak trends for Boğaz, Girne, and Karpaz stations, strong trends for Kantara and Lefkoşa stations, and very strong trends for İskele, Güzelyurt, Lefke, and Magusa stations. In terms of Sen's slope values, a decrease was observed at Boğaz, Girne, Güzelyurt, Kantara, Karpaz, and Lefke stations, amounting to 0.6, 0.3, 0.5, 0.1, 0.8, and 0.5 mm/season, respectively. On the other hand, a minor increase of 0.1 mm/season was noticed at İskele, Lefkoşa, and Magusa stations. Findings for the stations İskele, Lefkoşa and Magusa are in line with the studies of Babaoumail et al. [133] and Lelieveld et al. [102] since they also detected slightly increasing precipitation for the second half of the century for some regions in Eastern Mediterranean. In addition, the results of the remaining stations are also in an agreement with Philandras et al. [101] and

Giannakopoulos et al. [76], where amounts of precipitation are projected to decrease significantly for eastern Mediterranean and Cyprus respectively.

CHAPTER 6

CONCLUSIONS AND RECOMMENDATIONS

6.1 Summary and Conclusions

There are some expected changes in the usual weather patterns of the Eastern Mediterranean due to the changing climate conditions of the region. They could reveal themselves either as an increase in the temperature which might result in a drought or as an increase in evaporation rates resulting in extreme rainfalls and floods. This region is already familiar with such extreme weather events, and due to its diversity, effects of these events are not proportional. In this study, the main focus was put on the Northern Cyprus region. The possible effects of climate change on precipitation which could be experienced in the future were examined. For that manner, several climate models were used to make projections on future events under different scenarios. To thoroughly investigate the alterations in precipitation trends throughout the island, our study encompasses a selection of nine strategically positioned precipitation stations: Girne, Lefkoşa, Magusa, Karpaz, Boğaz, İskele, Güzelyurt, Kantara, and Lefke. Observational data were sourced from the Meteorological office in Northern Cyprus, while model simulations encompassing historical and future periods were obtained from the EURO-CORDEX database.

In this study, the datasets from EURO-CORDEX structure for 14 different GCM-RCM combinations were adopted. All datasets were based on daily precipitation values. As stated earlier, both GCM and downscaled RCM simulations had biases that needed to be evaluated to address any existing bias and to correct them. In this regard, to evaluate the accuracy of various EURO-CORDEX climate models over Northern Cyprus in predicting historical precipitation records the period spanning from 1978 to 2005 was selected as a mutual timeframe for comparing historical

observed and model data. This facilitated the identification of potential biases in these models. Subsequently, the bias correction methods were applied, and the identical time interval from 1978 to 2005 was selected to ensure the assessment of the bias correction technique's reliability. In this context, two commonly used bias correction methods, EQM and GQM, and their results were compared against each other to assess the effectiveness of two commonly employed bias correction techniques for our study region in enhancing the quality of projected data series for all selected stations, using observed data as a basis. The results suggested that that EQM performed superior than GQM for this study area and the correction of biases for the projected data was carried out by using EQM method.

Subsequently, to explore the local changes in precipitation for observed data across annual and seasonal timeframes an examination of historical observed data took place to ascertain the precipitation trends in the region spanning from the past to the present. During this analysis, three distinct aspects were assessed, which are the direction, significance, and the magnitude of the trend. This investigation was performed by utilizing the methods of Modified Mann-Kendall Trend Test and Innovative Trend Analysis, and Sen's Slope Estimator. Overall, the trend analysis of data from the past and present timeframes revealed a mixed pattern in station trends. While certain stations exhibited decreasing trends, others displayed an upward trend. It is noteworthy that the downward trends tended to be either very weak or weak in strength. On the contrary, stations experiencing an increase demonstrated strong and even very strong trends.

Moreover, to analyze alterations in precipitation patterns under two distinct emission pathways for future projections, the most effective five GCM-RCM combinations were determined, and more effective bias correction method of EQM was applied to future simulations to fix biases in future datasets as well for two different future sub-periods of near and far future taking two different scenarios as a reference, RCP4.5 and RCP8.5. Following that, the precipitation trends were subjected to separate analyses for each climate scenario to ensure the consistent assessment of the three aforementioned aspects across the distinct time periods. As a general result of the

analysis, in both climate scenarios all three trend tests (MMK, ITA, and Sen's slope estimator) estimated decreasing trends for near future (2024-2062) on both annual and seasonal basis. For the far-future (2063-2100) trend tests detected an overall increasing trend in RCP4.5 scenario on both annual and seasonal levels. The stations that showed decreasing trends were only a few with a very low significance. However, for the RCP8.5 scenario all trend tests showed a decreasing trend on annual, winter season, and spring season analyses. For the autumn season, although the general agreement of the trend tests for a decreasing trend, there were also few stations detected with an increasing trend. However, their strength was generally found to be very weak or weak. It can be seen that except the RCP4.5 far future analysis, there is a decrease in precipitation rates is expected for the Northern part of the Cyprus. Although this decreasing trend is more evident on annual level, it also shows itself on seasonal level as well. Given this observation, the local authorities are urged to adopt necessary precautions and accord significance to analogous investigations, aiming to enhance their insights into this matter. It is worth noting that the anticipation of future climate change impacts on precipitation patterns and their subsequent effects on national water resources holds significant importance in ensuring the sustainable development of the country.

6.2 Recommendations for Future Studies

Examining forthcoming patterns in precipitation holds significance in comprehending the potential repercussions of climate change on diverse geographical areas. To undertake an all-encompassing analysis of precipitation trends, it would be prudent to contemplate the subsequent suggestions:

- Gathering high-quality precipitation data from sources, such as satellites and various climatic models allows for comparison and testing to ensure the consistency of the findings.

- Examining data at local, regional, and global scales facilitates comprehension of both local variations and larger trends, providing insights into short and long-term temporal patterns.
- Climate simulations to predict precipitation trends based on different emission scenarios can be analyzed to discuss forthcoming alterations in precipitation patterns in a detailed manner, aiding decision-makers and researchers in preparing for and adapting to potential shifts in the climate.
- The variation of extreme precipitation events can be studied based on climate models, which can inform more effective strategies for managing the impacts of intense precipitation events and contribute to improved disaster preparedness and resilience measures.
- It is crucial to carry out an extensive hydrologic research in order to build a link between future projections and the nation's water supplies. Thus, it may be useful in developing water management plans, ensuring sustainable resource use, and addressing possible problems due to the changes in precipitation patterns.

REFERENCES

- [1] National Oceanic and Atmospheric Administration, “Carbon dioxide now more than 50% higher than pre-industrial levels,” Jun. 03, 2022. <https://www.noaa.gov/news-release/carbon-dioxide-now-more-than-50-higher-than-pre-industrial-levels> (accessed Aug. 03, 2023).
- [2] United States Environmental Protection Agency, “Global Greenhouse Gas Emissions Data,” Jan. 12, 2016. <https://www.epa.gov/ghgemissions/global-greenhouse-gas-emissions-data> (accessed Aug. 03, 2023).
- [3] F. Giorgi and P. Lionello, “Climate change projections for the Mediterranean region,” *Glob Planet Change*, vol. 63, no. 2–3, pp. 90–104, Sep. 2008, doi: 10.1016/j.gloplacha.2007.09.005.
- [4] C. Torma, F. Giorgi, and E. Coppola, “Added value of regional climate modeling over areas characterized by complex terrain—Precipitation over the Alps,” *Journal of Geophysical Research: Atmospheres*, vol. 120, no. 9, pp. 3957–3972, May 2015, doi: 10.1002/2014JD022781.
- [5] C. Giannakopoulos, P. Hadjinicolaou, E. Kostopoulou, K. V. Varotsos, and C. Zerefos, “Precipitation and temperature regime over Cyprus as a result of global climate change,” *Advances in Geosciences*, vol. 23, pp. 17–24, Feb. 2010, doi: 10.5194/adgeo-23-17-2010.
- [6] Elias Giannakis, Despina Serghides, Stella Dimitriou, and George Zittis, “Land transport CO2 emissions and climate change: evidence from Cyprus,” 2020, Accessed: Aug. 04, 2023. [Online]. Available: <https://www.tandfonline.com/doi/full/10.1080/14786451.2020.1743704>
- [7] “Annex VII: Glossary,” in *Climate Change 2021 – The Physical Science Basis*, Cambridge University Press, 2023, pp. 2215–2256. doi: 10.1017/9781009157896.022.

- [8] T. S. Ledley, E. T. Sundquist, S. E. Schwartz, D. K. Hall, J. D. Fellows, and T. L. Killeen, “Climate change and greenhouse gases,” *Eos, Transactions American Geophysical Union*, vol. 80, no. 39, pp. 453–458, Sep. 1999, doi: 10.1029/99EO00325.
- [9] Maarten K. van Aalst, “The impacts of climate change on the risk of natural disasters,” May 2006.
- [10] M. Lynas, B. Z. Houlton, and S. Perry, “Greater than 99% consensus on human caused climate change in the peer-reviewed scientific literature,” *Environmental Research Letters*, vol. 16, no. 11, p. 114005, Oct. 2021, doi: 10.1088/1748-9326/ac2966.
- [11] “Greenhouse Gases.” <https://www.twinkl.pl/teaching-wiki/greenhouse-gases> (accessed Aug. 04, 2023).
- [12] NASA, “World of Change: Global Temperatures,” 2023.
- [13] “AR5 Synthesis Report: Climate Change 2014 — IPCC.” <https://www.ipcc.ch/report/ar5/syr/> (accessed Aug. 04, 2023).
- [14] “Topic 2: Future changes, risks and impacts — IPCC.” https://ar5-syr.ipcc.ch/topic_futurechanges.php (accessed Aug. 04, 2023).
- [15] N. Lana-Renault, E. Morán-Tejeda, M. Moreno de las Heras, J. Lorenzo-Lacruz, and N. López-Moreno, “Land-use change and impacts,” *Water Resources in the Mediterranean Region*, pp. 257–296, Jan. 2020, doi: 10.1016/B978-0-12-818086-0.00010-8.
- [16] F. Giorgi, “Climate change hot-spots,” *Geophys Res Lett*, vol. 33, no. 8, p. 8707, Apr. 2006, doi: 10.1029/2006GL025734.
- [17] D. Jacob *et al.*, “EURO-CORDEX: New high-resolution climate change projections for European impact research,” *Reg Environ Change*, vol. 14, no. 2, pp. 563–578, Jul. 2014, doi: 10.1007/S10113-013-0499-2/FIGURES/8.

- [18] S. M. Vicente-Serrano *et al.*, “Evidence of increasing drought severity caused by temperature rise in southern Europe,” *Environmental Research Letters*, vol. 9, no. 4, p. 044001, Apr. 2014, doi: 10.1088/1748-9326/9/4/044001.
- [19] C.-F. Schleussner *et al.*, “Differential climate impacts for policy-relevant limits to global warming: the case of 1.5 °C and 2 °C,” *Earth System Dynamics*, vol. 7, no. 2, pp. 327–351, Apr. 2016, doi: 10.5194/esd-7-327-2016.
- [20] “Environmental science, data, and analysis of the highest quality Independent, non-governmental, and open-source. - Berkeley Earth.” <https://berkeleyearth.org/> (accessed Aug. 04, 2023).
- [21] “Homepage - MedECC.” <https://www.medecc.org/> (accessed Aug. 04, 2023).
- [22] K. E. Taylor, R. J. Stouffer, and G. A. Meehl, “An Overview of CMIP5 and the Experiment Design,” *Bull Am Meteorol Soc*, vol. 93, no. 4, pp. 485–498, Apr. 2012, doi: 10.1175/BAMS-D-11-00094.1.
- [23] R. L. Wilby *et al.*, “A review of climate risk information for adaptation and development planning,” *International Journal of Climatology*, vol. 29, no. 9, pp. 1193–1215, Jul. 2009, doi: 10.1002/joc.1839.
- [24] J. Chen, F. P. Brissette, D. Chaumont, and M. Braun, “Finding appropriate bias correction methods in downscaling precipitation for hydrologic impact studies over North America,” *Water Resour Res*, vol. 49, no. 7, pp. 4187–4205, Jul. 2013, doi: 10.1002/wrcr.20331.
- [25] U. Ghimire, G. Srinivasan, and A. Agarwal, “Assessment of rainfall bias correction techniques for improved hydrological simulation,” *International Journal of Climatology*, vol. 39, no. 4, pp. 2386–2399, Mar. 2019, doi: 10.1002/joc.5959.
- [26] Richard Seager and Gabriel A. Vecchi, “Greenhouse warming and the 21st century hydroclimate of southwestern North America,” Dec. 2010.

- [27] G. H. Fang, J. Yang, Y. N. Chen, and C. Zammit, “Comparing bias correction methods in downscaling meteorological variables for a hydrologic impact study in an arid area in China,” *Hydrol Earth Syst Sci*, vol. 19, no. 6, pp. 2547–2559, Jun. 2015, doi: 10.5194/hess-19-2547-2015.
- [28] “Climate Models | NOAA Climate.gov,” 2012. <https://www.climate.gov/maps-data/climate-data-primer/predicting-climate/climate-models> (accessed Aug. 04, 2023).
- [29] IPCC, “AR4 Climate Change 2007: Synthesis Report,” 2007, Accessed: Aug. 04, 2023. [Online]. Available: <https://www.ipcc.ch/report/ar4/syr/>
- [30] A. Farmer, “A REVIEW OF DOWNSCALING METHODS FOR CLIMATE CHANGE PROJECTIONS,” Sep. 2014. Accessed: Aug. 04, 2023. [Online]. Available: http://www.ciesin.org/documents/Downscaling_CLEARED_000.pdf
- [31] M. Turco, M. C. Llasat, S. Herrera, and J. M. Gutiérrez, “Bias correction and downscaling of future RCM precipitation projections using a MOS-Analog technique,” *Journal of Geophysical Research: Atmospheres*, vol. 122, no. 5, pp. 2631–2648, Mar. 2017, doi: 10.1002/2016JD025724.
- [32] H. von Storch, E. Zorita, and U. Cubasch, “Downscaling of Global Climate Change Estimates to Regional Scales: An Application to Iberian Rainfall in Wintertime,” Jun. 1993, Accessed: Aug. 04, 2023. [Online]. Available: https://journals.ametsoc.org/view/journals/clim/6/6/1520-0442_1993_006_1161_dogcce_2_0_co_2.xml
- [33] J. Chen, C. Xu, S. Guo, H. Chen, and, “Progress and Challenge in Statistically Downscaling Climate Model Outputs,” *Journal of Water Resources Research* vol. 5, no. 4, 2016, Accessed: Aug. 04, 2023. [Online]. Available: <http://www.hanspub.org/journal/jwrrhttp://creativecommons.org/licenses/by/4.0/>

- [34] F. Lijun, F. Congbin, and CHEN Deliang, “REVIEW ON CREATING FUTURE CLIMATE CHANGE SCENARIOS BY STATISTICAL DOWNSCALING TECHNIQUES□□,” *Advances in Earth Science*, vol. 20, no. 3, p. 320, Mar. 2005, doi: 10.11867/J.ISSN.1001-8166.2005.03.0320.
- [35] C. Teutschbein and J. Seibert, “Bias correction of regional climate model simulations for hydrological climate-change impact studies: Review and evaluation of different methods,” *J Hydrol (Amst)*, vol. 456–457, pp. 12–29, Aug. 2012, doi: 10.1016/j.jhydrol.2012.05.052.
- [36] A. Di Luca, R. de Elía, and R. Laprise, “Potential for added value in precipitation simulated by high-resolution nested Regional Climate Models and observations,” *Clim Dyn*, vol. 38, no. 5–6, pp. 1229–1247, Mar. 2012, doi: 10.1007/s00382-011-1068-3.
- [37] J. Chen, F. P. Brissette, D. Chaumont, and M. Braun, “Performance and uncertainty evaluation of empirical downscaling methods in quantifying the climate change impacts on hydrology over two North American river basins,” *J Hydrol (Amst)*, 2013.
- [38] H. C. Thoeun, “Observed and projected changes in temperature and rainfall in Cambodia,” *Weather Clim Extrem*, vol. 7, pp. 61–71, Mar. 2015, doi: 10.1016/j.wace.2015.02.001.
- [39] W. Buytaert, M. Vuille, A. Dewulf, R. Urrutia, A. Karmalkar, and R. Céleri, “Uncertainties in climate change projections and regional downscaling in the tropical Andes: Implications for water resources management,” *Hydrol Earth Syst Sci*, vol. 14, no. 7, pp. 1247–1258, 2010, doi: 10.5194/HESS-14-1247-2010.
- [40] M. B. Switanek *et al.*, “Scaled distribution mapping: a bias correction method that preserves raw climate model projected changes,” *Hydrol Earth Syst Sci*, vol. 21, no. 6, pp. 2649–2666, Jun. 2017, doi: 10.5194/hess-21-2649-2017.

- [41] R. A. I. Wilcke, T. Mendlik, and A. Gobiet, “Multi-variable error correction of regional climate models,” *Clim Change*, vol. 120, no. 4, pp. 871–887, Oct. 2013, doi: 10.1007/S10584-013-0845-X/FIGURES/7.
- [42] C. Fu *et al.*, “Regional Climate Model Intercomparison Project for Asia,” *Bull Am Meteorol Soc*, vol. 86, no. 2, pp. 257–266, Feb. 2005, doi: 10.1175/BAMS-86-2-257.
- [43] F. Giorgi, C. Jones, and G. R. Asrar, “Addressing climate information needs at the regional level: the CORDEX framework,” *WMO Bulletin*, vol. 58, no. 3, 2009, Accessed: Aug. 04, 2023. [Online]. Available: <http://wcrp.ipsl>.
- [44] F. Giorgi and W. J. Gutowski, “Regional Dynamical Downscaling and the CORDEX Initiative,” <https://doi.org/10.1146/annurev-environ-102014-021217>, vol. 40, pp. 467–490, Nov. 2015, doi: 10.1146/ANNUREV-ENVIRON-102014-021217.
- [45] D. Jacob *et al.*, “Regional climate downscaling over Europe: perspectives from the EURO-CORDEX community,” *Reg Environ Change*, vol. 20, no. 2, p. 51, Jun. 2020, doi: 10.1007/s10113-020-01606-9.
- [46] D. P. van Vuuren, J. A. Edmonds, M. Kainuma, K. Riahi, and J. Weyant, “A special issue on the RCPs,” *Clim Change*, vol. 109, no. 1, pp. 1–4, Nov. 2011, doi: 10.1007/S10584-011-0157-Y.
- [47] B. C. O’Neill *et al.*, “A new scenario framework for climate change research: The concept of shared socioeconomic pathways,” *Clim Change*, vol. 122, no. 3, pp. 387–400, 2014, doi: 10.1007/S10584-013-0905-2.
- [48] “Topic 3: Future Pathways for Adaptation, Mitigation and Sustainable Development — IPCC.” https://ar5-syr.ipcc.ch/topic_pathways.php (accessed Aug. 04, 2023).
- [49] M. Meinshausen *et al.*, “The RCP greenhouse gas concentrations and their extensions from 1765 to 2300,” *Clim Change*, vol. 109, no. 1, pp. 213–241, Nov. 2011, doi: 10.1007/S10584-011-0156-Z/TABLES/5.

- [50] M. Höök, A. Sivertsson, and K. Aleklett, “Validity of the Fossil Fuel production outlooks in the IPCC Emission Scenarios,” *Natural Resources Research*, vol. 19, no. 2, pp. 63–81, Jun. 2010, doi: 10.1007/S11053-010-9113-1/FIGURES/14.
- [51] Z. Hausfather and G. P. Peters, “Emissions – the ‘business as usual’ story is misleading,” *Nature* 2021 577:7792, vol. 577, no. 7792, pp. 618–620, Jan. 2020, doi: 10.1038/d41586-020-00177-3.
- [52] R. Mehrotra and A. Sharma, “An improved standardization procedure to remove systematic low frequency variability biases in GCM simulations,” *Water Resour Res*, vol. 48, no. 12, Dec. 2012, doi: 10.1029/2012WR012446.
- [53] H. J. Fowler and M. Ekström, “Multi-model ensemble estimates of climate change impacts on UK seasonal precipitation extremes,” *International Journal of Climatology*, vol. 29, no. 3, pp. 385–416, Mar. 2009, doi: 10.1002/joc.1827.
- [54] H. J. Fowler, S. Blenkinsop, and C. Tebaldi, “Linking climate change modelling to impacts studies: recent advances in downscaling techniques for hydrological modelling,” *International Journal of Climatology*, vol. 27, no. 12, pp. 1547–1578, Oct. 2007, doi: 10.1002/joc.1556.
- [55] D. Maraun *et al.*, “Precipitation downscaling under climate change: Recent developments to bridge the gap between dynamical models and the end user,” *Reviews of Geophysics*, vol. 48, no. 3, p. RG3003, Sep. 2010, doi: 10.1029/2009RG000314.
- [56] G. Lenderink, A. Buishand, and W. van Deursen, “Estimates of future discharges of the river Rhine using two scenario methodologies: direct versus delta approach,” *Hydrol Earth Syst Sci*, vol. 11, no. 3, pp. 1145–1159, May 2007.
- [57] A. Barkhordarian, H. von Storch, E. Zorita, and J. J. Gómez-Navarro, “An attempt to deconstruct recent climate change in the Baltic Sea basin,” *Journal*

- of Geophysical Research: Atmospheres*, vol. 121, no. 22, pp. 13,207-13,217, Nov. 2016, doi: 10.1002/2015JD024648.
- [58] F. Johnson and A. Sharma, “A nesting model for bias correction of variability at multiple time scales in general circulation model precipitation simulations,” *Water Resour Res*, vol. 48, no. 1, Jan. 2012.
- [59] C. Volosciuk, D. Maraun, M. Vrac, and M. Widmann, “A combined statistical bias correction and stochastic downscaling method for precipitation,” *Hydrol Earth Syst Sci*, vol. 21, no. 3, pp. 1693–1719, Mar. 2017, doi: 10.5194/hess-21-1693-2017.
- [60] G. H. Fang, J. Yang, Y. N. Chen, and C. Zammit, “Comparing bias correction methods in downscaling meteorological variables for a hydrologic impact study in an arid area in China,” *Hydrol Earth Syst Sci*, vol. 19, no. 6, pp. 2547–2559, Jun. 2015, doi: 10.5194/hess-19-2547-2015.
- [61] J. Teng *et al.*, “How does bias correction of regional climate model precipitation affect modelled runoff?,” *Hydrol Earth Syst Sci*, vol. 19, no. 2, pp. 711–728, Feb. 2015, doi: 10.5194/hess-19-711-2015.
- [62] A. Halmstad, M. R. Najafi, and H. Moradkhani, “Analysis of precipitation extremes with the assessment of regional climate models over the Willamette River Basin, USA,” *Hydrol Process*, vol. 27, no. 18, pp. 2579–2590, Aug. 2013, doi: 10.1002/HYP.9376.
- [63] S. T. Ngai, F. Tangang, and L. Juneng, “Bias correction of global and regional simulated daily precipitation and surface mean temperature over Southeast Asia using quantile mapping method,” *Glob Planet Change*, vol. 149, pp. 79–90, Feb. 2017, doi: 10.1016/j.gloplacha.2016.12.009.
- [64] M. Mendez, B. Maathuis, D. Hein-Griggs, and L.-F. Alvarado-Gamboa, “Performance Evaluation of Bias Correction Methods for Climate Change Monthly Precipitation Projections over Costa Rica,” *Water (Basel)*, vol. 12, no. 2, p. 482, Feb. 2020, doi: 10.3390/w12020482.

- [65] C. G. de C. Menéndez, A. Sorensson, and J.-P. Boulanger, “CLARIS Project: towards climate downscaling in South America,” *Meteorologische Zeitschrift*, vol. 19, no. 4, pp. 357–362, Aug. 2010, doi: 10.1127/0941-2948/2010/0459.
- [66] M. Mendez, L.-A. Calvo-Valverde, B. Maathuis, and L.-F. Alvarado-Gamboa, “Generation of Monthly Precipitation Climatologies for Costa Rica Using Irregular Rain-Gauge Observational Networks,” *Water (Basel)*, vol. 11, no. 1, p. 70, Jan. 2019, doi: 10.3390/w11010070.
- [67] K. Schamm *et al.*, “Global gridded precipitation over land: A description of the new GPCP First Guess Daily product,” *Earth Syst Sci Data*, vol. 6, no. 1, pp. 49–60, Jan. 2014, doi: 10.5194/ESSD-6-49-2014.
- [68] C. G. Jones, U. Willén, A. Ullerstig, and U. Hansson, “The Rossby Centre Regional Atmospheric Climate Model Part I: Model Climatology and Performance for the Present Climate over Europe,” *AMBIO: A Journal of the Human Environment*, vol. 33, no. 4, pp. 199–210, Jun. 2004, doi: 10.1579/0044-7447-33.4.199.
- [69] A. Mehran, A. AghaKouchak, and T. J. Phillips, “Evaluation of CMIP5 continental precipitation simulations relative to satellite-based gauge-adjusted observations,” *Journal of Geophysical Research: Atmospheres*, vol. 119, no. 4, pp. 1695–1707, Feb. 2014, doi: 10.1002/2013JD021152.
- [70] V. Todaro, M. D’Oria, D. Secci, A. Zanini, and M. G. Tanda, “Climate Change over the Mediterranean Region: Local Temperature and Precipitation Variations at Five Pilot Sites,” *Water (Basel)*, vol. 14, no. 16, p. 2499, Aug. 2022, doi: 10.3390/w14162499.
- [71] D. Jacob *et al.*, “EURO-CORDEX: new high-resolution climate change projections for European impact research,” *Reg Environ Change*, vol. 14, no. 2, pp. 563–578, Apr. 2014, doi: 10.1007/s10113-013-0499-2.
- [72] “Climate Change 2013: The Physical Science Basis: Working Group I ... - Google Kitaplar,” 2013.

https://books.google.com.cy/books?hl=tr&lr=&id=o4gaBQAAQBAJ&oi=fnd&pg=PR1&dq=Climate+Change+2013:+The+Physical+Science+Basis:+Working+Group+I+Contribution+to+the+Fifth+Assessment+Report+of+the+Intergovernmental+Panel+on+Climate+Change&ots=Whsu7QAvNm&sig=9whiEpzSGjCvaEF4NznvkpFPppc&redir_esc=y#v=onepage&q=Climate%20Change%202013%3A%20The%20Physical%20Science%20Basis%3A%20Working%20Group%20I%20Contribution%20to%20the%20Fifth%20Assessment%20Report%20of%20the%20Intergovernmental%20Panel%20on%20Climate%20Change&f=false (accessed Aug. 05, 2023).

- [73] G. Zittis, A. Bruggeman, and C. Camera, “21st Century Projections of Extreme Precipitation Indicators for Cyprus,” *Atmosphere (Basel)*, vol. 11, no. 4, p. 343, Mar. 2020, doi: 10.3390/atmos11040343.
- [74] W. C. Skamarock *et al.*, “A Description of the Advanced Research WRF Version 3,” 2008.
- [75] L. Fita *et al.*, “CORDEX-WRF v1.3: Development of a module for the Weather Research and Forecasting (WRF) model to support the CORDEX community,” *Geosci Model Dev*, vol. 12, no. 3, pp. 1029–1066, Mar. 2019, doi: 10.5194/GMD-12-1029-2019.
- [76] C. Giannakopoulos, P. Hadjinicolaou, E. Kostopoulou, K. V. Varotsos, and C. Zerefos, “Precipitation and temperature regime over Cyprus as a result of global climate change,” *Advances in Geosciences*, vol. 23, pp. 17–24, 2010, doi: 10.5194/ADGEO-23-17-2010.
- [77] G. Lenderink, A. van Ulden, B. van den Hurk, and F. Keller, “A study on combining global and regional climate model results for generating climate scenarios of temperature and precipitation for the Netherlands,” *Clim Dyn*, vol. 29, no. 2–3, pp. 157–176, Aug. 2007, doi: 10.1007/S00382-007-0227-Z/FIGURES/15.
- [78] G. Zittis, A. Bruggeman, C. Camera, P. Hadjinicolaou, and J. Lelieveld, “The added value of convection permitting simulations of extreme precipitation

- events over the eastern Mediterranean,” *Atmos Res*, vol. 191, pp. 20–33, Jul. 2017, doi: 10.1016/j.atmosres.2017.03.002.
- [79] E. Kostopoulou and P. D. Jones, “Comprehensive analysis of the climate variability in the eastern Mediterranean. Part I: map-pattern classification,” *International Journal of Climatology*, vol. 27, no. 9, pp. 1189–1214, Jul. 2007, doi: 10.1002/JOC.1467.
- [80] M. C. Peel, B. L. Finlayson, and T. A. McMahon, “Updated world map of the Köppen-Geiger climate classification,” *Hydrol Earth Syst Sci*, vol. 11, no. 5, pp. 1633–1644, Oct. 2007, doi: 10.5194/hess-11-1633-2007.
- [81] C. Christofi, A. Bruggeman, C. Kuells, and C. Constantinou, “Hydrochemical evolution of groundwater in gabbro of the Troodos Fractured Aquifer. A comprehensive approach,” *Applied Geochemistry*, vol. 114, pp. 104–524, Mar. 2020, doi: 10.1016/J.APGEOCHEM.2020.104524.
- [82] E. Kostopoulou and P. D. Jones, “Comprehensive analysis of the climate variability in the eastern Mediterranean. Part II: relationships between atmospheric circulation patterns and surface climatic elements,” *International Journal of Climatology*, vol. 27, no. 10, pp. 1351–1371, Aug. 2007, doi: 10.1002/JOC.1466.
- [83] J. G. Pinto, U. Ulbrich, and P. Speth, “The Variability of Cyclonic Activity in the Mediterranean Area in the last 40 Years and its Impact on Precipitation,” 2001.
- [84] H. Zaifoğlu, B. Akıntuğ, and A. M. Yanmaz, “Quality Control, Homogeneity Analysis, and Trends of Extreme Precipitation Indices in Northern Cyprus,” *J Hydrol Eng*, vol. 22, no. 12, Dec. 2017, doi: 10.1061/(ASCE)HE.1943-5584.0001589.
- [85] “CDO User Guide Climate Data Operators Version 1.8.1 Uwe Schulzweida-MPI for Meteorology,” 2017.

- [86] E. Pastén-Zapata, J. M. Jones, H. Moggridge, and M. Widmann, “Evaluation of the performance of Euro-CORDEX Regional Climate Models for assessing hydrological climate change impacts in Great Britain: A comparison of different spatial resolutions and quantile mapping bias correction methods,” *J Hydrol (Amst)*, vol. 584, p. 124653, May 2020, doi: 10.1016/j.jhydrol.2020.124653.
- [87] R. M. Hirsch and J. R. Slack, “A Nonparametric Trend Test for Seasonal Data With Serial Dependence,” *Water Resour Res*, vol. 20, no. 6, pp. 727–732, Jun. 1984, doi: 10.1029/WR020i006p00727.
- [88] H. B. Mann, “Nonparametric Tests Against Trend,” *Econometrica*, vol. 13, no. 3, p. 245, Jul. 1945, doi: 10.2307/1907187.
- [89] P. D. Valz and A. I. McLeod, “A simplified derivation of the variance of kendall’s rank correlation coefficient,” *American Statistician*, vol. 44, no. 1, pp. 39–40, 1990, doi: 10.1080/00031305.1990.10475691.
- [90] “Rank correlation methods.” <https://psycnet.apa.org/record/1948-15040-000> (accessed Aug. 21, 2023).
- [91] D. KOUTSOYIANNIS, “Climate change, the Hurst phenomenon, and hydrological statistics,” *Hydrological Sciences Journal*, vol. 48, no. 1, pp. 3–24, Feb. 2003, doi: 10.1623/hysj.48.1.3.43481.
- [92] K. H. Hamed, “Trend detection in hydrologic data: The Mann–Kendall trend test under the scaling hypothesis,” *J Hydrol (Amst)*, vol. 349, no. 3–4, pp. 350–363, Feb. 2008, doi: 10.1016/j.jhydrol.2007.11.009.
- [93] P. K. Sen, “Estimates of the Regression Coefficient Based on Kendall’s Tau,” *J Am Stat Assoc*, vol. 63, no. 324, pp. 1379–1389, Dec. 1968, doi: 10.1080/01621459.1968.10480934.
- [94] S. H. Bari, M. T. U. Rahman, M. A. Hoque, and Md. M. Hussain, “Analysis of seasonal and annual rainfall trends in the northern region of Bangladesh,”

- Atmos Res*, vol. 176–177, pp. 148–158, Jul. 2016, doi: 10.1016/j.atmosres.2016.02.008.
- [95] Z. Şen, “Innovative Trend Analysis Methodology,” *J Hydrol Eng*, vol. 17, no. 9, pp. 1042–1046, Sep. 2012, doi: 10.1061/(ASCE)HE.1943-5584.0000556.
- [96] P. Sonali and D. Nagesh Kumar, “Review of trend detection methods and their application to detect temperature changes in India,” *J Hydrol (Amst)*, vol. 476, pp. 212–227, Jan. 2013, doi: 10.1016/j.jhydrol.2012.10.034.
- [97] S. Alashan, “An improved version of innovative trend analyses,” *Arabian Journal of Geosciences*, vol. 11, no. 3, p. 50, Feb. 2018, doi: 10.1007/s12517-018-3393-x.
- [98] P. Alpert, “The paradoxical increase of Mediterranean extreme daily rainfall in spite of decrease in total values,” *Geophys Res Lett*, vol. 29, no. 11, p. 1536, 2002, doi: 10.1029/2001GL013554.
- [99] C. Onyutha, H. Tabari, A. Rutkowska, P. Nyeko-Ogiramoi, and P. Willems, “Comparison of different statistical downscaling methods for climate change rainfall projections over the Lake Victoria basin considering CMIP3 and CMIP5,” *Journal of Hydro-environment Research*, vol. 12, pp. 31–45, Sep. 2016, doi: 10.1016/J.JHER.2016.03.001.
- [100] A. Hilal, N. Vakitbilir, and B. Akıntuğ, “Spatial and Temporal Analysis of Daily, Monthly, and Seasonal Rainfall Characteristics across Northern Cyprus,” *J Hydrol Eng*, vol. 26, no. 12, Dec. 2021, doi: 10.1061/(ASCE)HE.1943-5584.0002136.
- [101] C. M. Philandras, P. T. Nastos, J. Kapsomenakis, K. C. Douvis, G. Tselioudis, and C. S. Zerefos, “Long term precipitation trends and variability within the Mediterranean region,” *Natural Hazards and Earth System Sciences*, vol. 11, no. 12, pp. 3235–3250, Dec. 2011, doi: 10.5194/nhess-11-3235-2011.

- [102] J. Lelieveld *et al.*, “Climate change and impacts in the Eastern Mediterranean and the Middle East,” *Clim Change*, vol. 114, no. 3–4, pp. 667–687, Oct. 2012, doi: 10.1007/s10584-012-0418-4.
- [103] P. Hadjinicolaou, C. Giannakopoulos, C. Zerefos, M. A. Lange, S. Pashiardis, and J. Lelieveld, “Mid-21st century climate and weather extremes in Cyprus as projected by six regional climate models,” *Reg Environ Change*, vol. 11, no. 3, pp. 441–457, Sep. 2011, doi: 10.1007/s10113-010-0153-1.
- [104] H. Babaousmail *et al.*, “Future changes in mean and extreme precipitation over the Mediterranean and Sahara regions using bias-corrected CMIP6 models,” *International Journal of Climatology*, vol. 42, no. 14, pp. 7280–7297, Nov. 2022, doi: 10.1002/joc.7644.

APPENDICES

A. Bias Correction Tables

Table A.1. Results of Comparison Between Observation, Raw Model, and EQM Corrected Model for Mean Precipitation and SD

GCM-RCM couplings	Stations	Mean Precipitation (mm)			Percent Bias (%)		Standard Deviation (mm)			Percent Bias (%)	
		Obs	Raw Mod	Corr Mod	obs-mod	obs-cor	Obs	Raw Mod	Corr Mod	obs-mod	obs-cor
1	Boğaz	1.06	0.50	1.06	52.96	0.28	4.72	2.32	4.68	50.90	0.89
	Lefkoşa	0.85	0.79	0.85	6.92	0.13	3.80	2.73	3.81	28.08	0.31
	Girne	1.31	1.48	1.35	12.90	3.35	6.20	4.80	6.91	22.66	11.42
	Magusa	0.91	1.14	0.91	24.14	0.56	4.21	4.20	4.14	0.27	1.60
	Karpaz	1.38	1.77	1.39	28.31	0.54	6.03	5.91	6.15	1.91	1.93
	Güzelyurt	0.79	2.12	0.78	169.46	0.20	3.27	7.20	3.25	120.44	0.65
	Lefke	0.81	1.34	0.80	65.37	0.95	3.37	4.12	3.25	22.16	3.82
	İskele	0.95	1.12	0.94	18.39	0.12	4.58	3.84	4.56	16.16	0.45
	kantara	1.54	0.76	1.53	50.28	0.26	6.57	3.23	6.54	50.83	0.54

2	Boğaz	1.06	1.56	1.06	46.50	0.45	4.72	4.73	4.66	0.20	1.26
	Lefkoşa	0.85	1.32	0.86	55.39	0.73	3.80	4.22	3.88	11.15	2.23
	Girne	1.31	1.56	1.34	18.75	2.66	6.20	4.73	6.75	23.74	8.84
	Magusa	0.91	0.97	0.90	6.34	1.24	4.21	3.77	4.07	10.43	3.34
	Karpaz	1.38	1.26	1.39	8.94	0.45	6.03	4.38	6.13	27.39	1.72
	Güzelyurt	0.79	1.69	0.80	115.16	1.31	3.27	5.26	3.43	61.06	4.81
	Lefke	0.81	2.51	0.81	209.67	0.51	3.37	6.85	3.33	103.12	1.48
	İskele	0.95	0.97	0.93	2.30	1.20	4.58	3.54	4.40	22.68	4.09
	kantara	1.54	1.34	1.53	12.70	0.34	6.57	4.16	6.51	36.70	0.98
3	Boğaz	1.06	1.18	1.06	11.04	0.15	4.72	3.38	4.77	28.38	1.06
	Lefkoşa	0.85	0.88	0.86	3.50	1.02	3.80	2.82	3.91	25.82	2.84
	Girne	1.31	1.10	1.36	16.17	3.72	6.20	3.36	7.05	45.77	13.60
	Magusa	0.91	1.03	0.92	13.03	0.12	4.21	3.31	4.21	21.43	0.15
	Karpaz	1.38	1.54	1.39	11.43	0.73	6.03	4.20	6.22	30.28	3.18
	Güzelyurt	0.79	0.72	0.78	7.72	0.40	3.27	2.34	3.22	28.50	1.52
	Lefke	0.81	0.88	0.81	8.37	0.53	3.37	2.74	3.30	18.68	2.10
	İskele	0.95	1.12	0.94	18.27	0.28	4.58	3.41	4.55	25.58	0.63
	kantara	1.54	1.33	1.55	13.42	0.99	6.57	3.70	6.79	43.72	3.34

4	Boğaz	1.06	0.70	1.05	33.83	0.85	4.72	3.62	4.57	23.37	3.12
	Lefkoşa	0.85	0.60	0.85	29.90	0.47	3.80	2.91	3.75	23.44	1.28
	Girne	1.31	0.85	1.33	35.36	1.58	6.20	4.16	6.53	32.88	5.33
	Magusa	0.91	0.70	0.91	23.05	0.80	4.21	3.81	4.11	9.39	2.31
	Karpaz	1.38	0.95	1.42	31.01	2.61	6.03	4.03	6.66	33.23	10.43
	Güzelyurt	0.79	0.60	0.79	23.11	1.03	3.27	2.80	3.40	14.47	3.93
	Lefke	0.81	0.69	0.80	14.94	1.01	3.37	3.22	3.25	4.45	3.60
	İskele	0.95	0.65	0.95	31.10	0.79	4.58	3.12	4.70	31.96	2.66
	kantara	1.54	0.68	1.53	55.47	0.40	6.57	3.06	6.48	53.39	1.41
5	Boğaz	1.06	0.97	1.06	8.69	0.10	4.72	3.80	4.72	19.57	0.03
	Lefkoşa	0.85	0.28	0.86	66.71	0.50	3.80	1.48	3.85	61.09	1.18
	Girne	1.31	0.89	1.32	32.22	0.68	6.20	3.22	6.32	48.04	1.90
	Magusa	0.91	0.82	0.91	10.78	0.64	4.21	3.13	4.12	25.54	2.07
	Karpaz	1.38	1.10	1.40	20.01	1.42	6.03	3.70	6.30	38.60	4.51
	Güzelyurt	0.79	0.28	0.78	64.65	1.11	3.27	1.58	3.15	51.75	3.68
	Lefke	0.81	0.31	0.80	62.37	1.08	3.37	1.65	3.23	51.13	4.35
	İskele	0.95	0.57	0.94	39.93	0.69	4.58	2.72	4.46	40.62	2.70
	kantara	1.54	1.02	1.53	33.38	0.44	6.57	4.12	6.48	37.27	1.41

6	Boğaz	1.06	1.06	1.06	0.13	0.29	4.72	3.50	4.77	25.84	1.10
	Lefkoşa	0.85	0.80	0.86	5.79	0.64	3.80	2.93	3.87	22.95	1.78
	Girne	1.31	1.04	1.34	20.91	2.05	6.20	3.45	6.67	44.44	7.58
	Magusa	0.91	0.97	0.91	6.22	0.00	4.21	3.35	4.21	20.36	0.03
	Karpaz	1.38	1.34	1.39	2.85	0.54	6.03	3.99	6.11	33.84	1.28
	Güzelyurt	0.79	0.61	0.79	21.85	0.69	3.27	2.19	3.34	32.86	2.17
	Lefke	0.81	0.79	0.81	3.01	0.33	3.37	2.91	3.32	13.74	1.70
	İskele	0.95	0.98	0.94	4.04	0.31	4.58	3.34	4.54	27.12	0.91
	kantara	1.54	1.15	1.55	25.03	0.72	6.57	3.59	6.73	45.32	2.42
7	Boğaz	1.06	0.95	1.06	10.34	0.61	4.72	3.77	4.64	20.11	1.80
	Lefkoşa	0.85	0.31	0.85	63.25	0.14	3.80	3.24	3.78	14.67	0.66
	Girne	1.31	0.86	1.34	34.16	2.69	6.20	1.58	6.74	74.50	8.66
	Magusa	0.91	0.83	0.91	9.61	0.17	4.21	2.89	4.19	31.30	0.40
	Karpaz	1.38	1.03	1.39	25.65	0.45	6.03	3.66	6.08	39.23	0.93
	Güzelyurt	0.79	0.29	0.79	62.76	0.99	3.27	1.61	3.37	50.59	3.04
	Lefke	0.81	0.33	0.80	59.36	0.94	3.37	1.57	3.26	53.61	3.31
	İskele	0.95	0.61	0.95	35.05	0.23	4.58	3.23	4.62	29.59	0.84
	kantara	1.54	1.04	1.53	32.09	0.68	6.57	4.23	6.43	35.60	2.19

8	Boğaz	1.06	0.63	1.05	40.30	1.42	4.72	2.76	4.50	41.56	4.59
	Lefkoşa	0.85	0.57	0.85	32.93	0.41	3.80	3.81	3.74	0.33	1.59
	Girne	1.31	0.90	1.34	31.60	2.00	6.20	2.77	6.57	55.27	5.87
	Magusa	0.91	0.77	0.91	15.62	0.63	4.21	3.24	4.13	23.09	1.78
	Karpaz	1.38	1.18	1.41	14.88	2.23	6.03	4.61	6.55	23.61	8.63
	Güzelyurt	0.79	0.61	0.79	22.39	0.05	3.27	2.95	3.27	9.69	0.03
	Lefke	0.81	0.66	0.80	18.20	1.12	3.37	2.63	3.23	21.99	4.30
	İskele	0.95	0.69	0.96	27.14	1.44	4.58	3.68	4.80	19.65	4.77
	kantara	1.54	0.75	1.55	51.43	0.74	6.57	3.24	6.73	50.65	2.34
9	Boğaz	1.06	0.57	1.05	46.66	1.13	4.72	2.02	4.56	57.17	3.42
	Lefkoşa	0.85	0.65	0.85	24.25	0.24	3.80	7.30	3.78	92.11	0.63
	Girne	1.31	1.94	1.31	47.88	0.13	6.20	3.49	6.16	43.79	0.69
	Magusa	0.91	1.08	0.91	18.26	0.13	4.21	2.76	4.19	34.33	0.48
	Karpaz	1.38	2.02	1.41	46.46	1.83	6.03	7.17	6.53	18.91	8.26
	Güzelyurt	0.79	1.14	0.78	45.46	0.14	3.27	3.22	3.25	1.48	0.47
	Lefke	0.81	0.86	0.80	6.00	1.58	3.37	2.21	3.19	34.63	5.60
	İskele	0.95	0.87	0.94	8.42	0.19	4.58	4.41	4.51	3.73	1.53
	kantara	1.54	0.45	1.53	70.56	0.23	6.57	2.00	6.54	69.53	0.53

10	Boğaz	1.06	1.80	1.06	69.49	0.37	4.72	2.09	4.67	55.64	1.17
	Lefkoşa	0.85	0.53	0.85	37.95	0.39	3.80	5.31	3.77	39.65	0.91
	Girne	1.31	0.80	1.34	39.06	2.37	6.20	3.98	6.71	35.78	8.13
	Magusa	0.91	0.99	0.91	8.46	0.46	4.21	3.21	4.15	23.71	1.43
	Karpaz	1.38	1.44	1.39	4.55	0.58	6.03	5.12	6.25	15.12	3.62
	Güzelyurt	0.79	0.49	0.79	37.83	0.65	3.27	2.05	3.35	37.43	2.36
	Lefke	0.81	0.41	0.82	50.07	0.39	3.37	2.30	3.41	31.99	1.09
	İskele	0.95	1.23	0.94	29.88	0.31	4.58	3.87	4.51	15.56	1.64
	kantara	1.54	1.79	1.53	16.43	0.17	6.57	5.48	6.56	16.66	0.12
11	Boğaz	1.06	0.78	1.06	26.05	0.28	4.72	1.86	4.77	60.68	1.07
	Lefkoşa	0.85	0.30	0.86	64.59	0.55	3.80	1.37	3.85	64.02	1.33
	Girne	1.31	0.39	1.33	69.93	1.34	6.20	1.51	6.50	75.61	4.78
	Magusa	0.91	0.52	0.91	43.61	0.81	4.21	2.90	4.10	31.07	2.56
	Karpaz	1.38	0.67	1.41	51.24	1.98	6.03	2.46	6.50	59.23	7.75
	Güzelyurt	0.79	0.27	0.79	65.98	0.12	3.27	1.34	3.27	58.88	0.06
	Lefke	0.81	0.28	0.81	65.26	0.73	3.37	2.38	3.28	29.58	2.92
	İskele	0.95	0.65	0.96	31.43	1.21	4.58	2.97	4.76	35.17	3.92
	kantara	1.54	0.84	1.53	45.38	0.47	6.57	3.19	6.52	51.54	0.85

12	Boğaz	1.06	1.51	1.06	42.42	0.02	4.72	4.68	4.72	0.88	0.00
	Lefkoşa	0.85	0.49	0.85	42.59	0.59	3.80	2.64	3.74	30.53	1.64
	Girne	1.31	0.62	1.34	52.48	2.07	6.20	1.86	6.57	70.07	5.94
	Magusa	0.91	0.79	0.91	13.56	0.74	4.21	3.66	4.12	12.95	2.03
	Karpaz	1.38	1.00	1.42	27.65	2.55	6.03	3.69	6.65	38.77	10.27
	Güzelyurt	0.79	0.40	0.80	49.28	1.23	3.27	2.01	3.41	38.50	4.35
	Lefke	0.81	0.45	0.80	44.70	0.92	3.37	2.04	3.27	39.63	3.03
	İskele	0.95	1.07	0.95	13.25	0.72	4.58	3.23	4.68	29.55	2.09
	kantara	1.54	1.46	1.55	5.17	1.11	6.57	4.84	6.83	26.42	3.94
13	Boğaz	1.06	0.41	1.06	61.58	0.34	4.72	2.03	4.67	56.94	1.06
	Lefkoşa	0.85	0.70	0.86	18.16	0.97	3.80	3.79	3.90	0.36	2.60
	Girne	1.31	1.06	1.32	19.44	0.81	6.20	5.59	6.33	9.85	2.00
	Magusa	0.91	0.86	0.91	5.96	1.05	4.21	3.23	4.09	23.37	2.86
	Karpaz	1.38	1.33	1.39	3.56	0.39	6.03	4.85	6.11	19.53	1.27
	Güzelyurt	0.79	1.54	0.78	95.97	0.21	3.27	3.67	3.22	12.15	1.35
	Lefke	0.81	1.04	0.80	27.50	0.89	3.37	2.57	3.24	23.98	3.86
	İskele	0.95	0.84	0.95	10.93	0.06	4.58	3.53	4.55	23.05	0.67
	kantara	1.54	0.53	1.54	65.45	0.48	6.57	2.54	6.70	61.32	1.91

	Boğaz	1.06	0.78	1.06	26.05	0.28	4.72	2.97	4.77	37.06	1.07
	Lefkoşa	0.85	0.30	0.86	64.59	0.55	3.80	1.86	3.85	51.16	1.33
	Girne	1.31	0.39	1.33	69.93	1.34	6.20	1.34	6.50	78.33	4.78
	Magusa	0.91	0.52	0.91	43.61	0.81	4.21	2.46	4.10	41.60	2.56
14	Karpaz	1.38	0.67	1.41	51.24	1.98	6.03	2.90	6.50	51.88	7.75
	Güzelyurt	0.79	0.27	0.79	65.98	0.12	3.27	1.37	3.27	58.16	0.06
	Lefke	0.81	0.28	0.81	65.26	0.73	3.37	1.51	3.28	55.18	2.92
	İskele	0.95	0.65	0.96	31.43	1.21	4.58	2.38	4.76	48.14	3.92
	kantara	1.54	0.84	1.53	45.38	0.47	6.57	3.19	6.52	51.54	0.85

Table A.2. Results of Comparison Between Observation, Raw Model, and GQM Corrected Model for Mean Precipitation and SD

GCM-RCM	Stations	Mean Precipitation (mm)			Percent Bias (%)		Standard Deviation (mm)			Percent Bias (%)	
		Obs	R Mod	Corr Mod	obs-mod	obs-cor	Obs	R Mod	Corr Mod	obs-mod	obs-cor
1	Boğaz	1.06	0.50	1.04	52.96	1.72	4.72	2.32	4.97	50.90	5.23
	Lefkoşa	0.85	0.79	0.89	6.92	4.93	3.80	2.73	3.99	28.08	5.10
	Girne	1.31	1.48	1.54	12.90	17.34	6.20	4.80	6.79	22.66	9.47
	Magusa	0.91	1.14	1.01	24.14	10.89	4.21	4.20	5.66	0.27	34.54
	Karpaz	1.38	1.77	1.68	28.31	21.93	6.03	5.91	7.73	1.91	28.29
	Güzelyurt	0.79	2.12	0.79	169.46	0.32	3.27	7.20	3.26	120.44	0.24
	Lefke	0.81	1.34	1.11	65.37	36.71	3.37	4.12	3.21	22.16	4.86
	İskele	0.95	1.12	0.99	18.39	4.48	4.58	3.84	4.85	16.16	5.80
kantara	1.54	0.76	1.55	50.28	0.69	6.57	3.23	7.35	50.83	11.83	

2	Boğaz	1.06	1.56	1.20	46.50	12.87	4.72	4.73	5.18	0.20	9.81
	Lefkoşa	0.85	1.32	0.94	55.39	10.17	3.80	4.22	4.14	11.15	8.88
	Girne	1.31	1.56	1.57	18.75	19.66	6.20	4.73	6.95	23.74	12.04
	Magusa	0.91	0.97	0.95	6.34	3.34	4.21	3.77	4.82	10.43	14.64
	Karpaz	1.38	1.26	1.52	8.94	10.40	6.03	4.38	6.57	27.39	8.96
	Güzelyurt	0.79	1.69	0.84	115.16	6.86	3.27	5.26	3.31	61.06	1.31
	Lefke	0.81	2.51	0.86	209.67	6.35	3.37	6.85	3.26	103.12	3.29
	İskele	0.95	0.97	1.01	2.30	6.31	4.58	3.54	5.02	22.68	9.56
	kantara	1.54	1.34	1.65	12.70	7.51	6.57	4.16	7.13	36.70	8.50
3	Boğaz	1.06	1.18	1.22	11.04	15.16	4.72	3.38	5.25	28.38	11.26
	Lefkoşa	0.85	0.88	1.03	3.50	20.58	3.80	2.82	5.10	25.82	34.30
	Girne	1.31	1.10	1.56	16.17	18.79	6.20	3.36	6.82	45.77	9.88
	Magusa	0.91	1.03	1.09	13.03	19.27	4.21	3.31	5.23	21.43	24.35
	Karpaz	1.38	1.54	1.59	11.43	14.81	6.03	4.20	5.97	30.28	0.92
	Güzelyurt	0.79	0.72	0.84	7.72	6.59	3.27	2.34	3.83	28.50	17.16
	Lefke	0.81	0.88	0.89	8.37	9.92	3.37	2.74	4.12	18.68	22.09
	İskele	0.95	1.12	1.13	18.27	19.41	4.58	3.41	5.32	25.58	16.18
	kantara	1.54	1.33	1.74	13.42	12.98	6.57	3.70	7.17	43.72	9.11

4	Boğaz	1.06	0.70	0.94	33.83	10.99	4.72	3.62	5.01	23.37	6.12
	Lefkoşa	0.85	0.60	0.81	29.90	4.55	3.80	2.91	4.46	23.44	17.27
	Girne	1.31	0.85	1.32	35.36	0.95	6.20	4.16	6.81	32.88	9.87
	Magusa	0.91	0.70	0.85	23.05	6.72	4.21	3.81	4.90	9.39	16.38
	Karpaz	1.38	0.95	1.43	31.01	3.28	6.03	4.03	6.56	33.23	8.89
	Güzelyurt	0.79	0.60	0.78	23.11	1.20	3.27	2.80	3.64	14.47	11.29
	Lefke	0.81	0.69	0.76	14.94	6.87	3.37	3.22	3.73	4.45	10.51
	İskele	0.95	0.65	0.94	31.10	0.60	4.58	3.12	5.29	31.96	15.35
	kantara	1.54	0.68	1.47	55.47	4.14	6.57	3.06	7.12	53.39	8.38
5	Boğaz	1.06	0.97	1.08	8.69	1.56	4.72	3.80	4.80	19.57	1.59
	Lefkoşa	0.85	0.28	0.82	66.71	3.68	3.80	1.48	4.25	61.09	11.90
	Girne	1.31	0.89	1.48	32.22	13.22	6.20	3.22	6.75	48.04	8.83
	Magusa	0.91	0.82	0.98	10.78	7.08	4.21	3.13	5.08	25.54	20.64
	Karpaz	1.38	1.10	1.65	20.01	19.42	6.03	3.70	7.26	38.60	20.42
	Güzelyurt	0.79	0.28	0.89	64.65	13.00	3.27	1.58	3.37	51.75	3.03
	Lefke	0.81	0.31	0.72	62.37	11.15	3.37	1.65	3.61	51.13	7.01
	İskele	0.95	0.57	0.89	39.93	5.78	4.58	2.72	4.68	40.62	2.12
	kantara	1.54	1.02	1.48	33.38	3.41	6.57	4.12	6.37	37.27	3.06

6	Boğaz	1.06	1.06	1.16	0.13	9.30	4.72	3.50	5.23	25.84	10.87
	Lefkoşa	0.85	0.80	0.95	5.79	11.83	3.80	2.93	4.78	22.95	25.82
	Girne	1.31	1.04	1.51	20.91	15.40	6.20	3.45	6.58	44.44	6.05
	Magusa	0.91	0.97	1.07	6.22	16.51	4.21	3.35	4.94	20.36	17.46
	Karpaz	1.38	1.34	1.59	2.85	14.95	6.03	3.99	5.95	33.84	1.37
	Güzelyurt	0.79	0.61	0.84	21.85	7.37	3.27	2.19	3.82	32.86	16.87
	Lefke	0.81	0.79	0.85	3.01	5.07	3.37	2.91	4.19	13.74	24.24
	İskele	0.95	0.98	1.10	4.04	16.08	4.58	3.34	5.16	27.12	12.53
	kantara	1.54	1.15	1.71	25.03	11.05	6.57	3.59	7.11	45.32	8.19
7	Boğaz	1.06	0.95	1.07	10.34	0.68	4.72	3.77	4.58	20.11	2.88
	Lefkoşa	0.85	0.31	0.81	63.25	4.58	3.80	3.24	4.10	14.67	7.96
	Girne	1.31	0.86	1.50	34.16	14.73	6.20	1.58	7.22	74.50	16.40
	Magusa	0.91	0.83	1.05	9.61	15.08	4.21	2.89	5.69	31.30	35.25
	Karpaz	1.38	1.03	1.66	25.65	20.01	6.03	3.66	7.91	39.23	31.25
	Güzelyurt	0.79	0.29	0.74	62.76	6.21	3.27	1.61	3.52	50.59	7.80
	Lefke	0.81	0.33	0.75	59.36	7.58	3.37	1.57	3.62	53.61	7.19
	İskele	0.95	0.61	0.94	35.05	1.01	4.58	3.23	4.66	29.59	1.73
	kantara	1.54	1.04	1.50	32.09	2.26	6.57	4.23	6.26	35.60	4.76

8	Boğaz	1.06	0.63	1.02	40.30	4.34	4.72	2.76	5.09	41.56	7.75
	Lefkoşa	0.85	0.57	0.79	32.93	7.03	3.80	3.81	4.35	0.33	14.41
	Girne	1.31	0.90	1.36	31.60	4.09	6.20	2.77	6.91	55.27	11.34
	Magusa	0.91	0.77	0.89	15.62	2.51	4.21	3.24	4.89	23.09	16.09
	Karpaz	1.38	1.18	1.45	14.88	4.87	6.03	4.61	6.87	23.61	13.92
	Güzelyurt	0.79	0.61	0.75	22.39	4.26	3.27	2.95	3.76	9.69	15.14
	Lefke	0.81	0.66	0.76	18.20	5.94	3.37	2.63	3.79	21.99	12.15
	İskele	0.95	0.69	0.95	27.14	0.90	4.58	3.68	5.45	19.65	18.89
	kantara	1.54	0.75	1.52	51.43	0.82	6.57	3.24	7.64	50.65	16.32
9	Boğaz	1.06	0.57	1.13	46.66	5.98	4.72	2.02	5.09	57.17	7.92
	Lefkoşa	0.85	0.65	0.92	24.25	8.42	3.80	7.30	4.30	92.11	13.25
	Girne	1.31	1.94	1.40	47.88	6.92	6.20	3.49	7.30	43.79	17.68
	Magusa	0.91	1.08	1.01	18.26	10.82	4.21	2.76	6.16	34.33	46.42
	Karpaz	1.38	2.02	1.65	46.46	19.36	6.03	7.17	7.84	18.91	30.12
	Güzelyurt	0.79	1.14	0.85	45.46	8.72	3.27	3.22	3.29	1.48	0.65
	Lefke	0.81	0.86	0.82	6.00	1.16	3.37	2.21	3.74	34.63	10.77
	İskele	0.95	0.87	1.07	8.42	12.95	4.58	4.41	4.80	3.73	4.72
	kantara	1.54	0.45	1.56	70.56	1.82	6.57	2.00	9.07	69.53	38.02

10	Boğaz	1.06	1.80	1.11	69.49	4.85	4.72	2.09	4.79	55.64	1.56
	Lefkoşa	0.85	0.53	0.84	37.95	1.44	3.80	5.31	4.39	39.65	15.39
	Girne	1.31	0.80	1.43	39.06	9.17	6.20	3.98	7.15	35.78	15.34
	Magusa	0.91	0.99	0.94	8.46	2.34	4.21	3.21	4.69	23.71	11.39
	Karpaz	1.38	1.44	1.44	4.55	3.99	6.03	5.12	6.42	15.12	6.57
	Güzelyurt	0.79	0.49	0.78	37.83	0.58	3.27	2.05	3.58	37.43	9.60
	Lefke	0.81	0.41	0.77	50.07	5.05	3.37	2.30	3.92	31.99	16.13
	İskele	0.95	1.23	1.00	29.88	5.83	4.58	3.87	4.84	15.56	5.66
	kantara	1.54	1.79	1.59	16.43	3.56	6.57	5.48	6.81	16.66	3.69
11	Boğaz	1.06	0.78	1.09	26.05	2.55	4.72	1.86	4.83	60.68	2.36
	Lefkoşa	0.85	0.30	0.83	64.59	2.72	3.80	1.37	4.23	64.02	11.30
	Girne	1.31	0.39	1.43	69.93	9.14	6.20	1.51	7.98	75.61	28.65
	Magusa	0.91	0.52	0.90	43.61	2.00	4.21	2.90	4.33	31.07	2.82
	Karpaz	1.38	0.67	1.42	51.24	2.60	6.03	2.46	6.27	59.23	3.97
	Güzelyurt	0.79	0.27	0.75	65.98	4.02	3.27	1.34	3.34	58.88	2.15
	Lefke	0.81	0.28	0.76	65.26	6.45	3.37	2.38	3.47	29.58	2.87
	İskele	0.95	0.65	0.99	31.43	4.36	4.58	2.97	4.56	35.17	0.57
	kantara	1.54	0.84	1.55	45.38	1.12	6.57	3.19	6.49	51.54	1.18

12	Boğaz	1.06	1.51	1.12	42.42	5.34	4.72	4.68	4.79	0.88	1.50
	Lefkoşa	0.85	0.49	0.84	42.59	0.90	3.80	2.64	4.11	30.53	8.21
	Girne	1.31	0.62	1.53	52.48	16.99	6.20	1.86	8.13	70.07	31.11
	Magusa	0.91	0.79	0.91	13.56	0.02	4.21	3.66	4.61	12.95	9.46
	Karpaz	1.38	1.00	1.47	27.65	6.29	6.03	3.69	6.25	38.77	3.74
	Güzelyurt	0.79	0.40	0.78	49.28	0.41	3.27	2.01	3.63	38.50	11.06
	Lefke	0.81	0.45	0.79	44.70	2.59	3.37	2.04	3.75	39.63	11.01
	İskele	0.95	1.07	1.00	13.25	5.49	4.58	3.23	4.81	29.55	5.01
	kantara	1.54	1.46	1.60	5.17	4.16	6.57	4.84	6.84	26.42	4.13
13	Boğaz	1.06	0.41	1.02	61.58	4.11	4.72	2.03	4.94	56.94	4.65
	Lefkoşa	0.85	0.70	0.89	18.16	4.66	3.80	3.79	4.04	0.36	6.41
	Girne	1.31	1.06	1.49	19.44	13.41	6.20	5.59	6.54	9.85	5.48
	Magusa	0.91	0.86	1.04	5.96	13.31	4.21	3.23	5.78	23.37	37.41
	Karpaz	1.38	1.33	1.73	3.56	25.09	6.03	4.85	7.97	19.53	32.12
	Güzelyurt	0.79	1.54	0.80	95.97	2.42	3.27	3.67	3.10	12.15	5.16
	Lefke	0.81	1.04	0.83	27.50	2.05	3.37	2.57	3.27	23.98	3.10
	İskele	0.95	0.84	1.01	10.93	7.08	4.58	3.53	4.81	23.05	5.02
	kantara	1.54	0.53	1.52	65.45	1.29	6.57	2.54	7.33	61.32	11.51

	Boğaz	1.06	0.78	1.09	26.05	2.55	4.72	2.97	4.83	37.06	2.36
	Lefkoşa	0.85	0.30	0.83	64.59	2.72	3.80	1.86	4.23	51.16	11.30
	Girne	1.31	0.39	1.43	69.93	9.14	6.20	1.34	7.98	78.33	28.65
	Magusa	0.91	0.52	0.90	43.61	2.00	4.21	2.46	4.33	41.60	2.82
14	Karpaz	1.38	0.67	1.42	51.24	2.60	6.03	2.90	6.27	51.88	3.97
	Güzelyurt	0.79	0.27	0.75	65.98	4.02	3.27	1.37	3.34	58.16	2.15
	Lefke	0.81	0.28	0.76	65.26	6.45	3.37	1.51	3.47	55.18	2.87
	İskele	0.95	0.65	0.99	31.43	4.36	4.58	2.38	4.56	48.14	0.57
	kantara	1.54	0.84	1.55	45.38	1.12	6.57	3.19	6.49	51.54	1.18

B. Trend Analysis Tables

Table B.1. Observed MMK and SS Results for Annual Analysis

Modified Mann-Kendall Test (Annual)					
Station	Test statistics		p-value	Sen's slope	Trend direction
Boğaz	2.129	***	0.0333	2.2	Positive
Girne	-0.150	*	0.8807	-0.2	Negative
İskele	-0.043	*	0.9659	-0.1	Negative
Güzelyurt	2.926	****	0.0034	1.1	Positive
Kantara	2.691	****	0.0071	1.8	Positive
Karpaz	-0.047	*	0.9627	-0.1	Negative
Lefke	4.584	****	0.0000	2.4	Positive
Lefkoşa	1.209	*	0.2266	1.0	Positive
Magusa	2.887	****	0.0039	1.6	Positive

Note: *, **, ***, and **** signs represent very weak, weak, strong, and very strong trends, respectively.

Table B.2. Observed ITA Results for Annual Analysis

Innovative Trend Analysis (Annual)									
Station	Trend Slope		Trend Indicator	Slope Standart Deviation	Sig. Level 90%	Sig. Level 95%	Sig. Level 99%	Trend Direction	
Boğaz	1.63	***	0.78	0.32	± 0.525	± 0.625	± 0.822	Positive	
Girne	-0.67	**	-0.26	0.35	± 0.573	± 0.683	± 0.897	Negative	
İskele	0.19	*	0.11	0.28	± 0.453	± 0.540	± 0.710	Positive	
Güzelyurt	0.85	****	0.57	0.16	± 0.267	± 0.318	± 0.418	Positive	
Kantara	1.29	***	0.44	0.60	± 0.984	± 1.173	± 1.541	Positive	
Karpaz	-0.26	*	-0.10	0.26	± 0.428	± 0.510	± 0.671	Negative	
Lefke	2.24	****	1.42	0.21	± 0.350	± 0.417	± 0.548	Positive	
Lefkoşa	2.09	****	1.36	0.27	± 0.448	± 0.534	± 0.701	Positive	
Magusa	-0.18	*	-0.10	0.33	± 0.546	± 0.650	± 0.854	Negative	

Note: *, **, ***, and **** signs represent very weak, weak, strong, and very strong trends, respectively.

Table B.3. Observed MMK and SS Results for Winter Season Analysis

Modified Mann-Kendall Test (Winter)					
Station	Test statistics		p-value	Sen's slope	Trend direction
Boğaz	3.362	****	0.0008	2.0	Positive
Girne	0.360	*	0.7188	0.3	Positive
İskele	0.474	*	0.6355	0.2	Positive
Güzelyurt	1.715	**	0.0864	0.6	Positive
Kantara	-0.675	*	0.4999	-0.6	Negative
Karpaz	0.362	*	0.7172	0.4	Positive
Lefke	2.481	***	0.0131	0.9	Positive
Lefkoşa	-0.380	*	0.7037	-0.2	Negative
Magusa	1.907	**	0.0565	1.0	Positive

Note: *, **, ***, and **** signs represent very weak, weak, strong, and very strong trends, respectively.

Table B.4. Observed ITA Results for Winter Season Analysis

Innovative Trend Analysis (Winter)								
Station	Trend Slope	Trend Indicator	Slope Standard Deviation	Sig. Level 90%	Sig. Level 95%	Sig. Level 99%	Trend Direction	
Boğaz	1.89 ****	1.64	0.16	± 0.259	± 0.3	± 0.405	Positive	
Girne	0.84 ***	0.55	0.34	± 0.563	± 0.7	± 0.881	Positive	
İskele	0.91 ****	0.93	0.15	± 0.249	± 0.297	± 0.390	Positive	
Güzelyurt	1.34 ****	1.67	0.11	± 0.185	± 0.220	± 0.289	Positive	
Kantara	0.38 *	0.24	0.30	± 0.500	± 0.596	± 0.783	Positive	
Karpaz	0.82 ****	0.52	0.30	± 0.495	± 0.589	± 0.775	Positive	
Lefke	0.90 ****	1.00	0.17	± 0.284	± 0.338	± 0.445	Positive	
Lefkoşa	0.75 ****	0.97	0.23	± 0.373	± 0.444	± 0.583	Positive	
Magusa	0.30 ***	0.29	0.14	± 0.234	± 0.279	± 0.367	Positive	

Note: *, **, ***, and **** signs represent very weak, weak, strong, and very strong trends, respectively.

Table B.5. Observed MMK and SS Results for Spring Season Analysis

Modified Mann-Kendall Test (Spring)					
Station	Test statistics		p-value	Sen's slope	Trend direction
Boğaz	-1.282	*	0.1999	-0.2	Negative
Girne	-4.199	****	0.0000	-0.8	Negative
İskele	0.087	*	0.9307	0.0	Positive
Güzelyurt	1.176	*	0.2395	0.3	Positive
Kantara	2.623	****	0.0087	0.8	Positive
Karpaz	-0.648	*	0.5169	-0.2	Negative
Lefke	3.119	****	0.0018	0.6	Positive
Lefkoşa	1.207	*	0.2275	0.4	Positive
Magusa	-0.442	*	0.6582	-0.1	Negative

Note: *, **, ***, and **** signs represent very weak, weak, strong, and very strong trends, respectively.

Table B.6. Observed ITA Results for Spring Season Analysis

Innovative Trend Analysis (Spring)										
Station	Trend Slope		Trend Indicator	Slope Standard Deviation	Sig. Level 90%	Sig. Level 95%	Sig. Level 99%	Trend Direction		
Boğaz	-0.45	****	-1.02	0.08	± 0.135	± 0.161	± 0.212	Negative		
Girne	-1.00	****	-2.09	0.12	± 0.199	± 0.237	± 0.311	Negative		
İskele	-0.47	****	-1.09	0.13	± 0.220	± 0.262	± 0.344	Negative		
Güzelyurt	0.02	*	0.06	0.06	± 0.101	± 0.120	± 0.158	Positive		
Kantara	0.71	****	1.17	0.20	± 0.328	± 0.252	± 0.514	Positive		
Karpaz	0.30	***	0.69	0.13	± 0.216	± 0.257	± 0.338	Positive		
Lefke	1.09	****	3.16	0.18	± 0.291	± 0.346	± 0.455	Positive		
Lefkoşa	0.97	****	2.54	0.16	± 0.266	± 0.317	± 0.417	Positive		
Magusa	-0.29	***	-0.77	0.11	± 0.186	± 0.222	± 0.291	Negative		

Note: *, **, ***, and **** signs represent very weak, weak, strong, and very strong trends, respectively.

Table B.7. Observed MMK and SS Results for Autumn Season Analysis

Modified Mann-Kendall Test (Autumn)					
Station	Test statistics		p-value	Sen's slope	Trend direction
Boğaz	1.060	*	0.2891	0.3	Positive
Girne	1.052	*	0.2926	0.3	Positive
İskele	-0.148	*	0.8824	0.0	Negative
Güzelyurt	-0.548	*	0.5835	-0.1	Negative
Kantara	0.046	*	0.9636	0.0	Positive
Karpaz	-2.059	***	0.0395	-1.0	Negative
Lefke	6.911	****	0.0000	0.8	Positive
Lefkoşa	1.676	**	0.0937	0.3	Positive
Magusa	2.389	***	0.0169	0.4	Positive

Note: *, **, ***, and **** signs represent very weak, weak, strong, and very strong trends, respectively.

Table B.8. Observed ITA Results for Autumn Season Analysis

Innovative Trend Analysis (Autumn)										
Station	Trend Slope		Trend Indicator	Slope Standard Deviation	Sig. Level 90%	Sig. Level 95%	Sig. Level 99%	Trend Direction		
Boğaz	0.36	**	0.89	0.20	± 0.324	± 0.386	± 0.508	Positive		
Girne	-0.36	***	-0.75	0.15	± 0.245	± 0.292	± 0.384	Negative		
İskele	-0.22	*	-0.62	0.14	± 0.237	± 0.282	± 0.371	Negative		
Güzelyurt	-0.39	***	-1.18	0.17	± 0.280	± 0.334	± 0.439	Negative		
Kantara	-0.15	*	-0.23	0.17	± 0.274	± 0.327	± 0.430	Negative		
Karpaz	-1.82	****	-2.81	0.18	± 0.298	± 0.355	± 0.467	Negative		
Lefke	0.45	****	1.58	0.10	± 0.166	± 0.197	± 0.260	Positive		
Lefkoşa	0.08	*	0.24	0.11	± 0.174	± 0.207	± 0.272	Positive		
Magusa	0.15	**	0.45	0.08	± 0.137	± 0.163	± 0.214	Positive		

Note: *, **, ***, and **** signs represent very weak, weak, strong, and very strong trends, respectively.

Table B.9. RCP4.5 Near-Future MMK and SS Results for Annual Analysis

Modified Mann-Kendall Test (Annual)					
Station	Test statistics		p-value	Sen's slope	Trend direction
Boğaz	-4.439	****	0.0000	-2.1	Negative
Girne	-5.637	****	0.0000	-3.1	Negative
İskele	-8.526	****	0.0000	-2.3	Negative
Güzelyurt	-5.132	****	0.0000	-1.4	Negative
Kantara	-6.616	****	0.0000	-3.2	Negative
Karpaz	-8.881	****	0.0000	-4.2	Negative
Lefke	-5.229	****	0.0000	-1.6	Negative
Lefkoşa	-5.880	****	0.0000	-1.6	Negative
Magusa	-7.868	****	0.0000	-2.5	Negative

Note: *, **, ***, and **** signs represent very weak, weak, strong, and very strong trends, respectively.

Table B.10. RCP4.5 Near-Future ITA Results for Annual Analysis

Innovative Trend Analysis (Annual)										
Station	Trend Slope		Trend Indicator	Slope Standard Deviation	Sig. Level 90%		Sig. Level 95%		Sig. Level 99%	Trend Direction
Boğaz	-2.05	****	-1.36	0.10	± 0.171	±	0.203	±	0.267	Negative
Girne	-3.68	****	-1.35	0.23	± 0.385	±	0.459	±	0.603	Negative
İskele	-2.29	****	-1.40	0.11	± 0.173	±	0.206	±	0.271	Negative
Güzelyurt	-1.87	****	-0.99	0.14	± 0.237	±	0.282	±	0.371	Negative
Kantara	-2.97	****	-1.43	0.16	± 0.262	±	0.313	±	0.411	Negative
Karpaz	-3.88	****	-1.35	0.12	± 0.195	±	0.232	±	0.305	Negative
Lefke	-1.56	****	-0.99	0.09	± 0.155	±	0.184	±	0.242	Negative
Lefkoşa	-1.76	****	-1.23	0.07	± 0.109	±	0.129	±	0.170	Negative
Magusa	-2.60	****	-1.53	0.11	± 0.175	±	0.209	±	0.274	Negative

Note: *, **, ***, and **** signs represent very weak, weak, strong, and very strong trends, respectively.

Table B.11. RCP4.5 Near-Future MMK and SS Results for Winter Season Analysis

Modified Mann-Kendall Test (Winter)					
Station	Test statistics		p-value	Sen's slope	Trend direction
Boğaz	-6.246	****	0.0000	-1.0	Negative
Girne	-5.445	****	0.0000	-2.1	Negative
İskele	-6.326	****	0.0000	-1.2	Negative
Güzelyurt	-3.135	****	0.0017	-0.7	Negative
Kantara	-4.995	****	0.0000	-1.3	Negative
Karpaz	-7.932	****	0.0000	-2.6	Negative
Lefke	-4.003	****	0.0001	-0.6	Negative
Lefkoşa	-3.315	****	0.0009	-0.6	Negative
Magusa	-6.841	****	0.0000	-1.4	Negative

Note: *, **, ***, and **** signs represent very weak, weak, strong, and very strong trends, respectively.

Table B.12. RCP4.5 Near-Future ITA Results for Winter Season Analysis

Innovative Trend Analysis (Winter)										
Station	Trend Slope		Trend Indicator	Slope Standard Deviation	Sig. Level 90%		Sig. Level 95%		Sig. Level 99%	Trend Direction
Boğaz	-1.12	****	-1.54	0.07	± 0.123	±	0.147	±	0.193	Negative
Girne	-2.72	****	-1.71	0.18	± 0.300	±	0.358	±	0.470	Negative
İskele	-1.34	****	-1.78	0.05	± 0.080	±	0.096	±	0.126	Negative
Güzelyurt	-1.34	****	-1.31	0.09	± 0.149	±	0.178	±	0.234	Negative
Kantara	-1.63	****	-1.54	0.11	± 0.174	±	0.207	±	0.272	Negative
Karpaz	-2.70	****	-1.65	0.14	± 0.229	±	0.273	±	0.359	Negative
Lefke	-0.85	****	-1.13	0.05	± 0.076	±	0.090	±	0.119	Negative
Lefkoşa	-0.91	****	-1.41	0.07	± 0.109	±	0.130	±	0.171	Negative
Magusa	-1.64	****	-1.82	0.09	± 0.140	±	0.167	±	0.219	Negative

Note: *, **, ***, and **** signs represent very weak, weak, strong, and very strong trends, respectively.

Table B.13. RCP4.5 Near-Future MMK and SS Results for Spring Season Analysis

Modified Mann-Kendall Test (Spring)				
Station	Test statistics	p-value	Sen's slope	Trend direction
Boğaz	-0.355 *	0.7229	-0.1	Negative
Girne	-1.430 *	0.1528	-0.3	Negative
İskele	-2.118 ***	0.0342	-0.5	Negative
Güzelyurt	-1.752 **	0.0798	-0.2	Negative
Kantara	-2.624 ****	0.0087	-0.6	Negative
Karpaz	-4.044 ****	0.0001	-0.9	Negative
Lefke	-1.283 *	0.1995	-0.2	Negative
Lefkoşa	-0.824 *	0.4100	-0.2	Negative
Magusa	-2.779 ****	0.0054	-0.4	Negative

Note: *, **, ***, and **** signs represent very weak, weak, strong, and very strong trends, respectively.

Table B.14. RCP4.5 Near-Future ITA Results for Spring Season Analysis

Innovative Trend Analysis (Spring)										
Station	Trend Slope		Trend Indicator	Slope Standard Deviation	Sig. Level 90%	Sig. Level 95%	Sig. Level 99%	Trend Direction		
Boğaz	-0.19	****	-0.48	0.05	± 0.088	± 0.105	± 0.138	Negative		
Girne	-0.26	****	-0.56	0.03	± 0.048	± 0.057	± 0.075	Negative		
İskele	-0.38	****	-0.77	0.07	± 0.110	± 0.131	± 0.172	Negative		
Güzelyurt	-0.21	****	-0.47	0.05	± 0.078	± 0.093	± 0.122	Negative		
Kantara	-0.51	****	-0.97	0.05	± 0.082	± 0.098	± 0.129	Negative		
Karpaz	-0.68	****	-1.34	0.05	± 0.087	± 0.103	± 0.136	Negative		
Lefke	-0.10	*	-0.24	0.08	± 0.131	± 0.156	± 0.205	Negative		
Lefkoşa	-0.13	****	-0.31	0.04	± 0.066	± 0.079	± 0.104	Negative		
Magusa	-0.25	****	-0.72	0.04	± 0.067	± 0.080	± 0.105	Negative		

Note: *, **, ***, and **** signs represent very weak, weak, strong, and very strong trends, respectively.

Table B.15. RCP4.5 Near-Future MMK and SS Results for Autumn Season Analysis

Modified Mann-Kendall Test (Autumn)					
Station	Test statistics		p-value	Sen's slope	Trend direction
Boğaz	-2.298	***	0.0216	-0.4	Negative
Girne	-1.720	**	0.0855	-0.4	Negative
İskele	-1.864	**	0.0623	-0.2	Negative
Güzelyurt	-2.356	***	0.0185	-0.3	Negative
Kantara	-3.116	****	0.0018	-0.7	Negative
Karpaz	-3.194	****	0.0014	-0.6	Negative
Lefke	-2.788	****	0.0053	-0.4	Negative
Lefkoşa	-3.510	****	0.0004	-0.4	Negative
Magusa	-2.872	****	0.0041	-0.4	Negative

Note: *, **, ***, and **** signs represent very weak, weak, strong, and very strong trends, respectively.

Table B.16. RCP4.5 Near-Future ITA Results for Autumn Season Analysis

Innovative Trend Analysis (Autumn)										
Station	Trend Slope		Trend Indicator	Slope Standard Deviation	Sig. Level 90%		Sig. Level 95%		Sig. Level 99%	Trend Direction
Boğaz	-0.58	****	-1.71	0.09	± 0.151	±	0.180	±	0.236	Negative
Girne	-0.53	****	-0.82	0.09	± 0.156	±	0.185	±	0.244	Negative
İskele	-0.42	****	-1.22	0.03	± 0.053	±	0.064	±	0.084	Negative
Güzelyurt	-0.22	****	-0.53	0.04	± 0.068	±	0.081	±	0.106	Negative
Kantara	-0.72	****	-1.55	0.08	± 0.131	±	0.156	±	0.205	Negative
Karpaz	-0.43	****	-0.60	0.07	± 0.119	±	0.141	±	0.186	Negative
Lefke	-0.47	****	-1.32	0.06	± 0.093	±	0.111	±	0.145	Negative
Lefkoşa	-0.47	****	-1.57	0.05	± 0.075	±	0.089	±	0.117	Negative
Magusa	-0.64	****	-1.52	0.04	± 0.070	±	0.083	±	0.109	Negative

Note: *, **, ***, and **** signs represent very weak, weak, strong, and very strong trends, respectively.

Table B.17. RCP4.5 Far-Future MMK and SS Results for Annual Analysis

Modified Mann-Kendall Test (Annual)					
Station	Test statistics		p-value	Sen's slope	Trend direction
Boğaz	2.382	***	0.0172	0.9	Positive
Girne	4.005	****	0.0001	5.7	Positive
İskele	3.002	****	0.0027	1.3	Positive
Güzelyurt	3.293	****	0.0010	1.4	Positive
Kantara	1.891	**	0.0586	0.7	Positive
Karpaz	5.747	****	0.0000	3.9	Positive
Lefke	4.481	****	0.0000	1.7	Positive
Lefkoşa	4.726	****	0.0000	1.4	Positive
Magusa	6.824	****	0.0000	2.7	Positive

Note: *, **, ***, and **** signs represent very weak, weak, strong, and very strong trends, respectively.

Table B.18. RCP4.5 Far-Future ITA Results for Annual Analysis

Innovative Trend Analysis (Annual)								
Station	Trend Slope	Trend Indicator	Slope Standard Deviation	Sig. Level 90%	Sig. Level 95%	Sig. Level 99%	Trend Direction	
Boğaz	1.24 ****	0.95	0.07	± 0.117	± 0.140	± 0.183	Positive	
Girne	5.65 ****	2.37	0.29	± 0.472	± 0.562	± 0.739	Positive	
İskele	2.18 ****	1.55	0.14	± 0.236	± 0.282	± 0.370	Positive	
Güzelyurt	1.52 ****	0.87	0.10	± 0.169	± 0.202	± 0.265	Positive	
Kantara	1.63 ****	0.90	0.12	± 0.193	± 0.230	± 0.303	Positive	
Karpaz	4.53 ****	1.83	0.22	± 0.362	± 0.431	± 0.566	Positive	
Lefke	1.94 ****	1.37	0.21	± 0.340	± 0.405	± 0.532	Positive	
Lefkoşa	1.80 ****	1.45	0.13	± 0.210	± 0.251	± 0.330	Positive	
Magusa	3.13 ****	2.19	0.13	± 0.212	± 0.252	± 0.331	Positive	

Note: *, **, ***, and **** signs represent very weak, weak, strong, and very strong trends, respectively.

Table B.19. RCP4.5 Far-Future MMK and SS Results for Winter Season Analysis

Modified Mann-Kendall Test (Winter)					
Station	Test statistics		p-value	Sen's slope	Trend direction
Boğaz	7.158	****	0.0000	1.5	Positive
Girne	6.223	****	0.0000	5.3	Positive
İskele	5.833	****	0.0000	1.3	Positive
Güzelyurt	6.603	****	0.0000	1.2	Positive
Kantara	4.361	****	0.0000	1.5	Positive
Karpaz	8.024	****	0.0000	2.8	Positive
Lefke	5.995	****	0.0000	1.0	Positive
Lefkoşa	8.633	****	0.0000	1.3	Positive
Magusa	7.901	****	0.0000	1.9	Positive

Note: *, **, ***, and **** signs represent very weak, weak, strong, and very strong trends, respectively.

Table B.20. RCP4.5 Far-Future ITA Results for Winter Season Analysis

Innovative Trend Analysis (Winter)									
Station	Trend Slope		Trend Indicator	Slope Standard Deviation	Sig. Level 90%	Sig. Level 95%	Sig. Level 99%	Trend Direction	
Boğaz	1.78	****	2.92	0.10	± 0.167	± 0.199	± 0.261	Positive	
Girne	5.10	****	3.76	0.27	± 0.440	± 0.524	± 0.689	Positive	
İskele	1.87	****	2.89	0.18	± 0.293	± 0.349	± 0.458	Positive	
Güzelyurt	1.25	****	1.32	0.08	± 0.125	± 0.149	± 0.196	Positive	
Kantara	2.16	****	2.37	0.12	± 0.200	± 0.238	± 0.313	Positive	
Karpaz	3.73	****	2.68	0.23	± 0.371	± 0.442	± 0.581	Positive	
Lefke	1.19	****	1.67	0.06	± 0.097	± 0.115	± 0.151	Positive	
Lefkoşa	1.55	****	2.74	0.09	± 0.143	± 0.170	± 0.224	Positive	
Magusa	2.70	****	3.61	0.19	± 0.314	± 0.374	± 0.492	Positive	

Note: *, **, ***, and **** signs represent very weak, weak, strong, and very strong trends, respectively.

Table B.21. RCP4.5 Far-Future MMK and SS Results for Spring Season Analysis

Modified Mann-Kendall Test (Spring)					
Station	Test statistics		p-value	Sen's slope	Trend direction
Boğaz	-0.931	*	0.3518	-0.1	Negative
Girne	1.274	*	0.2025	0.2	Positive
İskele	-0.399	*	0.6900	-0.1	Negative
Güzelyurt	2.260	***	0.0238	0.3	Positive
Kantara	-1.895	**	0.0581	-0.4	Negative
Karpaz	2.424	***	0.0154	0.4	Positive
Lefke	3.393	****	0.0007	0.5	Positive
Lefkoşa	1.868	**	0.0618	0.3	Positive
Magusa	-0.432	*	0.6656	-0.1	Negative

Note: *, **, ***, and **** signs represent very weak, weak, strong, and very strong trends, respectively.

Table B.22. RCP4.5 Far-Future ITA Results for Spring Season Analysis

Innovative Trend Analysis (Spring)										
Station	Trend Slope		Trend Indicator	Slope Standard Deviation	Sig. Level 90%		Sig. Level 95%		Sig. Level 99%	Trend Direction
Boğaz	-0.27	****	-0.73	0.04	± 0.068	±	0.081	±	0.106	Negative
Girne	0.11	*	0.24	0.08	± 0.132	±	0.157	±	0.207	Positive
İskele	0.00	*	0.00	0.06	± 0.094	±	0.112	±	0.148	Negative
Güzelyurt	0.04	*	0.08	0.06	± 0.104	±	0.124	±	0.163	Positive
Kantara	-0.35	****	-0.74	0.08	± 0.129	±	0.154	±	0.202	Negative
Karpaz	0.08	*	0.19	0.07	± 0.108	±	0.129	±	0.170	Positive
Lefke	0.44	****	1.13	0.10	± 0.168	±	0.200	±	0.262	Positive
Lefkoşa	0.11	**	0.28	0.06	± 0.106	±	0.127	±	0.166	Positive
Magusa	-0.04	*	-0.12	0.04	± 0.062	±	0.074	±	0.097	Negative

Note: *, **, ***, and **** signs represent very weak, weak, strong, and very strong trends, respectively.

Table B.23. RCP4.5 Far-Future MMK and SS Results for Autumn Season Analysis

Modified Mann-Kendall Test (Autumn)					
Station	Test statistics		p-value	Sen's slope	Trend direction
Boğaz	-3.539	****	0.0004	-0.6	Negative
Girne	0.628	*	0.5303	0.5	Positive
İskele	0.576	*	0.5644	0.2	Positive
Güzelyurt	0.042	*	0.9665	0.0	Positive
Kantara	-2.743	****	0.0061	-0.9	Negative
Karpaz	1.138	*	0.2552	0.6	Positive
Lefke	0.894	*	0.3713	0.2	Positive
Lefkoşa	-1.361	*	0.1736	-0.2	Negative
Magusa	0.233	*	0.8156	0.1	Positive

Note: *, **, ***, and **** signs represent very weak, weak, strong, and very strong trends, respectively.

Table B.24. RCP4.5 Far-Future ITA Results for Autumn Season Analysis

Innovative Trend Analysis (Autumn)											
Station	Trend Slope		Trend Indicator	Slope Standard Deviation		Sig. Level 90%		Sig. Level 95%		Sig. Level 99%	Trend Direction
Boğaz	-0.34	****	-1.15	0.06	±	0.104	±	0.124	±	0.164	Negative
Girne	0.64	****	1.10	0.12	±	0.201	±	0.239	±	0.314	Positive
İskele	0.45	****	1.56	0.07	±	0.089	±	0.083	±	0.109	Positive
Güzelyurt	0.19	****	0.52	0.04	±	0.073	±	0.087	±	0.114	Positive
Kantara	-0.22	****	-0.53	0.07	±	0.111	±	0.132	±	0.174	Negative
Karpaz	0.67	****	1.07	0.09	±	0.151	±	0.179	±	0.236	Positive
Lefke	0.18	****	0.63	0.02	±	0.039	±	0.046	±	0.061	Positive
Lefkoşa	-0.06	*	-0.23	0.05	±	0.085	±	0.101	±	0.133	Negative
Magusa	0.39	****	1.09	0.07	±	0.123	±	0.146	±	0.192	Positive

Note: *, **, ***, and **** signs represent very weak, weak, strong, and very strong trends, respectively.

Table B.25. RCP8.5 Near-Future MMK and SS Results for Annual Analysis

Modified Mann-Kendall Test (Annual)					
Station	Test statistics		p-value	Sen's slope	Trend direction
Boğaz	-5.008	****	0.0000	-2.3	Negative
Girne	-5.632	****	0.0000	-3.1	Negative
İskele	-5.054	****	0.0000	-1.4	Negative
Güzelyurt	-5.760	****	0.0000	-1.3	Negative
Kantara	-6.162	****	0.0000	-2.2	Negative
Karpaz	-3.827	****	0.0001	-1.9	Negative
Lefke	-7.084	****	0.0000	-2.1	Negative
Lefkoşa	-6.810	****	0.0000	-2.3	Negative
Magusa	-6.124	****	0.0000	-1.1	Negative

Note: *, **, ***, and **** signs represent very weak, weak, strong, and very strong trends, respectively.

Table B.26. RCP8.5 Near-Future ITA Results for Annual Analysis

Innovative Trend Analysis (Annual)										
Station	Trend Slope		Trend Indicator	Slope Standard Deviation	Sig. Level 90%		Sig. Level 95%		Sig. Level 99%	Trend Direction
Boğaz	-3.48	****	-1.71	0.10	± 0.164	±	0.196	±	0.258	Negative
Girne	-3.34	****	-1.21	0.21	± 0.342	±	0.407	±	0.535	Negative
İskele	-1.96	****	-1.16	0.13	± 0.206	±	0.245	±	0.322	Negative
Güzelyurt	-1.40	****	-0.91	0.09	± 0.156	±	0.186	±	0.244	Negative
Kantara	-3.49	****	-1.19	0.21	± 0.349	±	0.416	±	0.547	Negative
Karpaz	-2.19	****	-0.80	0.22	± 0.358	±	0.426	±	0.560	Negative
Lefke	-2.28	****	-1.45	0.11	± 0.185	±	0.220	±	0.289	Negative
Lefkoşa	-2.91	****	-1.78	0.12	± 0.201	±	0.240	±	0.315	Negative
Magusa	-1.39	****	-0.84	0.10	± 0.167	±	0.199	±	0.261	Negative

Note: *, **, ***, and **** signs represent very weak, weak, strong, and very strong trends, respectively.

Table B.27. RCP8.5 Near-Future MMK and SS Results for Winter Season Analysis

Modified Mann-Kendall Test (Winter)				
Station	Test statistics	p-value	Sen's slope	Trend direction
Boğaz	-0.563 *	0.5736	-0.2	Negative
Girne	-0.767 *	0.4434	-0.4	Negative
İskele	-2.664 ****	0.0077	-0.5	Negative
Güzelyurt	-1.742 **	0.0815	-0.6	Negative
Kantara	-2.076 ***	0.0379	-0.6	Negative
Karpaz	-0.183 *	0.8550	0.0	Negative
Lefke	-3.870 ****	0.0001	-0.4	Negative
Lefkoşa	-6.786 ****	0.0000	-0.5	Negative
Magusa	-3.650 ****	0.0003	-0.6	Negative

Note: *, **, ***, and **** signs represent very weak, weak, strong, and very strong trends, respectively.

Table B.28. RCP8.5 Near-Future ITA Results for Winter Season Analysis

Innovative Trend Analysis (Winter)									
Station	Trend Slope		Trend Indicator	Slope Standard Deviation	Sig. Level 90%	Sig. Level 95%	Sig. Level 99%	Trend Direction	
Boğaz	-0.25	****	-0.29	0.08	± 0.132	± 0.157	± 0.206	Negative	
Girne	-0.20	*	-0.14	0.15	± 0.239	± 0.285	± 0.375	Negative	
İskele	-0.58	****	-0.75	0.10	± 0.173	± 0.206	± 0.270	Negative	
Güzelyurt	-0.25	***	-0.32	0.10	± 0.168	± 0.200	± 0.262	Negative	
Kantara	-0.84	****	-0.59	0.08	± 0.134	± 0.160	± 0.210	Negative	
Karpaz	-0.57	****	-0.37	0.13	± 0.206	± 0.246	± 0.323	Negative	
Lefke	-0.36	****	-0.49	0.05	± 0.077	± 0.091	± 0.120	Negative	
Lefkoşa	-0.55	****	-0.78	0.05	± 0.076	± 0.091	± 0.119	Negative	
Magusa	-0.53	****	-0.59	0.07	± 0.121	± 0.144	± 0.189	Negative	

Note: *, **, ***, and **** signs represent very weak, weak, strong, and very strong trends, respectively.

Table B.29. RCP8.5 Near-Future MMK and SS Results for Spring Season Analysis

Modified Mann-Kendall Test (Spring)					
Station	Test statistics		p-value	Sen's slope	Trend direction
Boğaz	-2.724	****	0.0064	-0.7	Negative
Girne	-1.724	**	0.0847	-0.3	Negative
İskele	-1.104	*	0.2698	-0.2	Negative
Güzelyurt	-2.613	****	0.0090	-0.3	Negative
Kantara	-2.262	***	0.0237	-0.6	Negative
Karpaz	0.439	*	0.6604	0.1	Positive
Lefke	-3.847	****	0.0001	-0.7	Negative
Lefkoşa	-3.773	****	0.0002	-0.8	Negative
Magusa	0.940	*	0.3474	0.1	Positive

Note: *, **, ***, and **** signs represent very weak, weak, strong, and very strong trends, respectively.

Table B.30. RCP8.5 Near-Future ITA Results For Spring Season Analysis

Innovative Trend Analysis (Spring)										
Station	Trend Slope		Trend Indicator	Slope Standard Deviation	Sig. Level 90%		Sig. Level 95%		Sig. Level 99%	Trend Direction
Boğaz	-1.10	****	-1.96	0.09	± 0.141	±	0.168	±	0.221	Negative
Girne	-0.10	*	-0.26	0.09	± 0.144	±	0.171	±	0.225	Negative
İskele	-0.32	****	-0.68	0.05	± 0.083	±	0.099	±	0.131	Negative
Güzelyurt	-0.49	****	-1.37	0.03	± 0.048	±	0.058	±	0.076	Negative
Kantara	-0.84	****	-1.23	0.10	± 0.157	±	0.187	±	0.246	Negative
Karpaz	0.26	****	0.72	0.09	± 0.150	±	0.179	±	0.235	Positive
Lefke	-0.79	****	-1.88	0.07	± 0.107	±	0.128	±	0.168	Negative
Lefkoşa	-0.96	****	-1.90	0.04	± 0.067	±	0.080	±	0.105	Negative
Magusa	0.09	****	0.34	0.03	± 0.055	±	0.065	±	0.086	Positive

Note: *, **, ***, and **** signs represent very weak, weak, strong, and very strong trends, respectively.

Table B.31. RCP8.5 Near-Future MMK and SS Results for Autumn Season Analysis

Modified Mann-Kendall Test (Autumn)					
Station	Test statistics		p-value	Sen's slope	Trend direction
Boğaz	-4.687	****	0.0000	-1.0	Negative
Girne	-5.332	****	0.0000	-1.6	Negative
İskele	-4.857	****	0.0000	-0.6	Negative
Güzelyurt	-3.684	****	0.0002	-0.5	Negative
Kantara	-4.031	****	0.0001	-1.1	Negative
Karpaz	-6.486	****	0.0000	-1.8	Negative
Lefke	-5.886	****	0.0000	-0.6	Negative
Lefkoşa	-4.339	****	0.0000	-0.6	Negative
Magusa	-4.212	****	0.0000	-0.6	Negative

Note: *, **, ***, and **** signs represent very weak, weak, strong, and very strong trends, respectively

Table B.32. RCP8.5 Near-Future ITA Results for Autumn Season Analysis

Innovative Trend Analysis (Autumn)									
Station	Trend Slope		Trend Indicator	Slope Standard Deviation	Sig. Level 90%	Sig. Level 95%	Sig. Level 99%	Trend Direction	
Boğaz	-1.75	****	-3.26	0.07	± 0.113	± 0.134	± 0.177	Negative	
Girne	-3.08	****	-3.52	0.31	± 0.517	± 0.616	± 0.810	Negative	
İskele	-0.81	****	-2.05	0.04	± 0.070	± 0.084	± 0.110	Negative	
Güzelyurt	-0.82	****	-2.19	0.06	± 0.099	± 0.118	± 0.155	Negative	
Kantara	-1.58	****	-2.04	0.14	± 0.225	± 0.268	± 0.353	Negative	
Karpaz	-1.78	****	-2.15	0.14	± 0.238	± 0.283	± 0.372	Negative	
Lefke	-0.98	****	-2.66	0.04	± 0.065	± 0.077	± 0.101	Negative	
Lefkoşa	-1.14	****	-3.03	0.03	± 0.052	± 0.062	± 0.081	Negative	
Magusa	-0.81	****	-1.79	0.09	± 0.141	± 0.168	± 0.221	Negative	

Note: *, **, ***, and **** signs represent very weak, weak, strong, and very strong trends, respectively.

Table B.33. RCP8.5 Far-Future MMK and SS Results for Annual Analysis

Modified Mann-Kendall Test (Annual)					
Station	Test statistics		p-value	Sen's slope	Trend direction
Boğaz	-3.137	****	0.0017	-1.6	Negative
Girne	-3.377	****	0.0007	-3.2	Negative
İskele	-2.932	****	0.0034	-1.4	Negative
Güzelyurt	-6.809	****	0.0000	-2.0	Negative
Kantara	-2.939	****	0.0033	-2.3	Negative
Karpaz	-6.921	****	0.0000	-2.9	Negative
Lefke	-3.449	****	0.0006	-1.5	Negative
Lefkoşa	-2.683	****	0.0073	-1.1	Negative
Magusa	-3.447	****	0.0006	-1.4	Negative

Note: *, **, ***, and **** signs represent very weak, weak, strong, and very strong trends, respectively.

Table B.34. RCP8.5 Far-Future ITA Results for Annual Analysis

Innovative Trend Analysis (Annual)									
Station	Trend Slope		Trend Indicator	Slope Standard Deviation	Sig. Level 90%	Sig. Level 95%	Sig. Level 99%	Trend Direction	
Boğaz	-1.66	****	-1.03	0.27	± 0.445	± 0.531	± 0.697	Negative	
Girne	-4.02	****	-1.70	0.36	± 0.588	± 0.701	± 0.921	Negative	
İskele	-1.57	****	-1.14	0.17	± 0.287	± 0.342	± 0.449	Negative	
Güzelyurt	-1.87	****	-1.44	0.06	± 0.103	± 0.123	± 0.161	Negative	
Kantara	-3.51	****	-1.46	0.40	± 0.652	± 0.776	± 1.020	Negative	
Karpaz	-2.92	****	-1.30	0.24	± 0.395	± 0.470	± 0.618	Negative	
Lefke	-1.81	****	-1.46	0.18	± 0.294	± 0.350	± 0.460	Negative	
Lefkoşa	-1.27	****	-0.99	0.24	± 0.401	± 0.478	± 0.629	Negative	
Magusa	-1.86	****	-1.40	0.20	± 0.322	± 0.384	± 0.505	Negative	

Note: *, **, ***, and **** signs represent very weak, weak, strong, and very strong trends, respectively.

Table B.35. RCP8.5 Far-Future MMK and SS Results for Winter Season Analysis

Modified Mann-Kendall Test (Winter)					
Station	Test statistics		p-value	Sen's slope	Trend direction
Boğaz	-2.564	***	0.0103	-1.1	Negative
Girne	-2.562	***	0.0104	-1.9	Negative
İskele	-2.699	****	0.0070	-0.9	Negative
Güzelyurt	-2.759	****	0.0058	-0.9	Negative
Kantara	-3.361	****	0.0008	-1.8	Negative
Karpaz	-5.041	****	0.0000	-2.4	Negative
Lefke	-3.427	****	0.0006	-0.9	Negative
Lefkoşa	-2.458	***	0.0140	-1.0	Negative
Magusa	-2.864	****	0.0042	-1.2	Negative

Note: *, **, ***, and **** signs represent very weak, weak, strong, and very strong trends, respectively.

Table B.36. RCP8.5 Far-Future ITA Results for Winter Season Analysis

Innovative Trend Analysis (Winter)									
Station	Trend Slope		Trend Indicator	Slope Standard Deviation	Sig. Level 90%	Sig. Level 95%	Sig. Level 99%	Trend Direction	
Boğaz	-1.50	****	-1.89	0.20	± 0.331	± 0.394	± 0.518	Negative	
Girne	-2.86	****	-2.00	0.32	± 0.531	± 0.633	± 0.832	Negative	
İskele	-1.19	****	-1.77	0.16	± 0.262	± 0.312	± 0.410	Negative	
Güzelyurt	-1.01	****	-1.43	0.08	± 0.140	± 0.166	± 0.219	Negative	
Kantara	-2.66	****	-2.09	0.28	± 0.454	± 0.540	± 0.710	Negative	
Karpaz	-2.65	****	-1.99	0.17	± 0.281	± 0.335	± 0.440	Negative	
Lefke	-1.12	****	-1.71	0.12	± 0.205	± 0.245	± 0.322	Negative	
Lefkoşa	-1.03	****	-1.67	0.11	± 0.183	± 0.218	± 0.287	Negative	
Magusa	-1.58	****	-2.14	0.23	± 0.375	± 0.447	± 0.587	Negative	

Note: *, **, ***, and **** signs represent very weak, weak, strong, and very strong trends, respectively.

Table B.37. RCP8.5 Far-Future MMK and SS Results for Spring Season Analysis

Modified Mann-Kendall Test (Spring)					
Station	Test statistics		p-value	Sen's slope	Trend direction
Boğaz	-1.937	**	0.0527	-0.2	Negative
Girne	-3.744	****	0.0002	-0.6	Negative
İskele	-0.743	*	0.4577	-0.1	Negative
Güzelyurt	-3.749	****	0.0002	-0.3	Negative
Kantara	-3.505	****	0.0005	-0.6	Negative
Karpaz	-2.279	***	0.0227	-0.5	Negative
Lefke	-0.121	*	0.9037	0.0	Negative
Lefkoşa	-0.392	*	0.6949	0.0	Negative
Magusa	-2.870	****	0.0041	-0.4	Negative

Note: *, **, ***, and **** signs represent very weak, weak, strong, and very strong trends, respectively.

Table B.38. RCP8.5 Far-Future ITA Results for Spring Season Analysis

Innovative Trend Analysis (Spring)									
Station	Trend Slope		Trend Indicator	Slope Standard Deviation	Sig. Level 90%	Sig. Level 95%	Sig. Level 99%	Trend Direction	
Boğaz	-0.23	****	-0.55	0.06	± 0.093	± 0.111	± 0.146	Negative	
Girne	-0.85	****	-2.23	0.09	± 0.143	± 0.170	± 0.224	Negative	
İskele	-0.50	****	-1.19	0.10	± 0.156	± 0.186	± 0.245	Negative	
Güzelyurt	-0.43	****	-1.49	0.03	± 0.050	± 0.059	± 0.078	Negative	
Kantara	-0.87	****	-1.43	0.12	± 0.205	± 0.245	± 0.322	Negative	
Karpaz	-0.60	****	-1.56	0.05	± 0.083	± 0.099	± 0.130	Negative	
Lefke	-0.17	****	-0.59	0.05	± 0.078	± 0.093	± 0.122	Negative	
Lefkoşa	-0.20	****	-0.53	0.07	± 0.122	± 0.145	± 0.191	Negative	
Magusa	-0.53	****	-1.89	0.06	± 0.096	± 0.114	± 0.150	Negative	

Note: *, **, ***, and **** signs represent very weak, weak, strong, and very strong trends, respectively.

Table B.39. RCP8.5 Far-Future MMK and SS Results For Autumn Season Analysis

Modified Mann-Kendall Test (Autumn)					
Station	Test statistics		p-value	Sen's slope	Trend direction
Boğaz	-3.057	****	0.0022	-0.6	Negative
Girne	-1.546	*	0.1222	-0.3	Negative
İskele	0.458	*	0.6468	0.1	Positive
Güzelyurt	-5.221	****	0.0000	-0.5	Negative
Kantara	-0.070	*	0.9444	0.0	Negative
Karpaz	-3.141	****	0.0017	-0.8	Negative
Lefke	-5.245	****	0.0000	-0.5	Negative
Lefkoşa	0.435	*	0.6638	0.1	Positive
Magusa	0.919	*	0.3580	0.1	Positive

Note: *, **, ***, and **** signs represent very weak, weak, strong, and very strong trends, respectively.

Table B.40. RCP8.5 Far-Future ITA Results for Autumn Analysis

Innovative Trend Analysis (Autumn)									
Station	Trend Slope		Trend Indicator	Slope Standard Deviation	Sig. Level 90%	Sig. Level 95%	Sig. Level 99%	Trend Direction	
Boğaz	-0.07	*	-0.13	0.12	± 0.191	± 0.228	± 0.299	Negative	
Girne	-0.21	*	-0.39	0.16	± 0.268	± 0.320	± 0.420	Negative	
İskele	0.28	****	1.10	0.05	± 0.085	± 0.102	± 0.134	Positive	
Güzelyurt	-0.31	****	-1.11	0.05	± 0.081	± 0.096	± 0.126	Negative	
Kantara	0.22	***	0.45	0.11	± 0.174	± 0.207	± 0.272	Positive	
Karpaz	-0.07	*	-0.13	0.12	± 0.191	± 0.228	± 0.299	Negative	
Lefke	-0.36	****	-1.38	0.04	± 0.058	± 0.070	± 0.091	Negative	
Lefkoşa	0.19	***	0.79	0.09	± 0.144	± 0.172	± 0.226	Positive	
Magusa	0.44	****	1.56	0.05	± 0.083	± 0.099	± 0.130	Positive	

Note: *, **, ***, and **** signs represent very weak, weak, strong, and very strong trends, respectively.